The Dissertation Committee for Nicholas Jay Hanovice Certifies that this is the approved version of the following dissertation:

PIGMENTATION AND REGENERATION OF THE ZEBRAFISH RETINAL PIGMENT EPITHELIUM

Committee:

Steven Vokes, Supervisor

Jeffrey M. Gross, Co-Supervisor

Seema Agarwala

Nigel Atkinson

Johann Eberhart

PIGMENTATION AND REGENERATION OF THE ZEBRAFISH RETINAL PIGMENT EPITHELIUM

by

Nicholas Jay Hanovice, B.S.

Dissertation

Presented to the Faculty of the Graduate School of

The University of Texas at Austin

in Partial Fulfillment

of the Requirements

for the Degree of

Doctor of Philosophy

The University of Texas at Austin

May, 2017

Dedication

To my parents: Cathryn and Ronald Hanovice

My most constant defenders, and source of my strength.

Acknowledgements

I first thank my advisor, Dr. Jeffrey Gross, for taking a chance on me, for providing me with space, resources and unfailingly insightful feedback throughout my graduate career, and for his trust and support. I have grown personally and professionally under his mentorship and I will always be grateful. Thank you to the members of my committee: Dr. Seema Agarwala, Dr. Nigel Atkinson, Dr. Johann Eberhart, and Dr. Steven Vokes, for providing me invaluable scientific and life advice.

Thank you to the members of the Gross Lab, who I count amongst my closest friends and fiercest critics, and who have provided invaluable guidance, advice, technical help, and companionship throughout the years. Thank you also to my colleagues in the Institute for Cellular and Molecular Biology, for your friendship and camaraderie as we all pushed our way through this arduous process together. I want to acknowledge the University of Texas at Austin, the National Institutes of Health, and the US taxpayer for my funding.

Finally, thank you to my family. To my father, for offering his ophthalmological expertise as I progressed through my dissertation, for instilling in me a love of learning, and for showing me the value and rewards of hard work. To my mother, for her constant support, unconditional love and for teaching me the art of concision in my writing. To my brother and sister, who have shaped me in so many ways. Lastly, thank you to Rebecca, who has been unconditionally generous, patient and forgiving throughout my graduate career, and who brings out the best in me. I am nothing without you all.

PIGMENTATION AND REGENERATION OF THE ZEBRAFISH RETINAL PIGMENT EPITHELIUM

Nicholas Jay Hanovice

The University of Texas at Austin, 2017

Supervisor: Steven Vokes

Co-Supervisor: Jeffrey Gross

The Retinal Pigment Epithelium (RPE) is a specialized monolayer of pigmented cells in the back of the eye that forms a functional unit with photoreceptor cells in the retina and is critical for photoreceptor function and eye development. As a flat sheet of progenitor cells develops, a series of complex morphogenetic changes occur which require coordinated changes in cellular morphology, cell cycle and motility. To aid the study of these processes, I have generated ten novel GAL4-inducible zebrafish transgenics that enable the tissue-specific modulation of Rho GTPase activity and demonstrated the utility of these lines in studying eye development. Diseases disrupting the normal pigmentation of the RPE, known as albinism, cause defects in retinal development and vision. Although many different alleles of albinism have been identified, it is likely that undiscovered loci responsible for causing albinism exist. To learn more about the genetic underpinnings of albinism, I have characterized two novel zebrafish albino mutants and found they result from mutations in the gene encoding N ethyl maleimide-sensitive factor B (*nsfb*) and have established a role for nsfb in the maturation of pigment in zebrafish RPE. Finally, diseases affecting the adult RPE have

dire consequences for vision. Geographic Age-related Macular Degeneration (AMD) is the third leading cause of blindness worldwide, and occurs when atrophy of the RPE causes irreversible death of underlying photoreceptors. Despite advances in stem-cell based RPE replacement therapies, very little is known about the process by which RPE cells can successfully regenerate and integrate into damaged retinal tissue. To study this process, I established a novel zebrafish model of AMD whereby specific ablation of the RPE leads to rapid degeneration of underlying photoreceptors. Using this model, I demonstrated for the first time that the zebrafish RPE is capable of regenerating after widespread damage and provide evidence that RPE ablation provokes a robust proliferative response during which cells from the periphery move into the injury site and contribute to regeneration, and that these cells likely derive from unablated RPE. This model provides a platform for supporting the development of AMD therapies.

Table of Contents

List of Tables

List of Figures

Chapter 1: Introduction to the Development, Pigmentation and Regeneration of the Retinal Pigment Epithelium

1.1: Development and function of the Retinal Pigment Epithelium

This dissertation focuses on the development and regeneration of the Retinal Pigment Epithelium (RPE) in zebrafish. The eye is a fantastically complex organ whose function is to sense and convert light from the environment into electrochemical signals and transmit them to the brain. The RPE is a polarized monolayer of hexagonal pigment-containing cells posterior to the retina whose apical surface is closely interdigitated with photoreceptive neurons called photoreceptors. Photoreceptors are responsible for the conversion of light into electrochemical signals, and ultimately form a functional unit with the RPE. The basal RPE surface abuts and helps form a multilaminar basement membrane known as Bruch's Membrane (BM), which helps create a barrier between the retina and nourishing vasculature called the choriocapillaris. Because RPE is critical for many crucial processes in eye development and visual function, any disruption to RPE development or integrity has dire consequences for vision.

Table 1.1: Common Abbreviations

Retinal Pigment Epithelium	RPE
Neural Retina	NR
Retinal Progenitor Cells	RPCs
Ciliary Marginal Zone	CMZ
Müller glia-derived progenitor cells	MGPCs
Interphotoreceptor Retinol Binding Protein	IRBP
Bruch's Membrane	BM
Age-Related Macular Degeneration	AMD
Proliferative Vitreoretinopathy	PVR
Photoreceptor Outer Segments	POS
Choroidal Neovascularization	CNV
Outer Plexiform Layer	OPL
Outer Nuclear Layer	ONL

1.1.1 Early Development

To fully understand RPE development, it is necessary to start at the beginning: the eye field. The eye field is a single patch of neuroepithelial cells located in the medial anterior plate, from which both the RPE and the neural retina derive. Despite minor differences, the genetic and morphogenetic mechanisms by which this single flat sheet of cells ultimately develops into two complex light sensing organs is well conserved between zebrafish and human (Chow and Lang, 2001; Fuhrmann, 2010; Schmitt and Dowling, 1994).

The eye field first forms in the medial anterior neural plate shortly after forebrain specification (Bailey et al., 2004; Mathers et al., 1997), and is defined by the co-expression of a group of transcription factors known as eye-field transcription factors (EFTFs) which are often both necessary and sufficient for proper eye development. These factors include rx, *rx3*, lhx2, pax6, six3 and optx2 (Zuber et al., 2003). For example, Pax6 mutants completely lack eyes in mouse (Quinn et al., 1996), and medaka (Loosli et al., 2001) while ectopic expression of Pax6 (Hill et al., 1991), six3 (Lagutin et al., 2003), and others leads to the formation of ectopic retinae (Bailey et al., 2004; Zuber et al., 2003). While the series of events that result in eye field specification are incompletely understood, research indicates that gradients of morphogens such as Wnt (Cavodeassi et al., 2005), Shh (Macdonald et al., 1995), and FGF (Moore et al., 2004) induce forebrain specification and create a competency state that enables the stabilization of EFTF expression via a self-regulating network (Zuber et al., 2003). Illustrating this, six3 is initially expressed across the anterior neural plate in both mouse and zebrafish, where it drives forebrain specification by inhibiting canonical Wnt signaling before becoming restricted to the eye field (Lagutin et al., 2003). EFTFs are only capable of directing the formation of ectopic retinae in regions that express *otx2*, a transcription factor first involved in forebrain induction and specification (Chuang & Raymond, 2002, Chow 1999, Martinez 2001). The transcription factors Otx2 and Sox2 are required for forebrain induction, and directly regulate Rx gene expression (Danno et al., 2008). *rx3* expression in zebrafish facilitates the partitioning of eye field cells from different forebrain compartments via Eph/Ephrin signaling (Cavodeassi et al., 2013). *Otx2* also activates critical transcription factors in the zebrafish EFTF network such as *lhx2* (Kennedy et al., 2004), which plays a role in future RPE development. Zebrafish possess three *rx* genes as opposed to the single rx gene in mammals (*rx1-3*) (Chuang et al., 1999) and *rx1-2* appear

to play a instructive role enabling eye field formation, while *rx3* is required for cell movements directing later eye morphogenetic events (Chuang and Raymond, 2001; Fuhrmann, 2010) .

Shortly after eye field formation, the first of two major sequences of morphogenetic movements occurs, ultimately resulting in the bisection of the eye field and morphogenesis of optic vesicles (Fuhrmann, 2010). This process, known as optic vesicle evagination, occurs during neurulation, a process whereby the neural plate folds about the midline to create the neural tube. In zebrafish, evagination occurs during neural keel formation, which is analogous to neurulation in mammals (Lowery and Sive, 2004; Papan and Campos-Ortega, 1994). Two major events occur coincidentally with optic vesicle formation: caudally-located diencephalon cells move rostrally to replace anterior eye field cells as they move laterally, and the telencephalon folds toward the midline to seal the neuropore and facilitate the migration of eye precursors into the optic vesicles (England et al., 2006). It was initially thought that these movements drive evagination by bisecting the eye field and forcing eye field cells laterally (eg. Varga et al. 1999; Li et al. 1997). However, other time-lapse analyses revealed that eye precursor cells migrate in a cell-autonomous fashion. These analyses revealed that eye precursor cells initially move toward the midline before changing direction and moving laterally into the forming optic vesicles, and that lateral migration is dependent upon rx3 (Rembold et al., 2006). This phenotype likely results from misregulation of cell adhesion proteins, such as as nlcam, that sensitize eye precursor cells to attractive cues from the midline (Brown et al., 2010). More recently, it was shown that eye field cells display different types of cell morphologies, with peripheral eye field cells precociously organizing into a polarized neuroepithelium into which centrally located migratory cells intercalate via a MET-like mechanism to drive evagination (Ivanovitch et al., 2013).

As the optic vesicles continue to evaginate and approach the overlying surface ectoderm, heretofore-multipotent optic vesicle cells become specified into RPE, NR, and optic stalk (Fig 1A-B) (Fuhrmann, 2010). RPE specification is initiated by the expression of the bHLH transcription factor Mitf and homeobox domain transcription factor otx2 (Fuhrmann et al., 2014). Mitf is one of the earliest genes specifically demarcating RPE from NR, and is a critical regulator of RPE pigmentation and differentiation. First identified in mouse (Hertwig, 1942; Hodgkinson et al., 1993), mutations of mitf result in microphthalmia (hence microphthalmia-associated transcription factor) and defects in the pigmentation and maturation of RPE cells. In mice, mitf is initially expressed throughout the optic vesicle before becoming restricted to the presumptive RPE when FGF signals from the surface ectoderm induce the expression of vsx2 in the distal optic cup (Nguyen and Arnheiter, 2000). vsx2, which is the earliest gene specifically demarcating NR from RPE, suppresses mitf expression (Zou and Levine, 2012) in the presumptive NR, leading to its restriction to dorsal optic vesicle cells. In contrast to mouse, mitf is not broadly expressed throughout the optic vesicles before becoming restricted to the presumptive RPE region in chick and zebrafish. In chick, *Mitf* is expressed in distal optic vesicle cells and becomes restricted to the dorsal optic cup (Müller et al., 2007), while in zebrafish, the two paralogs of mitf, *mitfa* and *mitfb*, are specifically expressed in the presumptive RPE, never having a broad expression domain in the optic vesicle (Lister et al., 2011). Otx2, the other transcription factor critical for RPE specification, has a similar expression pattern to *Mitf* in chick—after initially being broadly expressed throughout the optic vesicle, it too is restricted to the presumptive RPE (Bovolenta et al., 1997), where it regulates pigmentation during RPE development (Martínez-Morales et al., 2004, 2003). Zebrafish possess three orthologs (*otx1a, otx1b*, and *otx2*) of the two mammalian Otx genes (otx1 and otx2) (Li et al., 1994; Mercier et al., 1995), which are restricted to the

presumptive RPE in early eye (Li et al., 1994). Interestingly, in zebrafish, otx signaling is necessary for RPE development while mitf signaling appears to be dispensable: mutations of both *mitfa* and *mitfb* do not cause major defects in RPE development (Lane and Lister, 2012). Otx and mitf transcription factors interact and positively regulate each other's activity (Martínez-Morales et al., 2003). Beyond this, the mechanisms regulating mitf expression are poorly understood, though lhx2 and rx genes play a prominent role. *rx3* is required both for *otx2* and *mitfa* expression in zebrafish (Rojas-Muñoz et al., 2005), while Lhx2 is required for Mitf expression in mice (Yun et al., 2009). During optic cup morphogenesis, extraocular mesenchyme is critical for induction of the RPE in mouse, via the TGFβ-family cytokine Activin (Fuhrmann et al., 2000) and BMP (Steinfeld et al., 2013). In addition to TGFβ, Wnt, (Fujimura et al., 2009; Westenskow et al., 2009), and Hippo (Miesfeld et al., 2015) signaling are also critical for RPE specification in the dorsal optic vesicle.

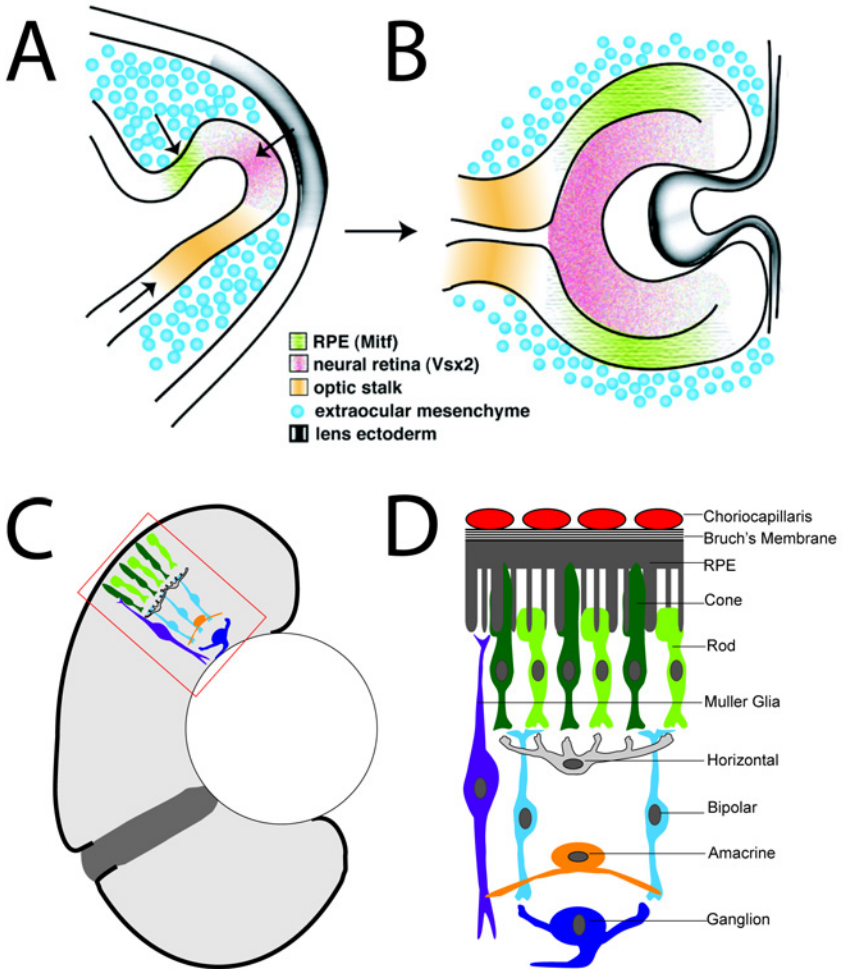

Figure 1.1: Vertebrate retinal morphogenesis. (A) As the optic vesicles evaginate and interacts with surrounding tissues, it becomes specified as RPE, retina or optic stalk. (B)Invagination of the optic vesicle forms the optic cup, with a lens-averse RPE layer and lens-facing retina layer. Image adapted from Fuhrmann 2010. (D) Cartoon representation of the retina, RPE and choroidal tissues contained in the red box. From proximal to distal: choriocapillaris, RPE, cone and rod photoreceptor cells, horizontal cell, bipolar cell, Müller Glia, amacrine cell, and retinal ganglion cell.

1.1.2: Maturation and Pigmentation

RPE maturation initiates during optic cup morphogenesis, which is the second series of major morphological changes that occur during the formation of the eye. After the optic vesicle and surface ectoderm make contact, the surface ectoderm involutes and begins forming the lens, while the optic vesicle invaginates to form bilayered optic cups with cells in the lens-facing layer comprising the neural retina (NR) and RPE cells comprising the lens-averse layer (Schmitt and Dowling, 1999). As the neural retina invaginates around the lens, it undergoes a marked increase in surface area and expands its cell population significantly. 4D analyses revealed that an epithelial flow of cells from the lens-averse layer into the lens-facing layer explains these changes (Heermann et al., 2015; Kwan et al., 2012; Li et al., 2000). As optic cup formation proceeds and the RPE monolayer and NR are brought into close proximity, a small amount of optic cup lumen becomes trapped between them. This lumen remnant is then filled by extracellular matrix and visual cycle proteins to form the interphotoreceptor matrix (Gonzalez-Fernandez, 2003; Stenkamp et al., 1998). Concurrent with interphotoreceptor matrix formation, (Tachibana, 2000) RPE cells begin terminal differentiation: they cease proliferating, transition from pseudostratified epithelium into flattened epithelial cells, and express tyrosinase. It is possible that this change in cell morphology provides the mechanical impetus to drive epithelial flow. As RPE cells transition from columnar pseudostratified epithelium to a flattened epithelium, they significantly increase their surface area and move in conjunction with presumptive NR cells, suggesting that this increase in surface area may drive epithelial flow. These findings are intriguing, as a significant body of literature posits that RPE tissue maintains bipotency late into optic cup morphogenesis and can trans-differentiate into NR (Araki et al., 2002; Bankhead et al., 2015; Sakaguchi et al., 1997). These findings raise the possibility that some of these phenotypes could

instead arise from a failure of cell migration rather than transdifferentiation of RPE into NR.

The formation of black pigment, known as melanogenesis, marks a critical step in the differentiation of RPE cells. Hypopigmentation of the RPE can lead to defects in retinal development (Grønskov et al., 2007) and abberrent routing of retinal ganglion axons in the optic nerve tract (Jeffery, 1997). During melanogenesis, black eumelanin pigment is synthesized and aggregated in lysosomal-related organelles called melanosomes (Seiji et al., 1963b; Videira et al., 2013). Tyrosinase, which is transcriptionally regulated in part by mitf (Yasumoto et al., 1994), pax6 (Raviv et al., 2014) and otx2 (Reinisalo et al., 2012), is an iron-containing membrane metalloenzyme that gets trafficked to developing melanosomes and performs the rate-limiting steps in the conversion of tyrosine to melanin (Korner and Pawelek, 1982). Immature melanosomes first form as early endosomes and become progressively more pigmented as they mature. Vesicles from the Golgi network are then trafficked to the early endosome and deliver melanogenic enzymes, cofactors and melanin precursors to developing melanosomes. Proper transport and sorting of these precursors is critical for melanogenesis, and depends in part on the action of small GTPase Rab38 and in multi-protein biogenesis of heteromeric lysosome-related organelle complexes (BLOCs). Rab38 has been found to mediate transport of tyrosinase to the melanosome in mice (Lopes et al., 2007; Wasmeier et al., 2006), while mutations in many BLOC components produce hypopigmentation defects in human (Huizing et al., 2008), mouse (Wei, 2006) and zebrafish (Daly 2013). Chapter 3 will address the stages of melanosomal maturation, and the requirement for proper vesicular fusion for melanogenesis, in greater detail. Once melanogenic precursors and enzymes are trafficked to the melanosome, the intracellular environment in melanosomes is tightly regulated to facilitate melanin synthesis and stability (d'Ischia,

2013). For example, regulation of pH is critical for melanin synthesis, (Ancans et al., 2001; Nuckels et al., 2009; Puri et al., 2000; Watabe et al., 2004).

After optic cup morphogenesis, the pseudostratified epithelium of the NR consists of rapidly proliferating retinal progenitor cells (RPCs). Interactions between the RPE and developing NR play critical roles in each tissue's development. For example, during RPC proliferation, RPE cells release ATP, which diffuses through the interphotoreceptor matrix to modulate the proliferation rate of RPCs (Martins and Pearson, 2008). RPE cells also continue to mature in two major ways: by further establishing apico-basal polarity and secreting growth factors to regulate retinal development. The basal RPE surface begins depositing collagen, which integrates with basement membrane from overlying endoderm, to create the Bruch's Membrane (Olson, 1979; Takei and Ozanics, 1975). Meanwhile, the apical surface begins to develop microvilli, and tight junctions between individual RPE cells form and mature, restricting membrane mixing across the apical/basal border and establishing a blood-retinal border. RPE cells also secrete growth factors that play major roles in directing RPC development, such as PEDF which in *Xenopus* is required for proper photoreceptor formation (Jablonski et al., 2000; Oetting and King, 1999).

As they proliferate, RPCs ultimately respond to environmental signals by differentiating and forming six retinal cell types (Agathocleous and Harris, 2009). This process terminates with the creation of three nuclear laminae, with photoreceptor cells populating the outermost layer adjacent to the RPE, bipolar, amacrine and horizontal cells in the inner nuclear layer, and retinal ganglion cells and displaced amacrine cells making up the innermost lamina (Fig I.1D-C). As specified photoreceptor cells interact with maturing RPE, both tissues undergo terminal differentiation in a cooperative fashion—RPE cells extend apical microvilli into the subretinal space and photoreceptors begin to

grow structures filled with tightly-stacked membrane disks containing phototransduction proteins called photoreceptor outer segments (POS). After interdigitation between POS and RPE microvilli, RPE cells express critical phototransduction proteins and this expression correlates with commencement of light responsiveness in photoreceptors (Bakall et al., 2003).

At this point, RPE development is largely complete. The RPE is now a highly polarized pigmented monolayer with membrane infoldings on its basal surface abutting the BM and microvilli extending from its apical surface to interdigitate with photoreceptor POS.

1.1.3 Function

During development, the RPE and photoreceptors establish themselves into a tight functional unit. One of the most illustrative examples of this is the role the RPE plays in the visual cycle, or the conversion of light to electrochemical information. *cis*-retinal is the light-sensing subunit of the rhodopsin complexes concentrated in photoreceptor POS. Upon absorbing a photon, *cis*-retinal isomerizes to all-*trans*-retinol, resulting in rhodopsin activation and phototransduction (Kuksa et al., 2003). Photoreceptors lack the requisite isomerases to recycle all-*trans*-retinal back to *cis*-retinal, so all-*trans*-retinal must be transported to the RPE. All-*trans*-retinal is exported from photoreceptors and binds interphotoreceptor retinol-binding protein (IRBP) (Edwards and Adler, 1994) as it is transported across the interphotoreceptor matrix to the RPE. Once it is in the RPE, the RPE-specific protein RPE65 performs the rate-limiting step in the retinoid cycle, which results in the conversion of all-*trans*-retinal to *cis*-retinal (Hamel et al., 1993; Redmond et al., 1998) Afterward, regenerated *cis*-retinal is exported, binds to IRBP in the subretinal space and is returned to the photoreceptors. Even with support from the retinoid cycle,

POS are constantly bombarded by light, progressively damaging their phototransduction machinery, which produces deleterious byproducts such as reactive oxygen and lipofuscin. Photoreceptors therefore constantly synthesize new outer segments and, in order to maintain outer segment length, shed photodamaged outer segment disks. These are phagocytosed by the RPE, which digests and eliminates toxic byproducts and recycles important phototransduction components back to the photoreceptors.

The RPE acts as the primary regulator of transport between the retina and circulatory system. Due to its apposition to Bruch's Membrane and tight junctions between RPE cells, the RPE creates the blood-retina barrier between the eye and the fenestrated endothelium of the choriocapillaris, as well as immune privilege in the eye (Streilein et al., 2002). Being a tight epithelium, the RPE transports water (Hamann, 2002), ions (Joseph 1991), and nutrients, such as glucose (Ban, 2000). The RPE also protects the retina from photo-oxidation and reactive oxygen, through absorption of light by its pigment and by expressing antioxidant enzymes (Cai, 2000). Finally, the RPE secretes a number of factors that are critical for the function and continued health of the retina, such as vascular endothelial growth factor (VEGF) (Adamis et al., 1993; Ford et al., 2011), PEDF (Dawson et al., 1999), and multiple FGF proteins (Strauss, 2005).

1.2: Regeneration of the Retinal Pigment Epithelium.

Due to its many critical and lifelong roles in maintaining retinal function and survival, diseases of the RPE result in debilitating consequences. This dissertation primarily focuses on two common diseases affecting the RPE: albinism and Age-Related Macular Degeneration. This section will detail the pathogenesis of these diseases, the

state of the field in their treatment and what is known about the extent to which the mammalian RPE is capable of repairing injuries.

1.2.1 Common diseases

Albinism refers to a group of inherited recessive autosomal genetic diseases characterized by a reduction or abrogation of melanogenesis in the skin and eyes (oculocutaneous albinism, OCA) or specifically in ocular structures including the RPE (ocular albinism, OA) (Dessinioti et al., 2009). There are currently seven known types of OCA, each associated with genes that regulate pigment synthesis. The two most common forms of OCA are OCA1 and OCA2, which respectively are caused by mutations in tyrosinase (Tomita, 1989) and the P (pink) protein, which is involved in in the transport and stabilization of tyrosinase (Orlow and Brilliant, 1999; Toyofuku et al., 2002). Albinism is associated with ocular defects that include nystagmus, foveal hypoplasia, and low acuity (Levin and Stroh, 2011). Hypopigmentation is also present in more severe syndromic diseases, such as Chediak-Higashi Syndrome and Hermansky-Pudlak. These diseases are caused by mutations in genes that regulate the formation of lysosomal related organelles and result in systemic phenotypes beyond albinism (Sitaram and Marks, 2012). Chediak-Higashi syndrome is characterized by the formation of giant intracellular granules, bleeding diasthesis and defects in immune system function, and is usually lethal during infancy. Hermansky-Pudlak syndrome is associated with classic features of albinism as well as defective platelet formation, bleeding diasthesis and pulmonary fibrosis (Huizing et al., 2008).

Age-related macular degeneration (AMD) is one of the leading causes of blindness worldwide, and is the leading cause of blindness in industrialized countries (Klein et al., 2011; Resnikoff, 2008; Wong et al., 2014). AMD is characterized by the

degeneration of the macula. The macula is a pigmented region within the central primate retina that contains the fovea. The fovea lies near the center of the macula, has no overlying inner retinal cell layers, and provides high-acuity vision. The most common form of AMD is geographic atrophy, or "Dry AMD," which is characterized by the degeneration of RPE cells in the macula, which leads to loss of the closely-apposed photoreceptors and loss of central field vision (Curcio et al., 1996; Lim et al., 2012a). A less-common, but more acute, variant of AMD is exudative, or "Wet AMD," is characterized by the invasion and exudative neovascularization of the choriocapillaris into the subretinal space (Lim et al., 2012a). Although peripheral vision is usually maintained in patients, since photoreceptors throughout the rest of the retina are unaffected, this blindness is still acutely debilitating. Onset of geographic AMD is most commonly scored by the appearance of Drusen, which form as membrane-rich deposits between the RPE and BM. These Drusen are primarily made of up of lipofuscin, a yellowish aggregation of photodamaged lipids and proteins which derive from phagocytosed photoreceptor material that the RPE cell was unable to effectively metabolize (Crabb et al., 2002; Mazzitello et al., 2009). The underlying causes of AMD are unclear, and controversy exists whether the disease is caused by pathology in photoreceptors, the RPE, the choroid, an autoimmune response, or whether multiple discrete diseases converge to cause AMD. Currently, the most well-accepted theory holds that AMD results from chronic inflammation, likely from accumulated oxidative stress from photoreceptors (Gnanaguru et al., 2016; Parmeggiani et al., 2012).

1.2.2: Current therapies for treating Retinal Pigment Epithelial degeneration

In most cases of albinism, symptoms are manageable with effective palliative care, such as protecting unpigmented skin from overexposure to the sun or using

corrective lenses to mitigate low visual acuity or nystagmus (Levin and Stroh, 2011). Since albinism is primarily a genetic disease, current research focuses either on gene therapy or pharmaceutical strategies to stimulate pigmentation, with the ultimate goal to rescue pigmentation during development to prevent developmentally related hypopigmentation. To this end, researchers are focusing on two routes: gene therapy to replace defective melanogenic machinery (Gargiulo et al., 2009; Surace et al., 2005) and pharmaceutical augmentation of melanin synthesis (Onojafe et al., 2011), although this work is still in its early stages.

The current standard of care for treating dry AMD relies upon early detection followed by administration of vitamin supplements to slow disease progression (Chew et al., 2012). Injection of VEGF inhibitors has proven to be an effective therapy controlling most forms of wet AMD, though this treatment relies upon routine and intrusive vitreal injections (Rofagha et al., 2013; Wykoff et al., 2014). No treatments currently exist that can replace RPE cells once they are lost, however one intriguing new study provides evidence that high doses of statins to treat Drusen halts progression and, in some rare cases, leads to the regression of drusenoid deposits (Vavvas et al., 2016). After initial failures (Binder et al., 2007), recent advances in stem cell technology have enabled researchers to differentiate RPE in vitro and begin experimenting with its implantation (Blenkinsop et al., 2013; Gamm et al., 2008; Haruta, 2004; Hu and Bok, 2001; Idelson et al., 2009; Krohne et al., 2012; Maminishkis et al., 2006; Zhu et al., 2013). Positive results in animal models, coupled with reports that stem cell-derived RPE implantation in primates does not elicit a damaging immune response (Schwartz et al., 2012) have led to multiple clinical trials examining the efficacy of transplants in humans. Indeed, physicians in Korea (Shim et al., 2017) and Japan (Kamao et al., 2017) have reported the

successful transplantation of hESC-derived RPE cells into dry AMD patients with no ill effects, and are currently moving toward expanding clinical trials.

1.2.3: Endogenous repair

Although researchers have long noted a limited endogenous capacity for repair of the RPE in mammals, little is known about the genetic mechanisms underlying the process by which RPE cells respond to and repair damage. A deeper understanding of these mechanisms is integral for developing therapies aimed at reversing RPE damage that occurs in diseases like AMD, and to facilitate a better understanding of the molecular underpinnings of stem-cell derived RPE formation and transplantation/integration into damaged tissue.

Studies in mammals indicate that the RPE fails to regenerate a functional monolayer following widespread damage. Photic maculopathy studies in rhesus monkeys noted that the RPE proliferated to form multilaminar structures post-injury (Tso, 1973). While multilaminar structures were capable of limited function, a fully functional RPE never formed, and the reasons for this are unknown. Similar results have been observed in penetrating trauma and retinal detachment paradigms (Cleary and Ryan, 1979a, 1979b; Machemer and Laqua, 1975). In these cases, the RPE response involves overproliferation, formation of multilaminar structures and RPE migration into the subretinal space, behaviors indicative of a potentially misregulated repair mechanism. Overproliferation of RPE is also a hallmark of proliferative vitreoretinopathy (PVR), a condition resulting from rhegmatagenous retinal detachment (Hiscott et al., 1999; Machemer et al., 1978; Weingeist et al., 1982). Although mammals fail to repair large injuries, they can regenerate functional RPE following small lesions. For example, the mammalian RPE is capable of generating new RPE following debridement, but newly-

formed RPE displays hypopigmentation and hyperplasia (Lopez 1995), or degradation of the choriocapillaris (Priore et al., 1995), which could result from overproliferation of RPE cells. Other studies using selective photocoagulation found that the RPE regained function within weeks (Negi and Marmor, 1984; Roider et al., 1992). Some noted a proliferative response surrounding the lesion, and it was presumed that daughter cells from these proliferative events migrated into the injury to effect regeneration. In earlier studies targeting damage to the RPE, researchers injected sodium iodate into rabbits to damage RPE in a patchy, but RPE-wide manner (Murray, 1953; Nilsson et al., 1977). Follow-up studies noted a slow electrophysiological recovery of RPE (Mizota and Adachi-Usami, 1997), which could either be the result of proliferating RPE cells, or that retinal glial cells replaced damaged tissue (Machalińska et al., 2013). One theory explaining the disparity between these findings is that the extent of RPE damage informs the nature of the response (Grierson et al., 1994), suggesting a model in which RPE cells are able to expand their size to fill in small lesions, but proliferate in response to large lesions. To date, the only study to use genetic ablation of RPE as an injury model expressed diphtheria toxin in the mouse RPE and assayed the effects on RPE recovery and function (Longbottom et al., 2009). Results showed that undamaged RPE expanded to encompass the area vacated by ablated cells; however, the expanded RPE was insufficient to support normal retinal function, and the authors hypothesized that the expanded cells were unable to meet the metabolic needs of an increased number of photoreceptors.

In contrast to mammals, the RPE in other vertebrates has higher regenerative capacity. In newt (Lopashov 1964, Haynes 2004) and embryonic chick (Luz-Madrigal et al., 2014; Spence et al., 2004, 2007), RPE cells are capable of regeneration and also of transdifferentiating and regenerating the entire neural retina after traumatic injury.

Studies in *Xenopus* revealed that a subpopulation of RPE cells delaminate from the Bruch's Membrane, and, in a process reminiscient of PVR, migrate to the retinal vascular membrane where they transdifferentiate and regenerate the neural retina (Yoshii et al., 2007). The newt RPE does not dissociate from Bruch's Membrane, but rather forms a bilayer reminiscent of an optic cup, with the retinal-facing layer proliferating to reform an intact retina as the BM-adherent layer regenerates the RPE (Chiba, 2014; Chiba et al., 2006; Susaki and Chiba, 2007). In both species, these processes seem to be dependent upon FGF signaling via the MEK-ERK pathways (Casco-Robles et al., 2016; Susaki and Chiba, 2007). Recently, a subpopulation of quiescent human RPE cells, termed RPE stem cells, was identified that can be induced to proliferate in vitro and to differentiate into either RPE or mesenchymal fates (Salero et al., 2012; Stern and Temple, 2015). The authors hypothesize that these RPE stem cells exist in vivo, and could potentially be harnessed for RPE regeneration. These findings are intriguing, particularly because they suggest that a population of human RPE cells might be capable of becoming induced to produce new RPE. However, the reason these cells are not able to trigger regeneration after injury is unknown.

As detailed above, many groups are exploring the implantation of RPE stem cells into diseased retina to reverse RPE degeneration. The majority of early research supporting these efforts focused on the Royal College of Surgeons rat model which lacks a critical enzyme for photoreceptor outer segment phagocytosis, leading to RPE/photoreceptor degeneration (Cruz et al., 2000). In a proof-of-concept study, healthy RPE transplanted into Royal College of Surgeons rats was able to attach to the retina and phagocytose POS (Jiang and Hamasaki, 1994; Lopez et al., 1989). Embryonic stem cells from mouse (Davis et al., 2016), human (Aoki et al., 2006; Little et al., 1998; Meyer et al., 2006) and primate (Haruta, 2004) sources, as well as iPSCs (Carr et al., 2009), have

been shown to restore some visual function in rat and murine models. Although these results provide support for the possible efficacy of RPE transplantation, there are caveats in their interpretation. In addition to the fact that rats lack a macula, completely unrelated cell populations such as Schwann cells rescue photoreceptor function upon transplantation (Lawrence et al., 2000; Pinilla et al., 2009), indicating that there may be confounding factors that cloud conclusions from these studies. In mouse experiments, researchers were able to chemically ablate RPE with sodium iodate, and transplanted hESC-derived RPE cells formed functional monolayers (Carido et al., 2014).

Although researchers have begun unraveling the signals required to differentiate RPE from stem cells, and have discovered a possible source of endogenous RPE stem cells, virtually nothing is known regarding the mechanisms by which RPE cells regenerate a functional monolayer, nor is it understood why mammalian systems possess only a modest ability to regenerate damaged RPE.

1.3: Zebrafish as a Model for Treating Blinding Disease

Research in this dissertation utilizes zebrafish to study RPE development and regeneration. Zebrafish represent an ideal tool for several key reasons. The development, structure and function of the retina and RPE are similar to human. Indeed, unlike rodents, which lack a cone-rich region analogous to the human macula, the zebrafish retina is cone-dense (Raymond et al., 1995) and therefore more analogous to the human macula. There is also a wealth of genetic tools available to aid in the interrogation of developmental and regenerative pathways in zebrafish. Most importantly, they possess a robust ability to regenerate damaged neural tissue, most notably the retina (Goldman, 2014), brain (Kizil et al., 2012), and spine (Becker et al., 1997). During retinal regeneration, two populations of adult stem cells contribute to the regenerative response.

The primary source of regenerated cells derive from Müller Glia, which respond by dedifferentiating, proliferating and giving rise to neuronal progenitor cells which migrate to the injury site and differentiate to regenerate lost tissue (Fausett and Goldman, 2006; Thummel et al., 2009). The zebrafish eye also contains a specialized population of adult stem cells in the eye periphery called the Ciliary Marginal Zone, which generates new retinal neurons throughout the life of the animal (Raymond et al., 2006), and contributes to the regenerative response in the periphery. In contrast, nothing is known about the response of the zebrafish RPE after widespread ablation.

In the first Chapter, a novel toolkit was generated which will aid the zebrafish community in investigation of eye development. The second Chapter characterizes a novel zebrafish model of oculocutaneous albinism and establishes a role for N-ethyl maleimide-sensitive factor B in melanosomal maturation. Finally, Chapter 3 establishes a novel zebrafish model of AMD, demonstrates that the zebrafish RPE is capable of regenerating an acute widespread injury, and characterizes the regenerative response. These results enable the identification of the genetic underpinnings of RPE regeneration, and will supplement the development of therapies to treat RPE degeneration.

Chapter 2: Generation and Validation of a GAL4-Inducible Toolkit for the *In Vivo* Modulation of Rho GTPase Activity in Zebrafish

Portions of this chapter are modified with permission from the authors. Hanovice, N.J., McMains, E., Gross, J.M., 2016. A GAL4-inducible transgenic toolkit for the in vivo modulation of Rho GTPase activity in zebrafish. Dev. Dyn. 844–853. JMG, NJH and EM concieved experiments and interpreted data. NJH and EM performed experiments and collected data.

2.1: INTRODUCTION:

Rho GTPases, a subfamily of Ras GTPases, are small monomeric G-proteins that play key roles in a myriad of cellular processes, including cell cycle progression, cytoskeletal dynamics, cellular polarity, and membrane trafficking (Etienne-Manneville and Hall, 2002; Takai et al., 2001). Rho GTPase activity depends upon a binary molecular switch: when bound to GTP, Rho GTPases are active, when bound to GDP, they are inactive. This switch is tightly regulated within the cell (Boguski and McCormick, 1993; Jaffe and Hall, 2005), as Rho proteins regulate numerous downstream processes through their interactions with a diverse array of effector proteins. Most studies of Rho GTPases have focused on the Rho subfamily proteins: Cdc42, Rac1 and RhoA. Cdc42 was first discovered in *Saccharomyces cerevisiae* as a protein required for proper cell polarity during budding (Adams et al., 1990). Since its discovery, Cdc42 has been shown to regulate membrane trafficking, actin filament polymerization to form filopodia, and numerous other cellular processes (Erickson and Cerione, 2001). Rac1 stimulates the assembly of lammellipodia and mediates the formation of cell adhesion structures (Bosco et al., 2009; Ridley et al., 1992). RhoA activity leads to the formation of actin stress

fibers (Hall, 1998), maturation of focal adhesions (Luo, 2002) and contraction of the cytokinesis furrow (Lai et al., 2005; Piekny et al., 2005). All three proteins are required for cell cycle progression (Olson et al., 1995). Rho GTPases are also involved in diverse developmental and pathological processes, including axon pathfinding (Bashaw and Klein, 2010; Jin et al., 2005), cell migration (Kardash et al., 2010; Raftopoulou and Hall, 2004), and oncogenesis (Ellenbroek and Collard, 2007; Sahai and Marshall, 2002).

However, these analyses have predominantly utilized cell culture or *in vitro* methods, limiting insight into how Rho GTPases function *in vivo*. Indeed, *in vivo* investigations of the molecular functions of Rho GTPases during animal development have been relatively rare, owing to the need for tissue specific approaches to manipulate their activity. For example, knockout of Cdc42 (Chen et al., 2000) or Rac1 (Sugihara et al., 1998) in mice results in severe pleiotropic defects and early embryonic lethality. Analysis of Rho GTPase activity and function *in vivo* therefore requires experimental approaches that allow modulation of activity in specific tissues or cell populations, and at specific time points (e.g. Chew et al., 2014; Govek et al., 2005; Heasman and Ridley, 2008; Heynen et al., 2013; Jackson et al., 2011; Luo et al., 1996; Ruchhoeft and Ohnuma, 1999; Wong and Faulkner-Jones, 2000; Xiang and Vanhoutte, 2011).

Zebrafish provide an excellent model for investigation of the molecular function of vertebrate Rho GTPases *in vivo* (Kardash et al., 2010; Lai et al., 2005; Salas-Vidal et al., 2005; Zhu et al., 2006). Previous studies of Rho GTPase function in developing zebrafish employed microinjection of mRNA to drive global overexpression of wild-type, constitutively active or dominant negative versions (Hsu et al., 2012; Xu et al., 2014; Yeh

et al., 2011; Zhu et al., 2008, 2006), or morpholino oligos for transient disruption of Rho GTPase expression (Hsu et al., 2012; Srinivas et al., 2007). Due to the central role of Rho GTPases in early embryogenesis, approaches that modulate global Rho GTPase activity must focus on events occurring very early during zebrafish development, and thus, have not been effective in analyzing the functions of these proteins during later developmental events. Following the development of highly efficient transgenesis techniques in zebrafish (Kwan et al., 2007), transgenic lines have been generated in which the expression of constitutively active and dominant negative versions of different Rho GTPase family members are driven by cell-type-specific promoters (Chew et al., 2014; Choe et al., 2013; Jung and Leem, 2013). Although these tools restrict Rho GTPase construct expression to specific cell and tissue types and, dependent on the promoter, allow functional investigations at later stages in development, systematic comparisons of functional roles of different Rho GTPase members in different tissues is limited to a small number of extant cell-type-specific promoter Rho GTPase transgenic lines (Chew et al., 2014; Choe et al., 2013; Jung and Leem, 2013). Moreover, this strategy necessitates the generation and validation of a new line for each desired promoter and/or Rho GTPase combination, an inefficient and time-consuming approach. The GAL4/UAS system is a powerful transgenic system for enabling the temporal-spatial control of transgene expression (Brand and Perrimon, 1993; Fischer et al., 1988; Ornitz et al., 1991; Scheer, 1999). In this system, a promoter fragment drives expression of the yeast transcription factor GAL4. GAL4 then binds an upstream activating sequence (UAS) to drive transgene expression. Gal4/UAS is widely used in zebrafish, and there are now

hundreds of published GAL4 drivers and UAS constructs listed on www.zfin.org. The strength of this system lies in its flexibility: a single GAL4 transgene can be used to drive expression of multiple UAS constructs, enabling researchers to express multiple transgenes within a defined cellular or tissue context.

Taking advantage of this approach, we have created a versatile transgenic toolkit that enables spatial and temporal modulation of Rho GTPase activity in zebrafish. In this Chapter, we generated and validated ten GAL4-inducible transgenic lines that express dominant negative, constitutively active, and wild type versions of Cdc42, RhoA, and Rac1, as well as a fluorescent protein marker to highlight expressing cells. We have confirmed GAL4-specific expression of these transgenes, and have demonstrated transgene functionality by reporting reproducible lens phenotypes in induced embryos. These lines now enable systematic tissue-specific investigation of the molecular function of Rho GTPases *in vivo*.

2.2: RESULTS:

2.2.1: Generation of GAL4-Inducible Rho GTPase Transgenics

To generate transgenic lines for GAL4-driven expression of Rho GTPases, we first designed and assembled transgenic constructs encoding wild-type (WT), dominant negative (DN) and constitutively active (CA) human Cdc42, RhoA, and Rac1 (Figure 2.1). An additional DN cdc42 was generated using *Xenopus* $Cdc42^{F37A}$ which has recently been utilized *in vivo* (Kieserman and Wallingford, 2009) and is 98% identical to human

Cdc42. We selected the 10X UAS element (Kwan et al., 2007) for our constructs due to this promoter's strong, GAL4-specific expression (Gabriel et al., 2012; Kwan et al., 2007). Although recent research has raised concern over multigenerational silencing of the repeat-heavy UAS element (Akitake et al., 2011; Goll et al., 2009), other reports have postulated that silencing may be reduced when UAS lines are maintained separately from GAL4 drivers (Choe et al., 2012). Cdc42 and RhoA constructs were assembled with the monomeric and highly photostable mCherry fluorescent protein (Shaner et al., 2004), while EGFP was chosen as the fluorescent reporter for Rac1 transgenics. A myc-tag was also added to enable detection of each Cdc42 and RhoA isoform, and there is a significant amount of literature reporting the use and effective function of C-terminal tags of Rho GTPases (Choe et al., 2012; Disanza et al., 2006; Hussain et al., 2001; Kim et al., 2008; Kroschewski et al., 1999; Lee et al., 2004; Sakurai-Yageta et al., 2008). Furthermore, our constructs were engineered using cDNAs that have been shown to be expressed and functional (Kieserman and Wallingford, 2009; Nobes and Hall, 1995). Nucleotide sequence encoding the self-cleaving viral peptide F2A was inserted between fluorescent reporters and Rho GTPase cDNA sequences to allow bicistronic expression of the fluorescent protein and the GTPase. Rather than requiring a second ribosomal binding event, as is the case for IRES, F2A peptides lead to two protein products via a ribosomal skipping mechanism (Donnelly and Luke, 2001; Szymczak et al., 2004), and when compared to IRES, F2A leads to more efficient bicistronic expression (Chan et al., 2011; Wang et al., 2011). With this rationale, we created three types of constructs: 10x*uas*:mCherry-F2A-myc-Cdc42^{XX} for the expression of mCherry-F2A and myc-Cdc42,

10x*uas*:EGFP-F2A-Rac1^{XX} to express EGFP-F2A and Rac1, and 10x*uas*:mCherry-F2A-myc-RhoA^{XX}, to express mCherry-F2A and myc-RhoA (Figure 2.1A). In all, we created a total of ten new transgenic constructs as elaborated in Figure 2.1B. All constructs include the *cmlc2:*egfp transgenesis marker to allow easy visualization of the presence of constructs. Germline transmission, scored by the appearance of offspring with ubiquitously GFP-positive hearts, occurred in outcrosses of roughly 25% of injected F0 fish.

A

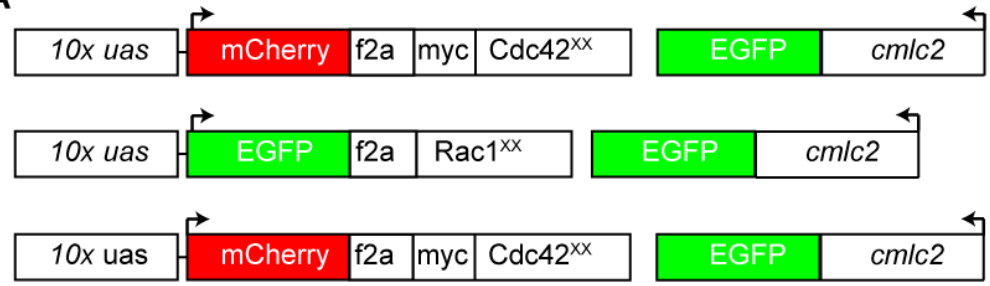

B

Allele	Construct	Mutation	Activity	Species
au66	*uas*:mCherry-F2A-myc-Cdc42^{WT}	———	Normal	Human
au68	*uas*:mCherry-F2A-myc-Cdc42^{CA}	G12V	↑	Human
au67	*uas*:mCherry-F2A-myc-CDC42^{DN} T17N	T17N	↓	Human
au69	*uas*:mCherry-F2A-myc-CDC42^{DN} F37A	F37A	↓	Xenopus
au70	*uas*:EGFP-F2A-Rac1^{WT}	———	Normal	Human
au72	*uas*:EGFP-F2A-Rac1^{CA}	G12V	↑	Human
au71	*uas*:EGFP-F2A-RAC1^{DN}	T17N	↓	Human
au73	*uas*:mCherry-F2A-myc-RhoA^{WT}	———	Normal	Human
au75	*uas*:mCherry-F2A-myc-RhoA^{CA}	Q63L	↑	Human
au74	*uas*:mCherry-F2A-myc-RhoA^{DN}	T19N	↓	Human

Figure 2.1: Overview of transgenic constructs. (A) myc-tagged Cdc42 and RhoA constructs are placed downstream of mCherry and the self-cleaving viral peptide f2a, enabling their bicistronic expression following activation of the 10xuas promoter. 10xuas activation leads to the bicistronic expression of egfp-f2a and Rac1. Each construct includes cmlc2:egfp oriented in reverse orientation (B) Chart detailing each specific isoform of Rho GTPase, with its predicted activity and species of origin.

To determine the spatial expression of F1 alleles while minimizing the potential for severe phenotypes arising from early induction, we crossed F0 adults with *hsp70l:gal4* zebrafish, globally heat shocked all transgenic embryos at ~54 hours post fertilization (hpf), and imaged reporter expression at 72hpf. Each line displayed robust and ubiquitous transgene expression following global heat shock (*data not shown*). No leakiness of transgene expression was observed before heat shock. PCR genotyping confirmed that fluorescent marker-positive embryos were also GAL4-positive and non-fluorescent embryos were GAL4-negative (*data not shown*), indicating that UAS-driven transgene expression was restricted to fish expressing GAL4 and that there was no observable leaky activation of the UAS promoter.

2.2.1: Validation of Transgene Expression and GAL4 Sensitivity

Non-equimolar expression of the second cistron following F2A ribosomal skipping has been reported (Chan et al., 2011). Because Rho GTPase function is dependent upon prenylation at the C-terminus, Rho GTPase sequence could not be placed upstream of the F2A element, as that would have resulted in the C-terminal fusion of the F2A peptide and the disruption of protein trafficking. Thus, to confirm that Gal4-mediated transgene induction results in expression of both the Rho GTPase and reporter proteins, we performed Western blot analyses of heat shocked F1 embryos of Cdc42 and RhoA constructs (Figure 2.2). GAL4-induced embryos displayed high levels of myc-tagged protein while no myc-tagged protein was observed in GAL4-negative embryos. This confirms that the F2A peptide is functioning properly by enabling bicistronic

expression of mCherry and myc-tagged Rho GTPase protein, both of which are only inducible by GAL4. Western blot analysis of heat shocked F1 embryos of Rac1 constructs using human Rac1 antibody showed strong Rac1 staining in both GFP^+ and GFP^- siblings, indicating that the Rac1 antibody also detects endogenous Rac1, an unsurprising result considering that human Rac1 protein sequence is 93% identical to zebrafish (data not shown).

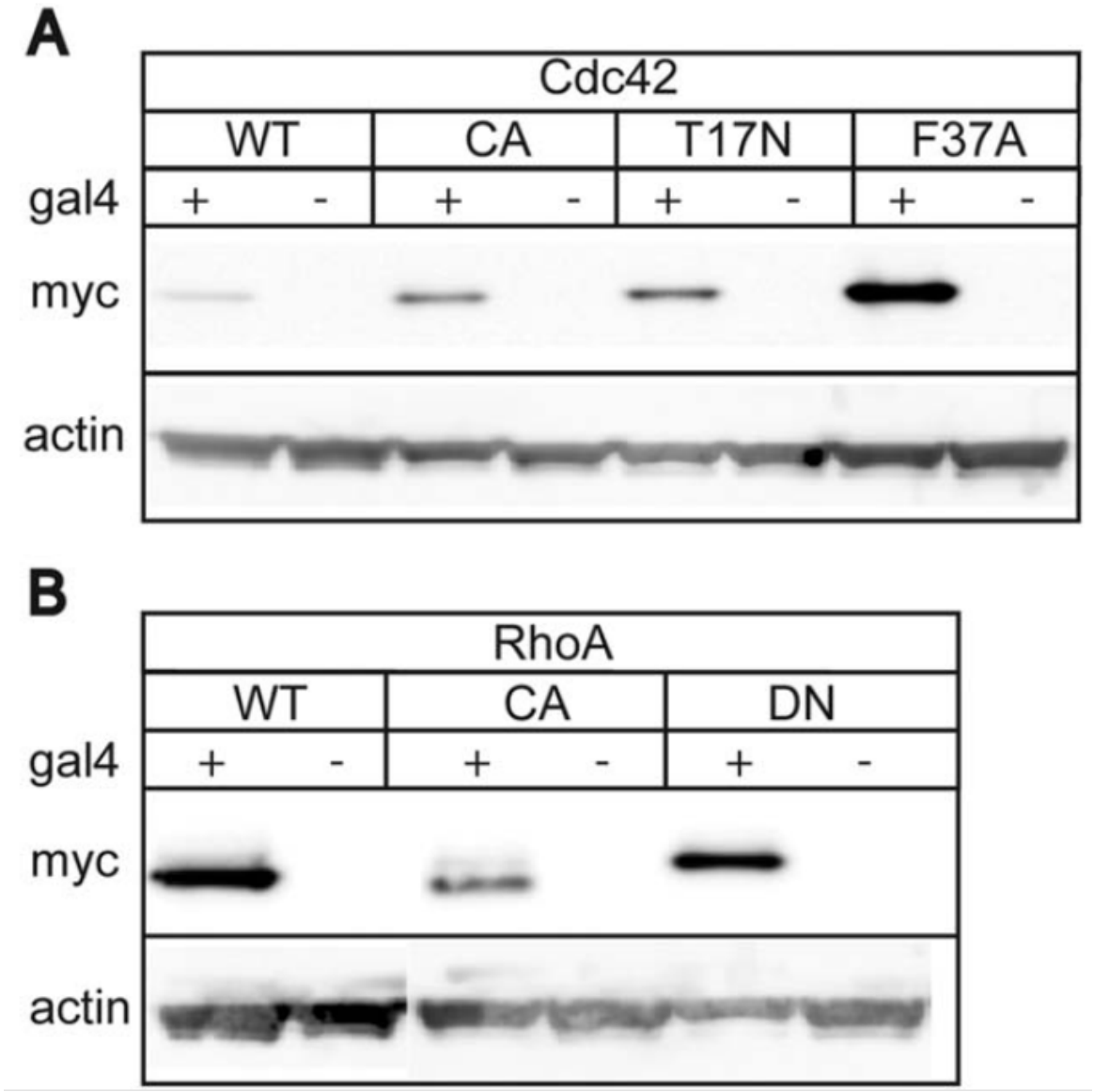

Figure 2.2: Induced embryos express myc-tagged protein. (A) Western blot analysis of myc-tagged cdc42 and β-actin in hsp70l:gal4-positive and negative Cdc42 transgenic embryos. Myc-labeled protein at the expected size of Cdc42 appears only in gal4-induced embryos. (B)Western blot analysis of myc-tagged RhoA and β-actin for each RhoA transgenic shows the presence of myc-RhoA only in gal4-induced embryos.

To confirm that the transgenes are spatially and temporally responsive to GAL4, F0 *uas:*mcherry-f2a-cdc42^{WT} transgenics were crossed to *pou4f3*:gal4, which express GAL4 in a subset (<20%) of retinal ganglion cells (RGCs), (Xiao and Baier, 2007a). To determine if Cdc42 expression is confined to RGCs in the retina, we cryosectioned 4dpf transgenic embryos and imaged the retina for mCherry fluorescence (Figure 2.3). mCherry fluorescence is confined to the RGC layer in a pattern consistent with previous studies utilizing the *pou4f3*:gal4 driver (Xiao et al., 2005), indicating our construct expression is restricted to RGCs, and that our transgenic constructs are amenable to cell-specific expression. To determine if cells expressing mCherry also express myc-Rho GTPase, we immunostained for myc in *uas:*mCherry-f2a-myc-Cdc42^{WT} embryos both with and without the *hsp70l:*gal4 transgene. Following heat shock, immunostaining reveals strong induction of both mCherry and myc throughout the retina (Figure 2.4A), which is entirely absent in mCherry-negative siblings (Figure 2.4B). Next, we crossed *uas*:GFP-f2a-Rac1^{WT} to *ptf1a:*gal4, a driver expressing GAL4 in amacrine cells and horizontal cells (Parsons et al., 2009), and stained retinal sections for human Rac1 (Penzes et al., 2000). Rac1 staining was detected throughout the retina, further supporting our hypothesis that this antibody detects endogenous Rac1. However, there does appear to be a higher degree of Rac1 signal in GFP-positive cells (Figure 2.4C), supporting *ptf1a:*gal4-driven cell specific induction of the construct. Similarly, immunostaining of *hsp70l:*GAL4*;UAS*:mCherry-f2a-RhoA^{WT} showed mCherry and myc colocalization only in mCherry-expressing cells (Figure 2.4D,E).

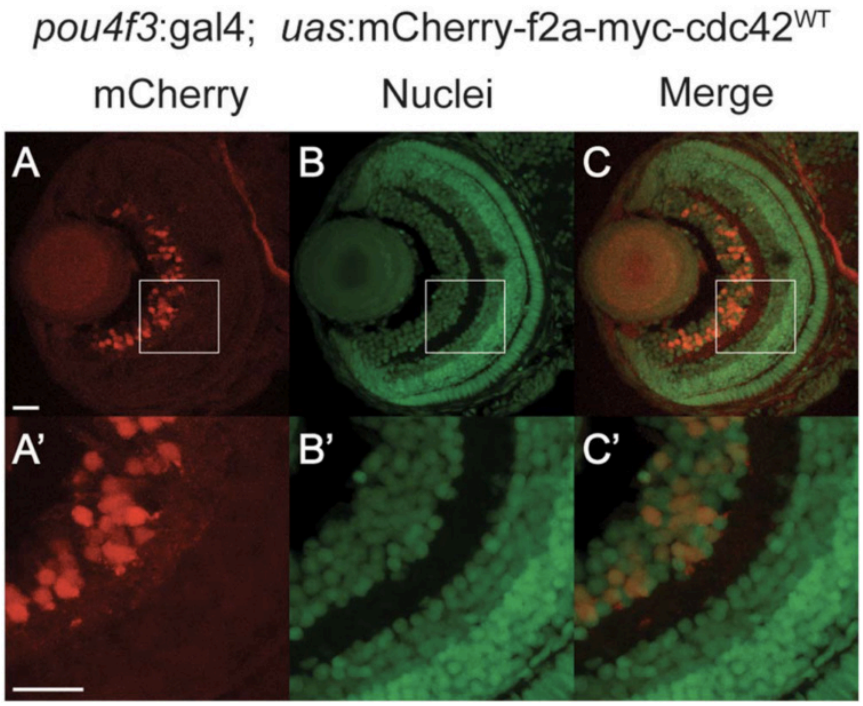

Figure 2.3: Tissue-specific control of transgene expression. Driven by *pou4f3*:gal4, mCherry (A,A') is specifically expressed in the RGC layer (B,B') of 4dpf *pou4f3:*gal4*;uas*:mcherry-f2a-cdc42^{WT} embryos. (A'-C') are magnified images taken from the boxed regions in (A-C). Scale bars=20μm.

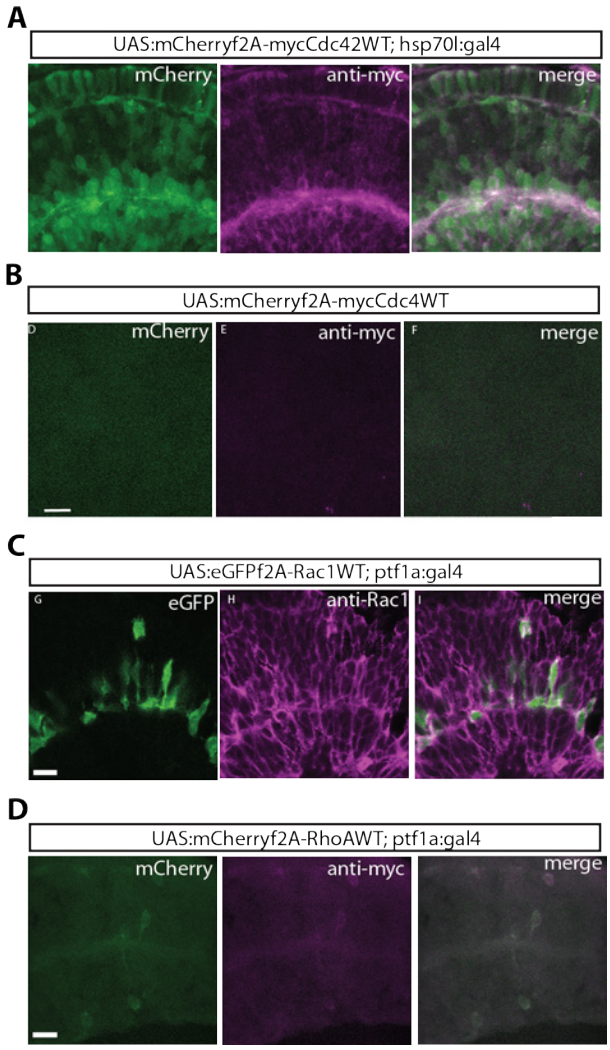

Figure 2.4: Antibody validation of transgene expression. (A) myc colocalization with mCherry expression in heat-shocked *hsp70l*:gal4*;uas:*mCherry-F2A-myc-Cdc42^{WT} embryos. (B) No signal for mCherry or myc was detected in *uas:*mCherry-F2A-myc-Cdc42^{WT} transgenics missing the *hsp70l*:gal4 transgene. (C) Rac1 antibody staining in *ptf1a*:gal4*;uas*:gfp-f2a-Rac1^{WT} embryos. (D) myc colocalization with mCherry expression in heat-shocked *hsp70l*:gal4*;uas*:mCherry-F2A-myc-RhoA^{WT} retinae. (D) No signal for mCherry or myc was detected in *uas*:mCherry-F2A-myc-RhoA^{WT} transgenics missing the *hsp70l:*gal4 transgene. Scale bar = 10μm.

Finally, we sought to validate transgene function by determining whether transgene expression leads to distinct morphological phenotypes. The majority of transgenics heat shocked at 3dpf did not display an overt phenotype by ~18 hours post heat shock, with two notable exceptions: induced $Cdc42^{CA}$ and $RhoA^{CA}$ embryos displayed widespread tissue disorganization and cardiac defects (*data not shown*). Such phenotypes are not surprising, as RhoA is required for cardiac development in chick (Kaarbø et al., 2003), and has been shown to be critical for proper heart morphogenesis and contractile function (Phillips et al., 2005; Sah et al., 1999), while cdc42 regulates sarcomere assembly during cardiomyocyte development (Nagai et al., 2003). Because heat shock in these cases occurred late during embryonic development, we reasoned that heat shocking embryos earlier during development will likely lead to more pronounced phenotypes. Therefore, we heat shocked F1 transgenics outcrossed to *hsp70l:GAL4,* at ~26hpf. At 50hpf, embryos were examined for overt embryonic phenotypes and transgene expression, and then were fixed, sectioned and stained for F-actin and DAPI to examine the structure of the eye. (Figures 2.5-7).

While no overt phenotype was detected in $Cdc42^{WT}$ embryos, the lens epithelium was thicker and lens fibers appeared mildly disorganized (Figure 2.5A). $Cdc42^{CA}$-expressing embryos displayed heart defects and edema, and they were microphthalmic. Cryosectioning revealed severe lens fiber disorganization (Fig. 2.5B). Despite the lack of gross morphological defects in embryos expressing either of the $Cdc42^{DN}$ isoforms, cryosections revealed severe lens fiber disorganization in both (Fig. 2.5C,D). Rac^{WT}-expressing embryos were microphthalmic but lens formation appeared largely normal

(Figure 2.6A). Rac^{CA}-expressing embryos displayed obvious morphological defects, including microphthalmia and cardiac edema, and severe disruption of lens fiber organization (Figure 2.6B). Rac^{DN}-expressing embryos display lower levels of cardiac edema, but sections revealed notable lens fiber disorganization (Figure 2.6C). Finally, overexpression of $RhoA^{WT}$ resulted in mild lens fiber disorganization (Figure 2.7A). Rho^{CA}-expressing embryos were microphthalmic and possessed heart defects, mild cardiac edema and severe lens fiber disorganization (Figure 2.7B). Embryos expressing Rho^{DN} were also microphthalmic and lens fibers were disorganized (Figure 2.7C).

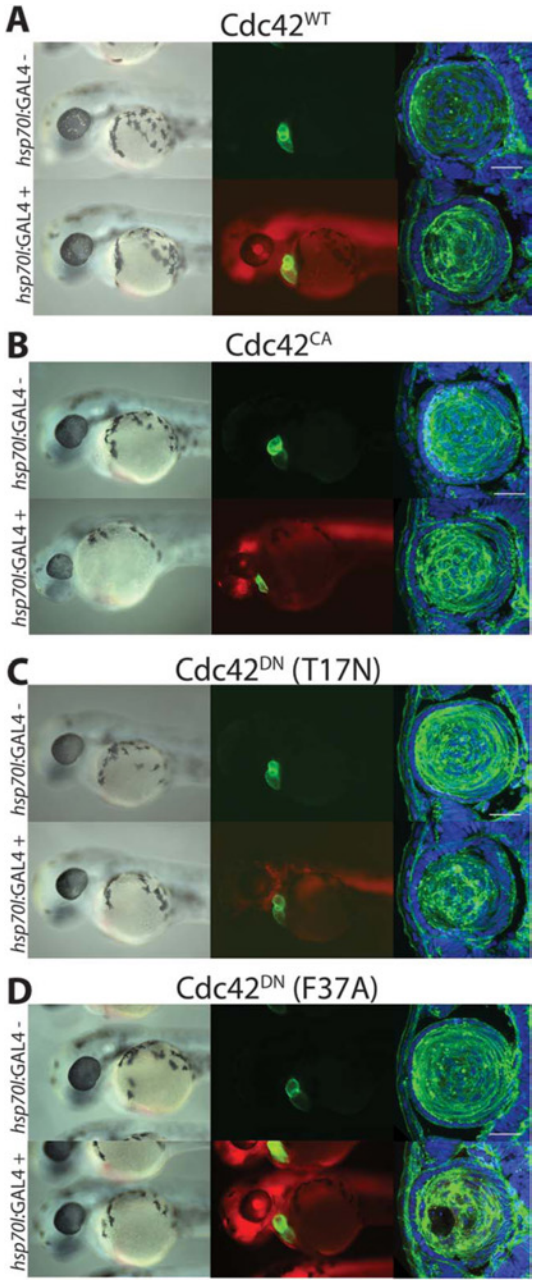

Figure 2.5: Construct expression and phenotypes of GAL4-positive and negative embryos of Cdc42 transgenics. Transgenic F1s were outcrossed to *hsp70l:gal4* zebrafish, and *cmlc2:*egfp^{+} embryos were heat shocked at ~26hpf and imaged at ~50hpf. Gross morphology, transgene expression and lens structure of *hsp70l:*gal4-positive and –negative (A) Cdc42^{WT}, (B) Cdc42^{CA} (C) Cdc42^{T17N}, (D) Cdc42^{F37A} embryos.. Scale bar = 25μm.

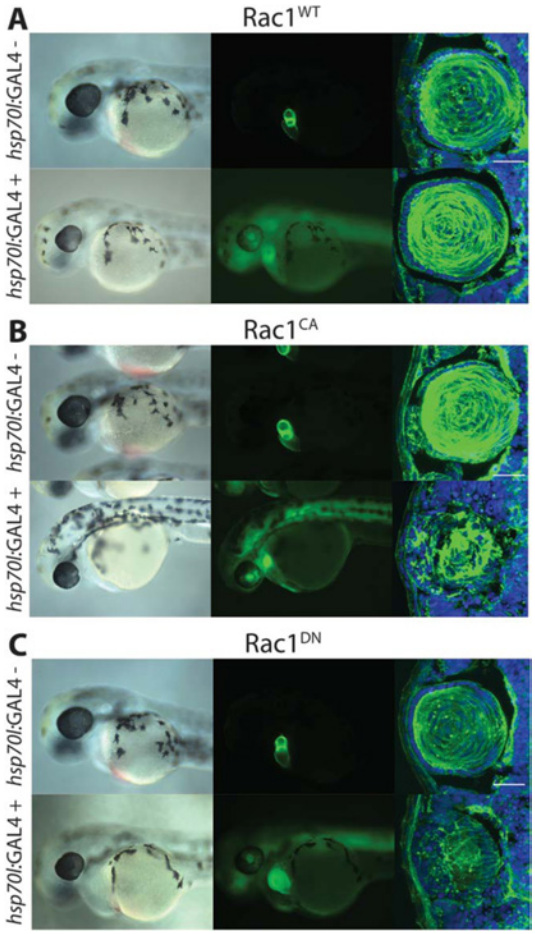

Figure 2.6: Construct expression and phenotypes of GAL4-positive and negative embryos of Rac transgenics. Transgenic F1s were outcrossed to *hsp70l:gal4* zebrafish, and *cmlc2:*egfp^{+} embryos were heat shocked at ~26hpf and imaged at ~50hpf. Gross morphology, transgene expression and lens structure of *hsp70l:*gal4-positive and –negative (A)Rac1^{WT}, (B) Rac1^{CA} (C) Rac1^{DN} embryos. Scale bar = 25µm.

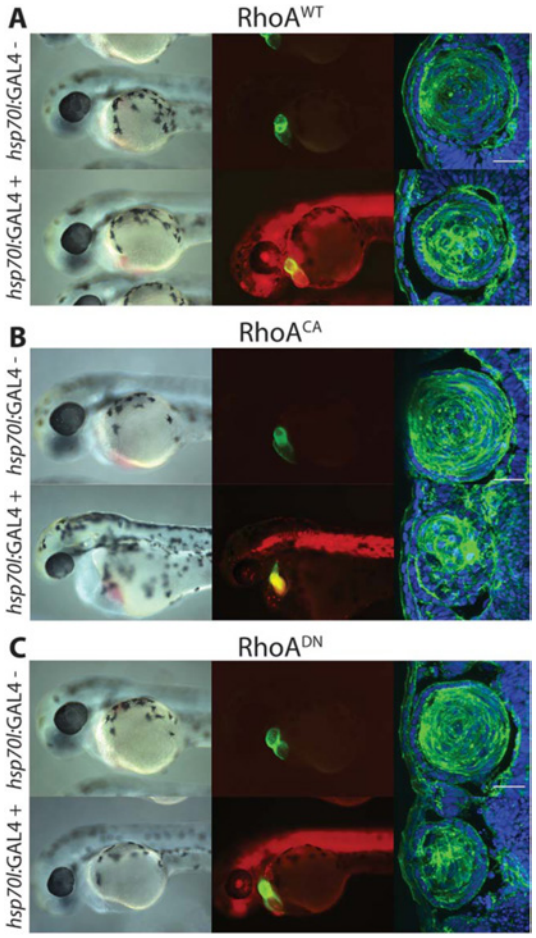

Figure 2.7: Construct expression and phenotypes of GAL4-positive and negative embryos of RhoA transgenics. Transgenic F1s were outcrossed to *hsp70l:gal4* zebrafish, and *cmlc2:*egfp^{+} embryos were heat shocked at ~26hpf and imaged at ~50hpf. Gross morphology, transgene expression and lens structure of *hsp70l:*gal4-positive and –negative (A) RhoA^{WT}, (B) RhoA^{CA} (C) RhoA^{T17N}. Scale bar = 25μm.

2.3: DISCUSSION:

These validated transgenic lines represent a versatile toolkit for the temporal-spatial modulation of Cdc42, RhoA and Rac1 activity. To our knowledge, these are the first UAS-inducible transgenic lines for the bicistronic expression of Rho GTPases and a fluorescent reporter. Furthermore, myc tags on Cdc42 and RhoA allow direct determination of protein expression, and potential experiments assaying the altered cellular localization and behaviors of mutant Rho GTPases. However, due to the requirement of Gal4 induction for construct expression and the inherent time delay therein, these transgenic lines are not optimal for studying Rho GTPase function during early developmental processes; their utility lies in modulating Rho GTPase activity during later development, during time points and in tissues that have been inaccessible using previous approaches.

While expression of all constructs was induced, $Cdc42^{F37A}$ displayed a higher level of expression than the other Cdc42 alleles. One potential explanation for this result is that *Xenopus* $Cdc42^{F37A}$ has greater stability in zebrafish compared to human Cdc42. However, there also appears to be higher expression of mCherry in $Cdc42^{F37A}$ embryos (Figure 2.5, data not shown). Our bicistronic constructs result in the expression of two separate proteins; mCherry should not display any species-dependent enhancement of stability. Tol2 transgenesis often leads to allelic quality differences between founders due to random integration events into the genome; therefore, a more likely explanation is that *uas*:mCherry-f2a-myc-$Cdc42^{F37A}$ is a particularly well-expressed allele due to its genomic location.

Cdc42, Rac1 and RhoA are all expressed in the lens (Chen et al., 2006), and have been implicated to play a critical role during lens formation in several studies. For example, knockout of RhoA and Rac1 in the mouse lens disrupts lens development, and defects include disorganization of the actin cytoskeleton within lens fibers (Maddala et al., 2011, 2004), and Cdc42 is required for lens pit invagination and early lens development (Chauhan et al., 2009; Muccioli et al., 2016). Thus, the lens phenotypes detailed here provide strong evidence that our transgenes express functional Rho GTPase proteins. However, it is important to note that numerous additional experiments must still be performed to definitively establish the role of Rho GTPases in lens and retinal development during these developmental windows, as it is equally plausible that the defects reported here arise indirectly from pleitropic disruption of general embryonic or ocular development following widespread modulation of GTPase function throughout the embryo and thus do not reflect a direct function of these RhoGTPase proteins during lens development.

As detailed in Chapter 1, an incredibly complex series of morphogenic changes occur in which eye progenitor cells must exert exquisite control over their morphology, directional migration and proliferation to ultimately produce a functional eye. Rho GTPases are critical modulators of these processes and therefore these transgenics will enable the future interrogation of the cell and molecular mechanisms underlying eye morphogenesis. For example, these tools will find immediate utility in studying a critical process during optic cup formation: choroid fissure closure (Bibliowicz et al., 2011; Graw, 2003). During optic cup morphogenesis, a transient opening forms in the ventral

surface of the optic cup that must be sealed to properly enclose the retina and RPE within the eye. A critical step in this process is the breakdown of basement membrane on the two opposing surfaces of the optic cup, which enables their fusion (James et al., 2016). These lines will enable the further interrogation of the pathways which regulate this process.

Chapter 3: N-ethylmaleimide-sensitive factor b (nsfb) is required for normal pigmentation of the zebrafish retinal pigment epithelium

Portions of this chapter are modified with permission from the authors. Hanovice, N.J., Daly, C.M.S., Gross, J.M., 2015. *N* -Ethylmaleimide–Sensitive Factor b (nsfb) Is Required for Normal Pigmentation of the Zebrafish Retinal Pigment Epithelium. Investig. Opthalmology Vis. Sci. 56, 7535. NJH, CMD and JMG conceived experiments and interpreted data. NJH and CMD performed experiments and collected data.

3.1: INTRODUCTION:

Albinism is a congenital disorder that affects roughly 1 in 17,000 people worldwide (Gargiulo et al., 2011; Grønskov et al., 2009; Hutton and Spritz, 2008) characterized by a complete or partial deficiency of melanin. Ocular defects associated with albinism include nystagmus, foveal hypoplasia, low acuity and photophobia (Grønskov et al., 2007; Levin and Stroh, 2011). Hypopigmentation can occur in the eyes and skin (oculocutaneous albinism, OCA), eyes only (ocular albinism, OA) or can be accompanied by more severe phenotypes in the relatively rare syndromic forms of albinism, such as Hermansky-Pudlak and Chediak-Higashi Syndromes. In all known forms of albinism, hypopigmentation results from mutations in genes encoding proteins involved in melanin synthesis (melanogenesis) (reviewed in (Grønskov et al., 2007; Sitaram and Marks, 2012)) or in melanosome transport (e.g. Bahadoran et al., 2001; Griscelli et al., 1978).

In the eye, albinism affects the Retinal Pigment Epithelium (RPE), a layer of pigmented cells closely apposed to the photoreceptors at the back of the retina. Proper pigmentation of the RPE is critical for normal retinal development and occurs during a process called melanogenesis, whereby pheomelanin and eumelanin pigments are

synthesized within specialized lysosome-related organelles called melanosomes (Jeffery, 1998). Pigmented melanosomes in the RPE aid the visual system by absorbing stray photons to prevent light scatter and focus light onto the photoreceptors and are also believed to aid in the breakdown of POS in phagosomes (Strauss, 2005). The process of melanogenesis requires the trafficking of melanogenic enzymes and substrates to forming melanosomes, and these drive melanosomal maturation by facilitating pigment synthesis and deposition. Melanosomal maturation occurs through several well defined stages (Abramowitz et al., 1977; Seiji et al., 1963a, 1963b; Turner et al., 1975) (Fig 3.1). In mammals, Stage I premelanosomes, which are still a part of the endocytic pathway, begin maturing by undergoing membrane invaginations to form intralumenal vesicles, and also by developing a proteinaceous fibril meshwork. This meshwork becomes fully formed in Stage II melanosomes. Melanin precursors and enzymes are trafficked to Stage II melanosomes, and melanin aggregates on the surface of the meshwork, generating a Stage III melanosome with characteristic pigmented striations. Melanin aggregation continues until the organelle is completely filled in and becomes a mature Stage IV melanosome. This process is well conserved amongst vertebrates, the only notable difference being that in fish melanin aggregates on the surfaces of intralumenal vesicles instead of on the striated meshwork (Navarro et al., 2008).

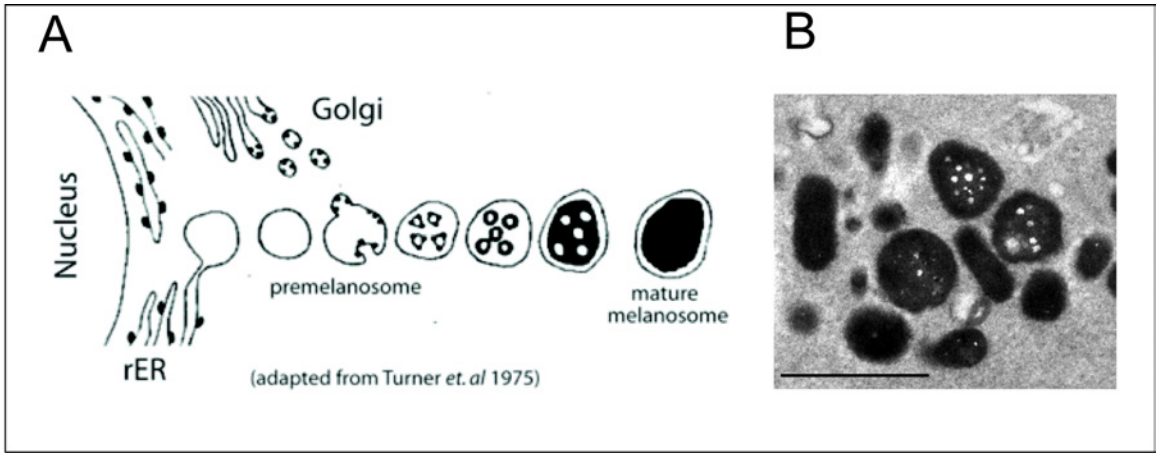

Figure 3.1: Overview of zebrafish melanogenesis. (A) Cartoon depicting the historical model of zebrafish melanosomal maturation based on TEM imagery. As melanosomes mature, melanin aggregates on intraluminal vesicle surfaces and they become progressively filled in. Adapted from Turner *et al,* 1975. (B) Representative TEM image of melanosomes at various stages of maturation. Scale bar = 1μm.

Melanogenesis depends upon proper vesicular targeting and membrane fusion. Indeed, mutations in the genes encoding a number of components of the endocytic pathway result in albinism (Huizing et al., 2008; Sitaram and Marks, 2012). Despite the number of albinism causing mutations identified in human patients and animal models, there remain a significant number of cases for which no mutation has yet been identified, suggesting that our understanding of the proteins involved in melanogenesis may be incomplete. Forward genetic screens in animal model systems can be very useful in this regard by utilizing a high throughout and unbiased screening approach to identify mutations in a process of interest. Highlighting this utility, our laboratory previously reported a forward genetic screen that identified ~20 mutations with defects in eye

development (Lee et al., 2012). Of this collection, two mutants presented with oculocutaneous albinism and in this study, we report the cloning and characterization of these mutations and identify them as mutant alleles affecting the *N-ethylmaleimide-sensitive factor* (*nsfb)* gene.

N-ethylmaleimide-sensitive factor (Nsf) is a critical regulator of membrane fusion. NSF was initially identified in yeast as an enzyme required for protein transport between Golgi stacks (Block et al., 1988; Melançon et al., 1987), and has since been identified as a AAA superfamily (ATPase Associated with various cellular Activities) protein that consists of three domains: two ATPase domains (D1 and D2) and an N-terminal domain (NSF-N) (Nagiec et al., 1995; Tagaya et al., 1993; Whiteheart et al., 1994). NSF protomers form a hexamer, and this constitutes part of the Soluble NSF Attachment Protein (SNAP) complex, which mediates vesicular fusion by disassembling SNARE (SNAP-Receptor) complexes. SNARE complexes form when SNARE proteins on different membranes interact and provide the requisite energy for membrane fusion by forming four-helix bundles and bringing the membranes into close apposition (Jahn and Scheller, 2006). As a part of the SNAP complex, NSF couples hydrolysis of ATP with the disassembly of SNARE complexes following membrane fusion, freeing individual SNARE proteins to participate in future vesicular fusion events (Banerjee et al., 1996; May et al., 2001; Whiteheart et al., 1994). Zebrafish possess two *nsf* genes: *nsfa* and *nsfb* (Kurrasch et al., 2009). *nsfa* is required for myelination of axons (Woods et al., 2006), the secretion of trophic factors during the maturation of hair cell synapses (Mo and Nicolson, 2011) and neuropeptide-dependent visually mediated background adaptation (Kurrasch et

al., 2009). In contrast, very little is known about *nsfb*. In this Chapter, we demonstrate that *nsfb* mutants display hypopigmentation of the RPE resulting from a defect in melanogenesis.

3.2: RESULTS:

3.2.1: *au13* and *au18* mutants display oculocutaneous albinism

au13 and *au18* mutants were isolated from an ENU mutagenesis screen for recessive mutations affecting eye development in zebrafish (Lee et al., 2012). Both *au13* and *au18* mutations are fully penetrant and strikingly similar in phenotype (Figure 3.2). *au13* fails to complement the *au18* mutation (data not shown), suggesting that the mutations affect the same gene. Phenotypically, hypopigmentation is noticeable in mutant embryos by 48hpf (Figure 3.2A,C), and the degree of hypopigmentation varies in severity, with mild and severe mutants present in the same clutch of embryos. Both severity classes are globally hypopigmented; in mild mutants, small areas of the RPE are completely devoid of pigment while others appear largely normal. Meanwhile, RPE in severely affected mutants contains numerous large regions lacking pigmentation. By 72hpf, severely affected mutants begin to display early signs of degeneration, and this includes brain necrosis and a slightly curved body axis.

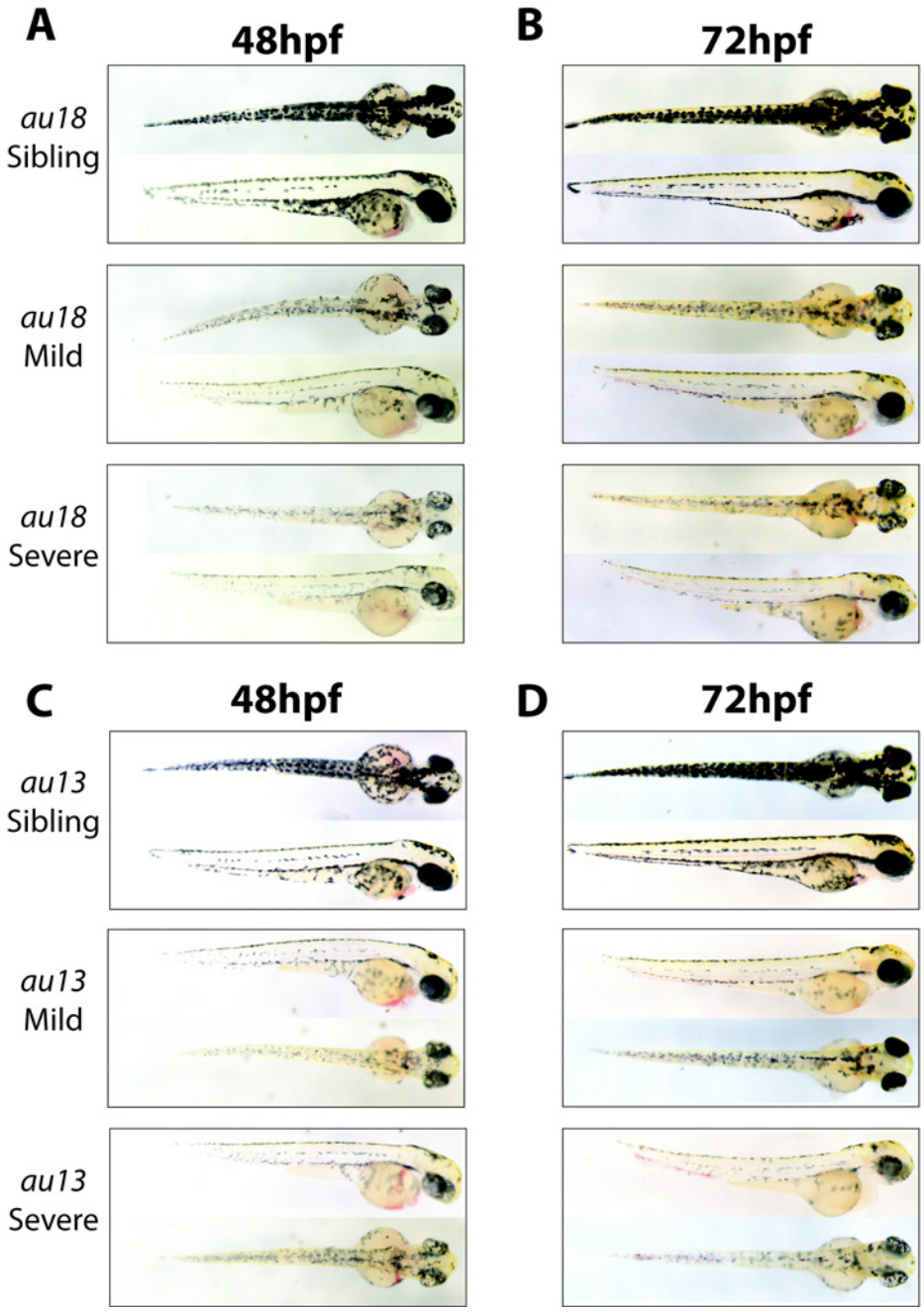

Figure 3.2: *au18* and *au13* mutants are oculocutaneous albinos. (A,B) lateral and dorsal whole embryo images of phenotypically wildtype sibling, mild, and severe *au18* mutants at 48hpf and 72hpf. (C,D) Images of phenotypically wild-type sibling, mild, and severe *au13* mutants at 48hpf and 72hpf. In both lines, severe mutants display large regions devoid of pigment in the RPE.

Given the likely allelic relationship between *au13* and *au18* mutants, and their phenotypic similarity, we focused our efforts on further characterizing the eye phenotype of *au18* mutants at 24, 48, 58, and 72 hpf. *au18* mutant embryos are histologically indistinguishable from WT siblings at 24hpf (Fig 3.3). At 48hpf, *au18* retinae are slightly microphthalmic, and appear to have fewer melanosomes in their RPE when compared to wild-type siblings (Fig. 3.3A-F). This difference in pigmentation becomes more pronounced over time; by 72hpf the mutant RPE contains markedly fewer melanosomes than that of wild-type siblings (Figure 3.3M-R). Beyond RPE hypopigmentation and mild microphthalmia, some of the most severely affected mutants possessed lens defects where the posterior of the lens was epithelialized (Fig. 3.3L,R). All other aspects of eye development appeared to be relatively normal in both mutants.

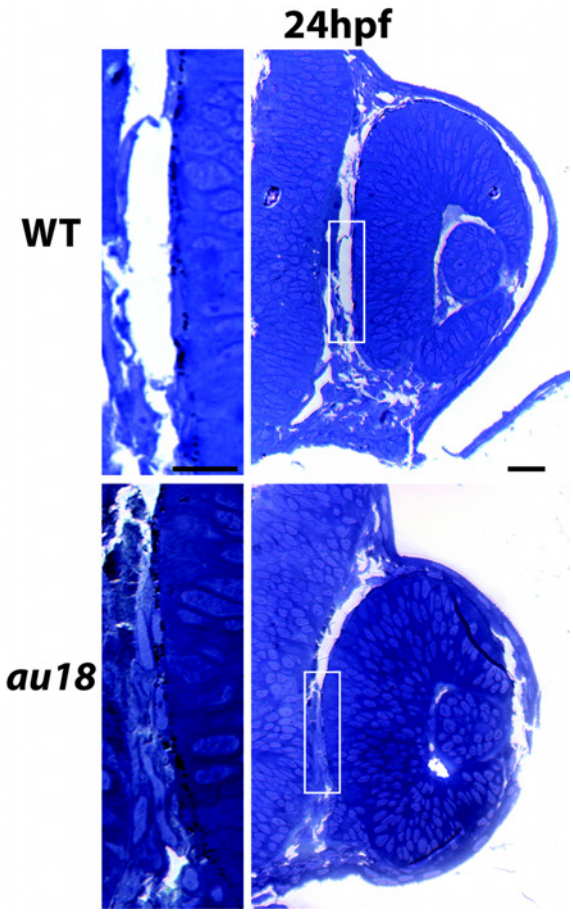

Figure 3.3: *au18* is histologically indistinguishable from sibling at 24hpf. Transverse histological sections of sibling and mutant embryos at 1 dpf reveal that homozygous *nsfb*^{au18} mutant retinae are histologically normal when compared to WT siblings (A,B). Scale bar = 20 μm. Additionally, there does not appear to be any reduction in pigmentation of the RPE (A',B'). Scale bar = 10 μm.

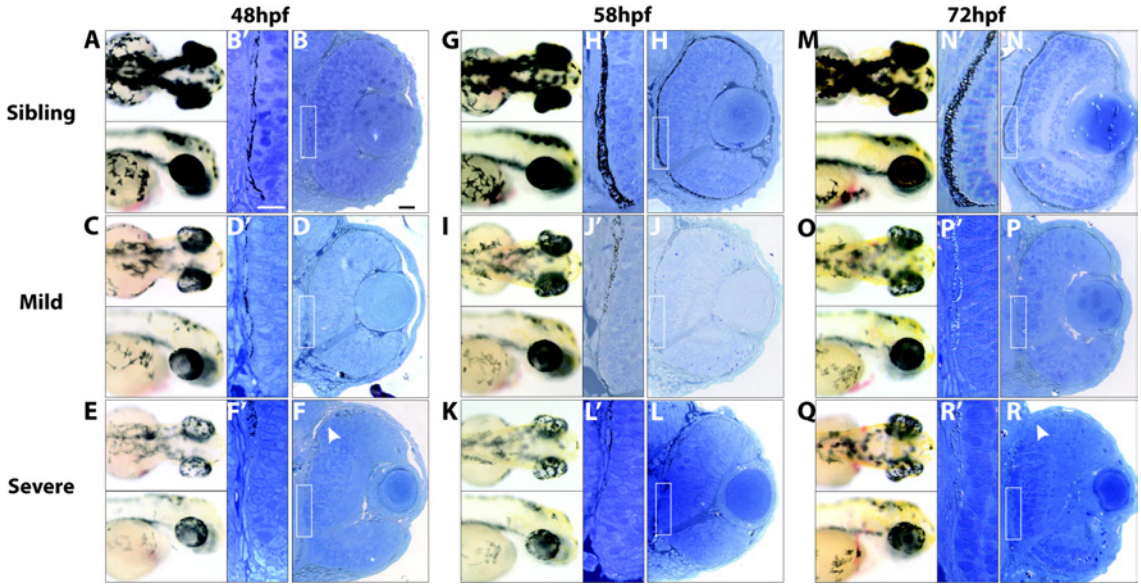

Figure 3.4: The RPE is disrupted in *au18* mutants. Images of sibling and mutant embryos show that the RPE of *au18* embryos is hypopigmented at 48 (A, C, E), 58 (G, I, K), and 72 hpf (M, O, Q). Transverse histologic sections of sibling and mutant embryos at 48 (B, D, F)58 (H, J, L), and 78 hpf (N, P, R) reveal that au18 eye is microphthalmic, but overall retina structure appears to be normal. Areas devoid of pigment are marked by white arrowheads. Scale bar: 20 μm. (B0, D0, F0, H0, J0, L0, N0, P0, R0) Magnified images of RPE show that RPE proximal to the optic nerve was consistently depigmented in au18 and confirm that au18 RPE appears to have fewer melanosomes than wild-type siblings. The posterior lens also appears to be cataractous in severe au18 mutants (F, L, R). Scale bar:10 μm.

3.2.2: *au13* and *au18* phenotypes are caused by mutations in *nsfb*

To identify the causative mutation in *au18*, we performed next-generation sequencing followed by SNP-mapping using the MegaMapper analysis pipeline (Obholzer et al., 2012). Whole-genome sequencing of *au18* mutants generated ~11X average coverage of the zebrafish genome. MegaMapper analysis identified a 6-megabase window on chromosome 12 as the likely location of the causative mutation. Within this window, a C-to-A transversion mutation at nucleotide 893 (C893T) of the *nsfb* coding sequence was predicted to be the mutation underlying the *au18* phenotype. This mutation is predicted to cause a premature stop codon at amino acid 297, truncating nsfb by 60% (S297X). cDNA sequencing confirmed the presence of this mutation in homozygous *au18* mutant embryos and its absence in wild-type embryos (Figure 3.4A). Nsfb contains three major domains: a N-terminal binding domain required for its association with SNAP-complex proteins, and two ATPase domains, D1 and D2 (Figure 3.4A). The first ATPase domain is required for overall ATPase activity of the protein, while the second ATPase mediates hexamerization during complex formation (Sumida et al., 1994; Whiteheart et al., 1994; Yu et al., 1999). The early stop codon in *au18* is predicted to truncate the protein within the first ATPase domain (red dotted line, Figure 3.4A), likely resulting in nonfunctional nsfb protein. To confirm that this mutation is causative of the *au18* phenotype, we performed an mRNA rescue experiment by injecting full-length $nsfb^{WT}$ and $nsfb^{au18}$ mRNA into homozygous mutant *au18* embryos. Injection of $nsfb^{WT}$ rescued pigmentation in *au18* mutant embryos (131/132), while $nsfb^{au18}$ failed to rescue the mutant phenotype (74/94) (Figure 3.4B,C).

Phenotypic rescue of homozygous *nsfb*^{au18} mutants was confirmed by genotyping in a subset of injected embryos (data not shown) (Neff et al., 1998). Based on these data, we conclude that *au18* possesses a nonsense mutation in *nsfb* and hereafter refer to this allele as *nsfb*^{au18} in accord with zebrafish nomenclature guidelines.

As mentioned above, *au13* fails to complement the *nsfb*^{au18} mutation, suggesting that they possess mutations in the same gene. However, we were unable to identify a causative mutation in the coding sequence of *nsfb* in *au13* mutants (data not shown). Injection of *nsfb*^{WT} mRNA rescued the mutant phenotype in embryos from an *au13* heterozygous incross (145/148), while injection of *nsfb*^{au18} failed to rescue the pigmentation phenotype in these clutches (46/60). Given the non-complementation between *nsfb*^{au18} mutants and *au13* mutants, and these rescue data, the most parsimonious explanation is that *au13* possesses a mutation in a regulatory region of *nsfb* that alters transcript expression. To test this possibility, we performed qPCR analysis of *nsfb* in *au13* and *nsfb*^{au18} mutants, which revealed that *nsfb* expression was reduced ~2.4-fold in both *nsfb*^{au18} and *au13* relative to wild-type embryos (Figure 3.4D). Thus, we conclude that the *au13* phenotype also results from a mutation in *nsfb*, and hereafter refer to this line as *nsfb*^{au13}.

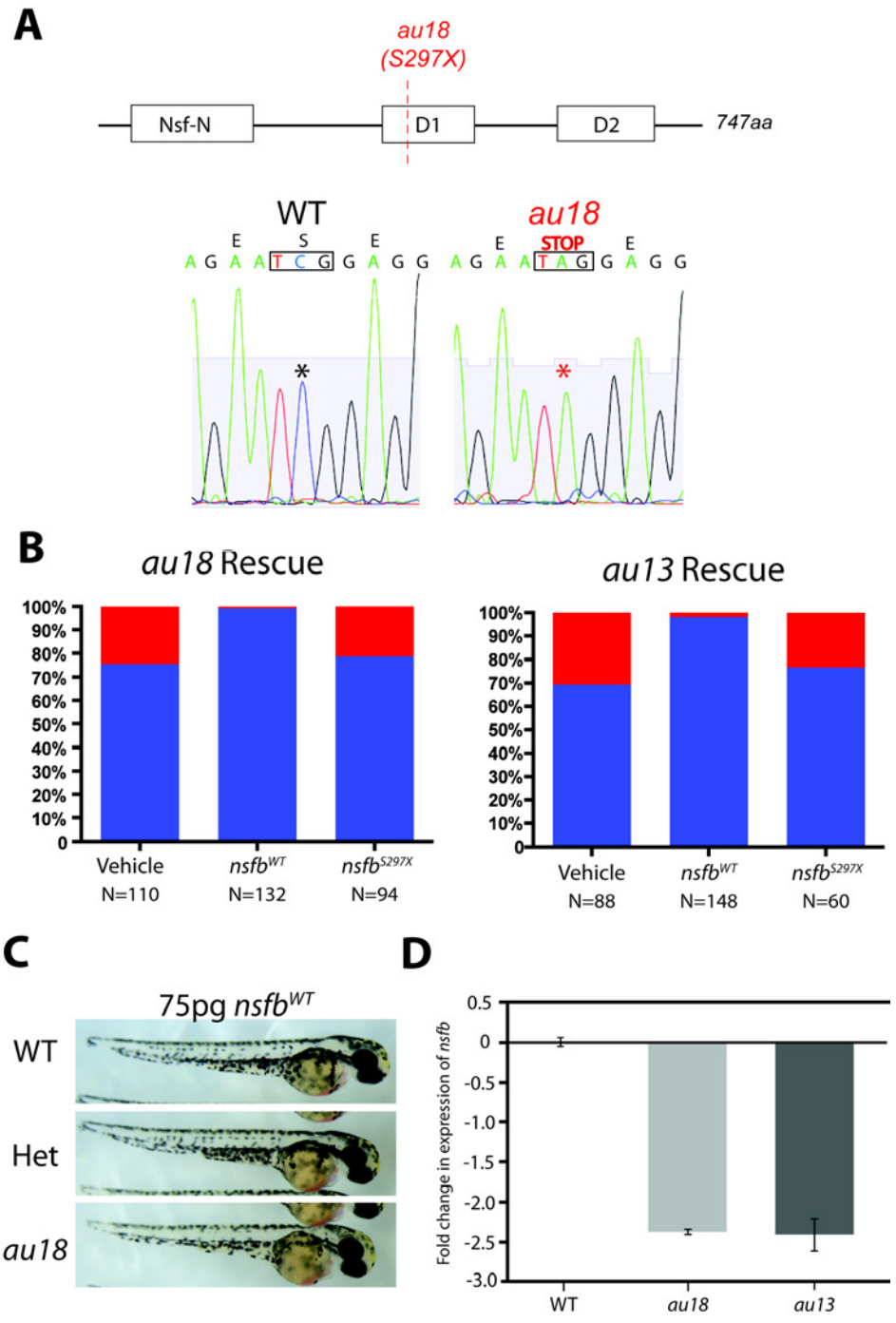
A
au18
(S297X)
Nsf-N
D1
D2
747aa
WT
au18
E S E
A G A A T C G G A G G
E STOP E
A G A A T A G G A G G
B
au18 Rescue
au13 Rescue
100%
90%
80%
70%
60%
50%
40%
30%
20%
10%
0
Vehicle
N=110
nsfbWT
N=132
nsfbS297X
N=94
Vehicle
N=88
nsfbWT
N=148
nsfbS297X
N=60
C
75pg nsfbWT
WT
Het
au18
D
Fold change in expression of nsfb
0.5
0
-0.5
-1.0
-1.5
-2.0
-2.5
-3.0
WT
au18
au13

Figure 3.5

Figure 3.5: *au13* and *au18* phenotypes are likely caused by mutations in nsfb. (A) Schematic of the nsfb protein. There are three major domains: the Nsf-N, ATPase domain 1 (D1), and ATPase domain 2 (D2). The mutation occurs at nucleotide 893 (C893T), and the dotted red line indicates the location of the premature stop codon at amino acid 297 (S297X) in *au18* mutants. This mutation is predicted to truncate the protein by 60%. (B) Graph illustrating the percentage of phenotypically mutant embryos in each clutch following injection of vehicle, $nsfb^{WT}$, and $nsfb^{au18}$ mRNA. Both *au13* and *au18* mutant phenotypes are rescued by injection of $nsfb^{WT}$, whereas injection of $nsfb^{au18}$ mRNA failed to rescue either the *au13* or *au18* mutant phenotype. (C) Representative images of WT, $au18^{-/+}$, and $au18^{-/-}$ embryos following $nsfb^{WT}$ injection. (D) Quantitative PCR quantification of the relative fold change of nsfb in $nsfb^{au13}$ and $nsfb^{au18}$ embryos at 48 hpf. Transcript levels were normalized to *act2b*. Error bars indicate SEM of five technical replicates for each experiment. N = 3 biological replicates.

3.2.3: *nsfb* is a ubiquitously expressed paralog of human NSF

The zebrafish genome contains two paralogs of human *NSF*: *nsfa* and *nsfb*, which likely arose from a genome duplication event in teleosts (Amores et al., 1998). Phylogenetic analysis of nsf genes suggests that *nsfb* is more distantly related to human *NSF* than *nsfa* (Figure 3.5A). *nsfa* is primarily expressed in the nervous system (Woods et al., 2006), but the expression pattern of *nsfb* is unknown. *In situ* hybridization revealed widespread expression, with apparently higher levels of expression in the somites at 24hpf. At 48hpf, *nsfb* mRNA expression appears to be more restricted to the anterior half of the embryo, with some enrichment in the otic vesicle and pectoral fins (Figure 3.5B).

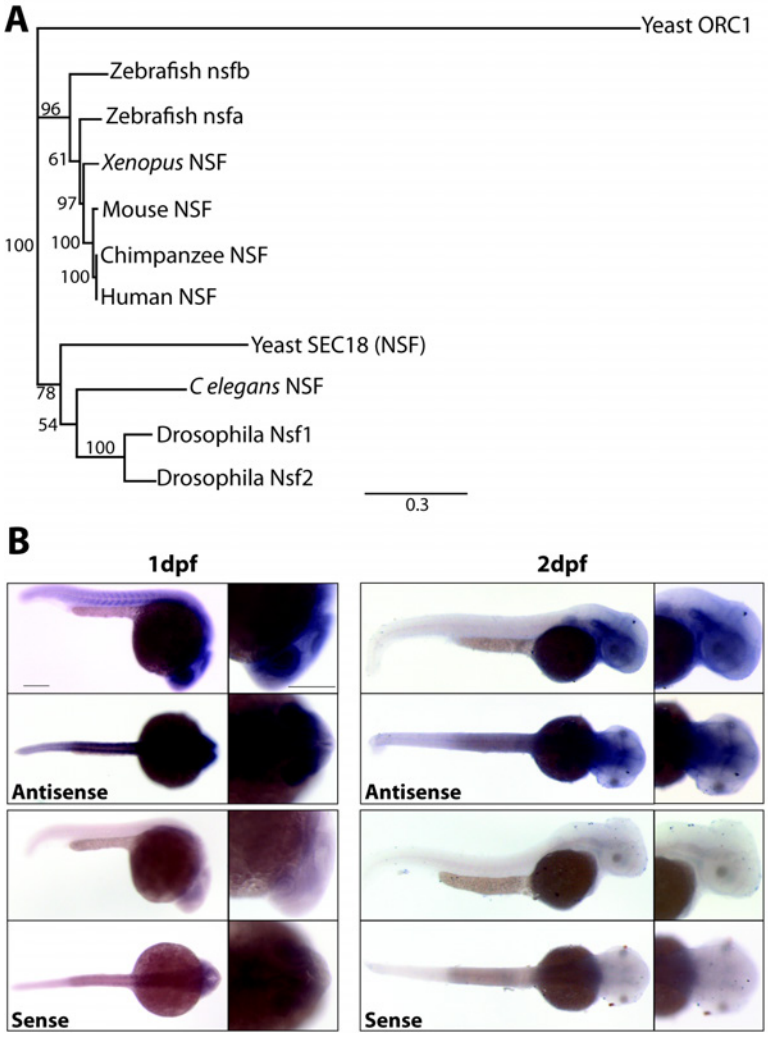

Figure 3.6: *nsfb* is a paralog of human NSF and is ubiquitously expressed during early embryo development. (A) Phylogenetic analysis of the relationship between *nsf* in vertebrates. This analysis was constructed using Geneious Tree Builder, based on an alignment of nsf amino acid sequences from human, chimpanzee, mouse, *Xenopus*, zebrafish, *Drosophila*, *C. elegans* and yeast. Origin recognition complex subunit 1 (ORC1) is an outgroup. Numbers at nodes represent bootstrap values after 1000 replicates. (B) *In situ* hybridization reveals that *nsfb* expression is widespread at 24hpf, with higher levels of staining in the somites and nervous system. At 48hpf, *nsfb* remains widely expressed in the head, with high levels of expression in the otic vesicle and pectoral fins, but is less apparent in the somites and posterior trunk. Lateral and dorsal views of embryos stained for antisense probe are on top and sense controls are on bottom. Scale bar: 200 μm.

3.2.4: Melanosome formation and maturation is disrupted in *nsfb*^{au18} mutants

Due to the importance of membrane trafficking and vesicular fusion during melanogenesis, we hypothesized that loss of nsfb function results in an arrest in melanosome maturation in *nsfb*^{au18} RPE. To test this hypothesis and assess melanogenesis in the *nsfb*^{au18} RPE, we performed TEM of *nsfb*^{au18} mutant and sibling RPE at 48, 58 and 72hpf, quantifying several aspects of melanosome formation from TEM images taken from the dorsal, central and ventral regions of the RPE (Figure 3.6A,B). Because hypopigmentation varies in *nsfb*^{au18} mutants, we continued to separate *nsfb*^{au18} embryos into mildly- and severely- hypopigmented cohorts to determine if there were quantitative differences in phenotypes between these groups. Quantification of melanosome density revealed that density increased between 58hpf and 72hpf in phenotypically wild-type sibling embryos ($p=0.001$). The average density of *nsfb*^{au18} mutants was significantly lower than sibling at all time points, and did not display a significant change over time (Figure 5C). Moreover, severely hypopigmented *nsfb*^{au18} mutants contained significantly fewer melanosomes than mild *nsfb*^{au18} mutants at 48 and 72hpf ($p<0.0001$).

Since melanosomes accumulate more pigment as they mature (Seiji et al., 1963a), the percentage of each melanosome containing pigment was quantified and this measure was used as a proxy for melanosome maturity. These analyses revealed that *nsfb*^{au18} melanosomes were significantly less mature than phenotypically wild-type siblings at all time points examined (Figure 3.6D), and melanosomes in severe *nsfb*^{au18} mutants were less mature than those in mild *nsfb*^{au18} mutants at 58 and 72hpf. While phenotypically wild-type

melanosomes grew more mature over all time points ($p<0.0001$), overall melanosomal maturity decreased between 48hpf and 58hpf in mildly affected ($p=0.0004$) and in severely affected embryos ($p<0.0001$).

Finally, quantification of melanosomal perimeter (Figure 3.6E) revealed that the average perimeter of melanosomes in phenotypically wild-type siblings did not significantly differ from mild *nsfb*^{au18} mutants. Melanosomal perimeter also increased significantly in sibling and mildly affected mutants between 48-58hpf ($p<0.0001$). However, the perimeter of melanosomes in severe *nsfb*^{au18} mutants was significantly reduced compared to sibling at 58 and 72hpf ($p<0.0001$). Also, unlike in phenotypically wild-type and mildly affected embryos, melanosomal perimeter decreased significantly between 48 and 58hpf in severely affected mutants ($p<0.0001$) (Figure 3.6E).

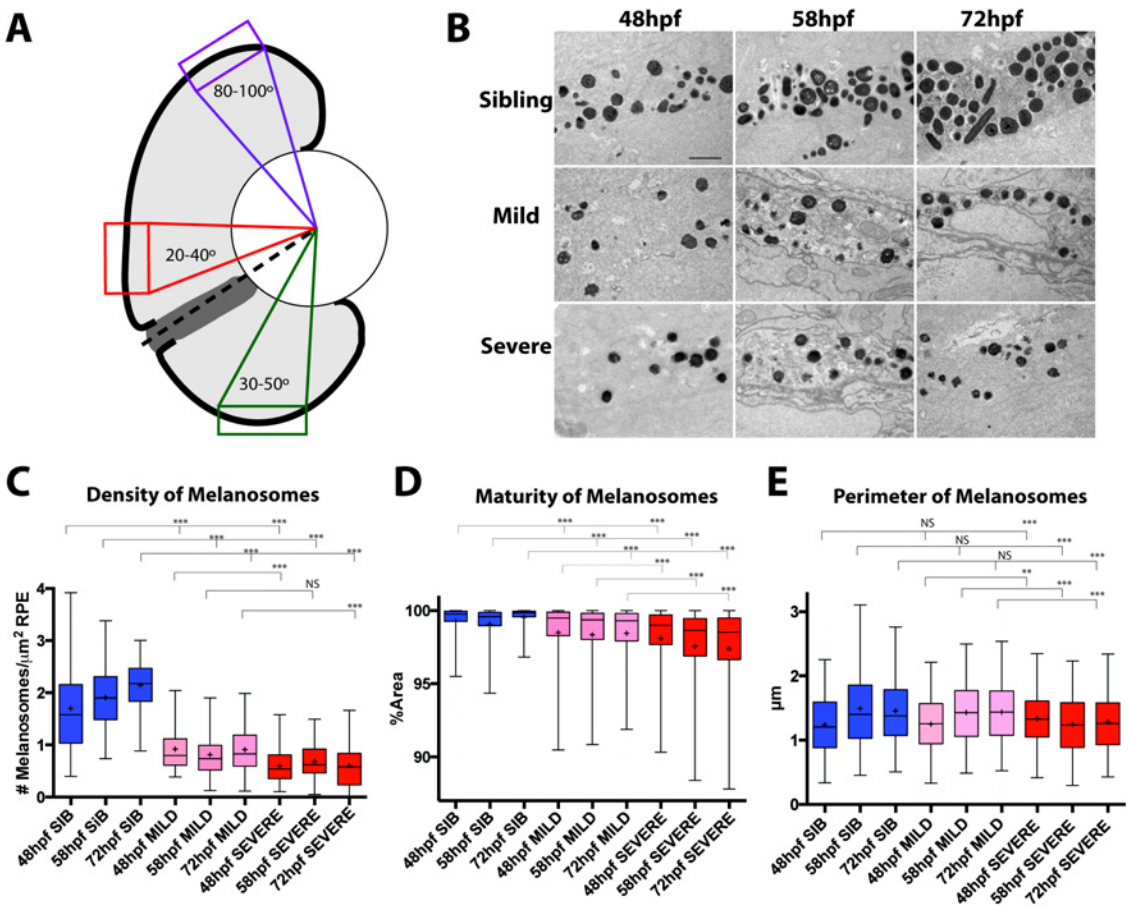
A
80-100°
20-40°
30-50°
B
48hpf
58hpf
72hpf
Sibling
Mild
Severe
C
Density of Melanosomes
Melanosomes/μm² RPE
D
Maturity of Melanosomes
%Area
E
Perimeter of Melanosomes
μm
48hpf SIB
58hpf SIB
72hpf SIB
48hpf MILD
58hpf MILD
72hpf MILD
48hpf SEVERE
58hpf SEVERE
72hpf SEVERE

Figure 3.7

Figure 3.7: Melanosome formation and maturation is disrupted in *nsfb*^{au18} mutants. (A) Cartoon schematic showing the dorsal, central, and ventral regions of the RPE that were analyzed. RPE between 20° and 40° clockwise from an imaginary line (dotted line) drawn between the center of the lens and the center of the optic nerve was defined as central, whereas RPE 80° to 100° was defined as dorsal. Finally, RPE contained within a box 30° to 50° counterclockwise was defined as ventral. (B) Representative TEM images of central RPE for sibling, mild, and severe *nsfb*^{au18} RPE at 48, 58, and 72 hours after fertilization. Images oriented distal (choroid) up, proximal (retina) down. Scale bar: 1 μm. (C) Quantification of the average number of melanosomes per square micrometer of RPE indicates that *nsfb*^{au18} mutants contained significantly fewer melanosomes than sibling at all time points, and severe *nsfb*^{au18} mutants contained significantly fewer melanosomes than mild *nsfb*^{au18} mutants at 48 and 72 hpf. (D) The graph depicting the average percentage of melanosomes containing pigment reveals that *nsfb*^{au18} melanosomes were significantly less mature than sibling at all time points and that severe mutants were less mature than mild. (E) Graph depicting the average perimeter of melanosomes. Although the average perimeter of melanosomes in sibling and mild *nsfb*^{au18} mutants was not significantly different, severe *nsfb*^{au18} melanosomes were significantly smaller than sibling. Furthermore, although melanosomal perimeter increased in sibling and mild RPE, severely affected mutant melanosomes decreased over time. (Mann-Whitney U test, *$P < 0.01$, **$P < 0.001$, ***$P < 0.0001$).

3.3: DISCUSSION:

Albinism results from mutations in a diverse collection of genes that regulate melanogenesis or melanosome trafficking (Oetting and King, 1999); however, data from human and animal studies suggest that we do not yet know the full complement of genes required for normal pigmentation. For example, although seven genetic subtypes of OCA have so far been identified: OCA1A and OCA1B (MIM 203100, 606952), OCA2 (MIM 203200), OCA3 (MIM 20390), OCA4 (MIM 606574), OCA5 (615312), OCA6 (MIM 113750), and OCA7 (MIM 615179,) the genes underlying OCA5-7 were discovered only very recently (Kausar et al., 2013; Montoliu et al., 2014), highlighting the probability that there are other undiscovered loci responsible for albinism. Here we report two novel zebrafish oculocutaneous albino mutants and establish a role for nsfb in melanogenesis.

Patients with albinism disorders often present with varying degrees of ocular defects, and these include foveal hypoplasia, nystagmus and improper retinal axon decussation (Grønskov et al., 2007; Levin and Stroh, 2011). Despite our growing understanding of the genetic etiology of OA, OCA and the syndromic types of albinism, we know comparatively less about the molecular and cellular underpinnings of these diseases, or how pigmentation affects the visual system. Zebrafish are a powerful model organism for gene discovery and mechanistic analysis of protein function during ocular development and disease due to tractable genetics and ability to perform a diverse array of molecular, biochemical, anatomical and behavioral studies (Gross and Perkins, 2008; Lieschke and Currie, 2007). Many pigmentation mutants have been identified and

characterized in zebrafish (Amsterdam et al., 2004; Daly et al., 2013; Golling et al., 2002; Haffter et al., 1996; Kelsh et al., 1996; Neuhauss et al., 1999; Ng et al., 2009; Nuckels et al., 2009; Odenthal et al., 1996; Streisinger et al., 1981), some of which directly model existing human pathologies (e.g. Krauss et al., 2014; Page-McCaw et al., 2004), while others presage the identification of human mutations. For example, the causative mutation of OCA6, *SLC24A5*, was identified in a zebrafish pigmentation mutant (Lamason et al., 2005) prior to in the mouse (Vogel et al., 2008) or in human patients (Wei et al., 2013). Thus, the zebrafish system represents a potent tool for studying the molecular and cellular regulation of melanogenesis, as well as identifying novel albinism genes in vertebrates.

Here, we report the cloning and characterization of two novel oculocutaneous albino mutants that result from mutations in *nsfb*: $nsfb^{au18}$, which results from a nonsense mutation, and $nsfb^{au13}$, whose causative mutation is unknown but is likely located in a noncoding regulatory region. Indeed, qPCR analysis demonstrated that *nsfb* expression is reduced in $nsfb^{au13}$ embryos, supporting this possibility. Interestingly, a comparable reduction of *nsfb* expression was also observed in $nsfb^{au18}$ mutant embryos. It is likely that this occurs via nonsense-mediated mRNA decay, a molecular phenotype frequently observed in zebrafish for genes that possess nonsense mutations (e.g. Fricke et al., 2001; Lamason et al., 2005; Obholzer et al., 2012; Xiao and Baier, 2007b).

nsfb mutants are oculocutaneous albinos and they are first identifiable at ~2dpf based on their hypopigmentation phenotype. *nsfb* is one of the two zebrafish *nsf* paralogs; *Nsf* is ubiquitously expressed in mammals (Magdaleno et al., 2006; Visel et al., 2004), though enriched in the nervous system (Betz, 1994). *nsfa* expression is limited to the

nervous system (Woods et al., 2006), while *nsfb* has more widespread expression (our data), suggesting that it may be more orthologous in function to *nsf* than *nsfa*. Interestingly, however, our phylogenetic analysis indicates the protein sequence of nsfa is more closely related to human NSF than is nsfb (Figure 4). Thus, while *nsfb* diverged evolutionarily from mammalian *Nsf*, it possibly retained its system-wide functions, while *nsfa* evolved to hold more limited or specialized functions.

Unlike nsfa, virtually nothing is known about the *in vivo* function(s) of nsfb. Here we demonstrate a critical requirement for nsfb in pigmentation and in regulating the maturation of melanosomes in the RPE. Defects in melanosomal maturation are accompanied by reductions in melanosome number (Figure 5). While phenotypes in both *nsfb* alleles were fully penetrant, there were differences in the expressivity of the pigmentation phenotype, with mildly- and severely- affected mutants detected within the same clutch of homozygous embryos. These data suggest that while melanogenesis is disrupted in both classes of mutants, it proceeds to a limited extent in mildly affected mutants, while it is significantly impaired in severely affected mutants. It is common in zebrafish to have variability in expressivity of a phenotype (e.g. Hartsock et al., 2014; Lee et al., 2008; Lee and Gross, 2007) and often this variability is ascribed to differing levels of maternal rescue in each embryo resulting from the deposition of mRNAs and proteins in the developing oocyte(Abrams and Mullins, 2010). More work is necessary to understand the molecular basis of this phenotypic variability in *nsfb* mutants, and, more generally, how maternal rescue contributes to phenotypic variability in recessive zebrafish mutants.

Our quantitative TEM data suggest a model in which nsfb activity is required for the maturation of melanosomes in the RPE. Although we limited our characterization to the RPE hypopigmentation phenotype, *nsfb* mutants possess widespread CNS degeneration by 3dpf, have reduced circulation, and typically die by 4dpf. Given the expanded and systemic severity of the phenotypes over those found in ocular albinism or oculocutaneous albinism patients, the *nsfb* phenotypes are more similar to those pathologies observed in patients with syndromic albinism. Indeed, patients with HPS or CHS often have additional, systemic defects such as pulmonary fibrosis and blood clotting defects, in addition to their albinism. Although mutations in *NSF* have not yet been linked to albinism in human, misregulation of NSF is linked to psychiatric diseases (Imai et al., 2001). It will be interesting to screen through existing albinism patients for whom a causative mutation has not yet been identified, and particularly those with more syndromic pathologies, to determine if mutations in NSF underlie their phenotypes. In summary, this Chapter identifies a role for nsfb during melanogenesis in the RPE, establishing an additional, and novel oculocutaneous albinism mutant in zebrafish through which the molecular and cellular underpinnings of melanogenesis can be further elucidated.

Chapter 4: Regeneration of the retinal pigment epithelium in a novel zebrafish model of macular degeneration

This chapter has contributions from other authors. Hanovice, N.J., Slater, K., Romanowicz, D.K., Collery R., Link, B., Gross, J.M., 2017. *Regeneration of the zebrafish retinal pigment epithelium in a novel model of macular degeneration*. In preparation. NJH and JMG conceived experiments and interpreted data. NJH, KS and DR performed experiments and collected data. RC and BL provided materials and technical advice.

4.1: INTRODUCTION

The Retinal Pigment Epithelium (RPE) is a polarized monolayer of hexagonal pigment-containing cells posterior to the retina whose apical surface is closely interdigitated with photoreceptive neurons called photoreceptors (Strauss, 2005). Photoreceptors are responsible for the conversion of light into electrochemical signals and form a functional unit with the RPE. The basal RPE surface abuts and helps form a multilaminar basement membrane known as Bruch's Membrane (BM), which helps create a barrier between the retina and overlying vasculature, known as the choriocapillaris. Due to its importance in visual system function, diseases affecting the RPE have serious consequences for vision. Age-related Macular degeneration (AMD) is the third leading cause of blindness in the world and the leading cause of blindness in industrialized countries (Klein et al., 2011; Resnikoff, 2008; Wong et al., 2014). AMD is divided into two types: geographic and exudative. In geographic AMD, RPE cells in the macula progressively degenerate, leading to the death of closely-apposed cone photoreceptors and debilitating loss of high-acuity vision (Curcio et al., 1996; Lim et al., 2012a). Exudative AMD is preceded by geographic atrophy and is marked by the invasion and neovascularization of the choroidal vasculature into the subretinal space, which is termed choroidal neovascularization (CNV) and accelerates retinal degeneration (Bird et al., 1995; Lim et al., 2012a). In both types, retinal degeneration from AMD is

irreversible and there are no FDA-approved therapies that are capable of recovering vision once it is lost.

A particularly attractive possibility for treating AMD is the transplantation of healthy RPE. In a proof-of-concept study, healthy RPE transplanted into Royal College of Surgeons rats was able to attach to the retina and phagocytose POS (Jiang and Hamasaki, 1994; Lopez et al., 1989). However, transplantation studies in human patients at first met mixed results due to factors such as rejection (Algvere et al., 1999, 1994; Algvere, 1997; Peyman et al., 1991), or from age-related defects in autologous RPE grafts . Advances over the past decade in stem cell technology have opened the possibility of the transplantation of stem-cell derived RPE cells (Choudhary et al., 2016; Leach and Clegg, 2015; Uygun et al., 2009), which could provide a non-immunogenic source of healthy RPE grafts. Experiments in rat and murine models demonstrated an improvement in visual function after the successful transplantation of embryonic stem cell-derived RPE from multiple sources, including human embryonic stem cells (hESC) (Aoki et al., 2006; Little et al., 1998; Meyer et al., 2006) and induced pluripotent stem cells (iPSC) (Carr et al., 2009). Aided in part by further developments in RPE cell scaffolds (Kamao et al., 2014), clinical trials are currently underway with promising early results (Kamao et al., 2017; Shim et al., 2017). Although this progress is encouraging, only rudimentary knowledge exists about the genetic and molecular mechanisms underlying the process by which RPE cells may respond to and successfully repair damage. In order for RPE transplantation to truly deliver on its promise, it of critical importance to improve our understanding of the process by which RPE cells can regenerate and reintegrate with retinal tissue.

The mammalian RPE is capable of limited regeneration but the success of regeneration is highly sensitive to the extent of the injury. Generally, mammalian RPE

cells respond to damage in one of two ways: they can regenerate small lesions by expanding to fill the open space, but fail to regenerate larger insults and often instead create further damage by overproliferating (Grierson et al., 1994). For example, mammalian RPE cells are capable of limited regeneration following small RPE debridement (Lopez et al., 1995; Priore et al., 1995) However, following large injuries such as retinal detachment, RPE cells respond by overproliferating to produce multilaminar structures while generating migratory cells that invade the subretinal space, behaviors indicative of what may be a misregulated repair mechanism (Cleary and Ryan, 1979a, 1979b; Machemer and Laqua, 1975). This proliferative response to injury can become deleterious and lead to Proilferative Vitreoretinopathy (PVR), during which RPE cells lose epithelial characteristics, overproliferate and migrate into the subretinal space, leading to further retinal detachment and blindness (Stern and Temple, 2015).

In contrast to mammals, the RPE of newt and embryonic chick has the remarkable capacity both to regenerate itself and to transdifferentiate and regenerate the neural retina (Barbosa-Sabanero et al., 2012; Haynes and Del Rio-Tsonis, 2004). Studies in *Xenopus* revealed that a subpopulation of RPE cells delaminate from the BM, and in a process reminiscent of PVR migrate to the retinal vascular membrane, where they transdifferentiate and regenerate the neural retina. The newt RPE does not dissociate from BM following injury but proliferates to forms a BM-attached bilayer which gives rise to a regenerated retina and RPE (Chiba, 2014; Chiba et al., 2006; Susaki and Chiba, 2007). Interestingly a subpopulation of quiescent human RPE cells, termed RPE stem cells, was recently identified in culture that can be induced to proliferate and differentiate into either RPE or mesenchymal fates (Salero et al., 2012; Stern and Temple, 2015), suggesting the existence of an analogous subpopulation of human RPE cells that could be induced to successfully regenerate retinal injuries. However, research in newt has to our

knowledge been mainly focused on the process of RPE-to-retina regeneration, while the specific molecular events underlying RPE-RPE regeneration are not well understood.

Zebrafish are highly amenable to forward and reverse genetic manipulation, have a fully sequenced genome and offer a wealth of genetic and *in vivo* imaging technologies. Importantly, zebrafish also possess a robust ability to regenerate damaged neural tissue, such as the brain (Kizil et al., 2012), spine (Becker et al., 1997) and retina (Goldman, 2014). In response to retinal injury, zebrafish Müller glia dedifferentiate and generate retinal progenitor cells, which then migrate to the injury site to replace lost neurons (Fausett and Goldman, 2006; Nagashima et al., 2013). In contrast, virtually nothing is known about the response of the zebrafish RPE to injury, or whether it is capable of regeneration following ablation. Here, we describe the establishment of a novel model of AMD using a zebrafish transgenic enabling the specific ablation of the RPE and demonstrate, for the first time, that the zebrafish RPE is capable of regeneration following widespread acute injury. We provide evidence that regeneration involves a robust proliferative response during which cells from the periphery move to the injury site and contribute to regeneration, and that these cells likely derive from uninjured RPE.

4.2: RESULTS

4.2.1 Specific ablation of the Retinal Pigment Epithelium leads to photoreceptor degeneration and blindness

To study the events underlying RPE regeneration in zebrafish, we obtained *rpe65a*:nfsb-GFP transgenic zebrafish from Dr. Brian Link (Medical College of Wisconsin). This transgenic uses a promoter element from *rpe65a* gene, which encodes a critical enzyme in the visual cycle (Hamel et al., 1993; Redmond et al., 1998), to drive

expression of the Nfsb-EGFP fusion protein specifically in mature RPE (Collery et al., 2016) (Fig 3.1A). Nfsb is an *E. coli* nitroreductase that converts the ordinarily benign prodrug metronidazole (MTZ) into a potent DNA crosslinking agent, leading to apoptosis in expressing cells (Bridgewater et al., 1995; Knox et al., 1988). The nitroreductase ablation system has been extensively validated in zebrafish as allowing for inducible ablation of target cells with limited bystander effect (e.g. Curado et al., 2007; Fraser et al., 2013; Hsu et al., 2010; Johnson et al., 2016; Li et al., 2012; Montgomery et al., 2010a; Pisharath et al., 2007; Shimizu et al., 2015; White and Mumm, 2013; White et al., 2011).

To ablate the RPE, *rpe65a*:nfsb-GFP outcrosses were prepared for ablation via treatment with the tyrosinase inhibitor phenylthiourea (PTU) (Westerfield, 2007), between 1-5dpf to suppress pigmentation of choroidal melanocytes, which interfere with analysis. Transgene expression is variable within each outcross clutch (data not shown). We screened out low-expressing embryos from each clutch and selected embryos with high transgene expression in the eye based upon GFP fluorescence. By 5dpf, eye formation and differentiation are complete and zebrafish have entered the larval stage of development (Kimmel et al., 1995). In the larval eye, nfsb-GFP is expressed specifically within the RPE layer apposed to the central retina (Fig 4.1B) and nicely labels RPE cell bodies and apical microvilli (Fig 4.1B, arrows). To ablate the RPE, larvae were removed from PTU treatment and then exposed to 10mM MTZ for 24 hours before being transferred to untreated fish system water to recover. After MTZ treatment, GFP+ apical microvilli are absent, and the GFP+ RPE monolayer becomes disrupted in the central two-thirds of the eye (Fig 4.1D). This disrupted area also fails to re-pigment after removal of PTU, indicating that RPE cell function is disrupted in ablated RPE cells (Fig 4.1F, compare to Fig 4.1C). Interestingly, nuclei in the outer nuclear layer (ONL)

immediately adjacent to ablated RPE become disorganized, some appearing to delaminate and become pyknotic (Fig 4.1D, arrows) while outer segment morphology degrades (Fig. 4.1F, compare to Fig 4.1C).

Although embryos were rigorously screened for high level of transgene expression prior to ablation, some variability in ablation severity was observed (data not shown), likely from variations in transgene expression and ablation efficiency. To mitigate this variability we screened ablated larvae at 2dpi and selected those with high levels of GFP signal disruption in the eye for further study. Mildly ablated larvae were excluded from analysis.

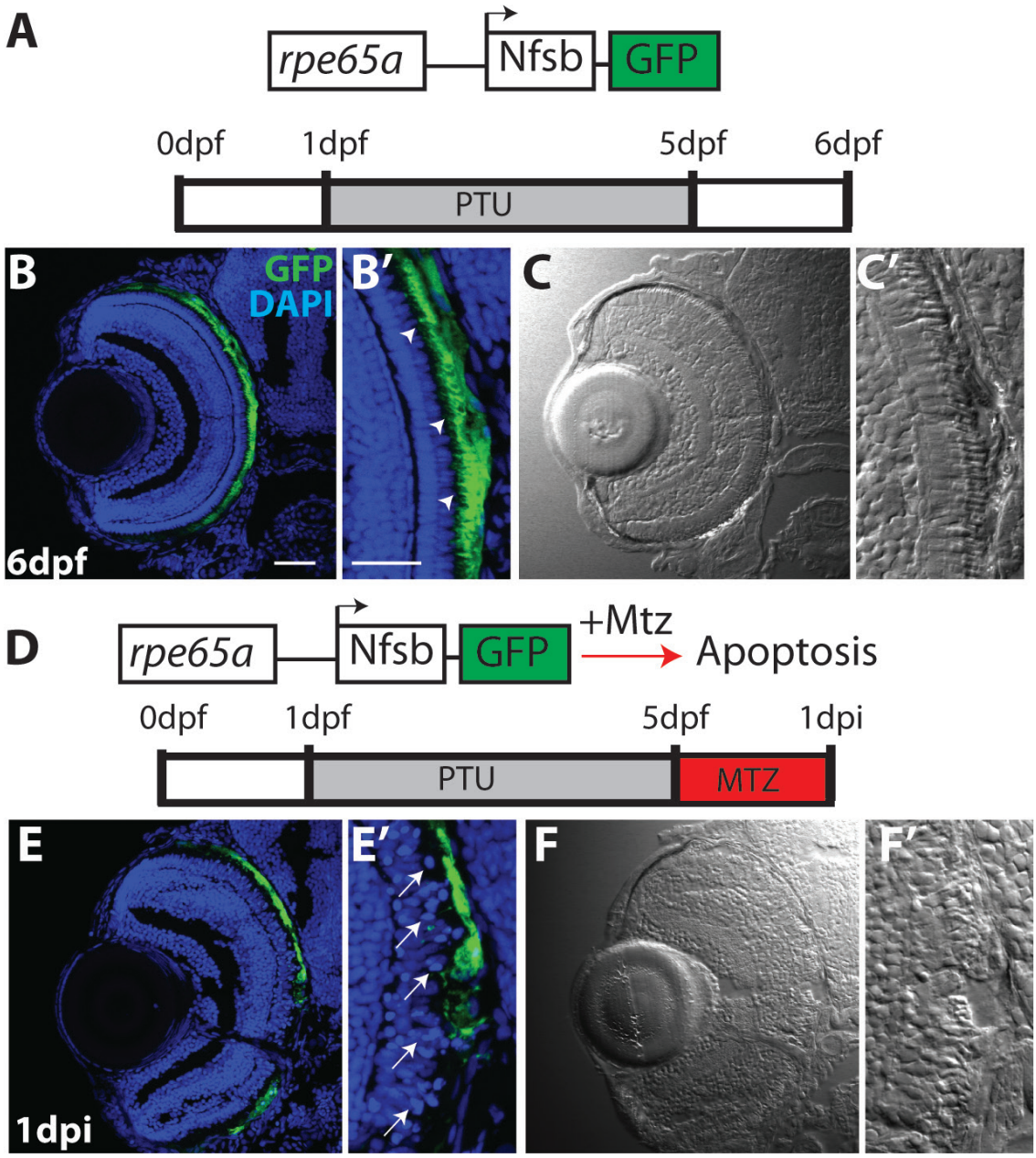

Figure 4.1: Paradigm of RPE ablation. (A) Cartoon depicting the *rpe65a*:Nfsb-GFP transgene and treatment course of unablated embryos. (B,B') Transverse cryosection of GFP and nuclei in an unablated 6dpf larva. GFP expression is strongest in the central two-thirds of RPE. Arrowheads indicate apical microvilli. (C,C') DIC channel. (D) Cartoon depicting nitroreductase-mediated ablation. (E,E') GFP and nuclei at 1dpi. Arrows indicate delaminated pyknotic nuclei. (F,F') DIC channel. Green=GFP, blue=nuclei. In all sections, dorsal is up and distal is left. Scale bar = 40μm.

In Geographic AMD, dysfunction and degeneration of RPE cells leads to the death of underlying photoreceptors (Curcio et al., 1996; Lim et al., 2012a). To determine the dynamics of RPE cell degeneration following ablation, and to determine whether RPE ablation leads to apoptosis of photoreceptor cells, we performed a time course analysis of apoptosis via TUNEL at 3, 6, 12, 18, 24 and 48 hours post injury (hpi) (Fig 4.2). While the ONL appears to be unchanged at 3hpi, slight disruptions in ablated RPE morphology are detectible: apical microvilli become shortened compared to control, and the occasional TUNEL+ nucleus appears in the RPE layer (Fig 4.2A-B, arrowhead). By 6hpi, TUNEL signal is significantly elevated in the RPE layer (Fig 4.2M). Meanwhile, apical microvilli have fully retracted, and GFP signal in the RPE layer becomes less diffuse and starts collecting into rounded blebs, indicating that RPE cell bodies are beginning to degrade. Nuclear organization in the ONL also begins to deteriorate at 6hpi. Starting at 12hpi, apoptosis is significantly increased in both the RPE layer and ONL (Fig 4.2M-N). ONL nuclei become less densely packed, and delaminated pyknotic nuclei appear. By 18hpi, apoptosis in the ONL peaks, and GFP signal in the RPE layer starts to accumulate in blebs, a process which begins to leave regions of the RPE entirely devoid of GFP signal (Fig 4.2G-H). RPE apoptosis peaks throughout the RPE layer at 24hpi, and the ONL continues to degrade (Fig 4.2I-J). Apoptosis, while still significantly elevated compared to control, begins to taper off in both layers by 48hpi. At this point, morphologically normal GFP+ RPE cells are completely absent from the RPE layer and have been replaced by irregular GFP+ blebs, likely consisting of degenerated cell debris. ONL nuclei are less densely-packed and clearly disorganized compared to control (Fig 4.2K-L).

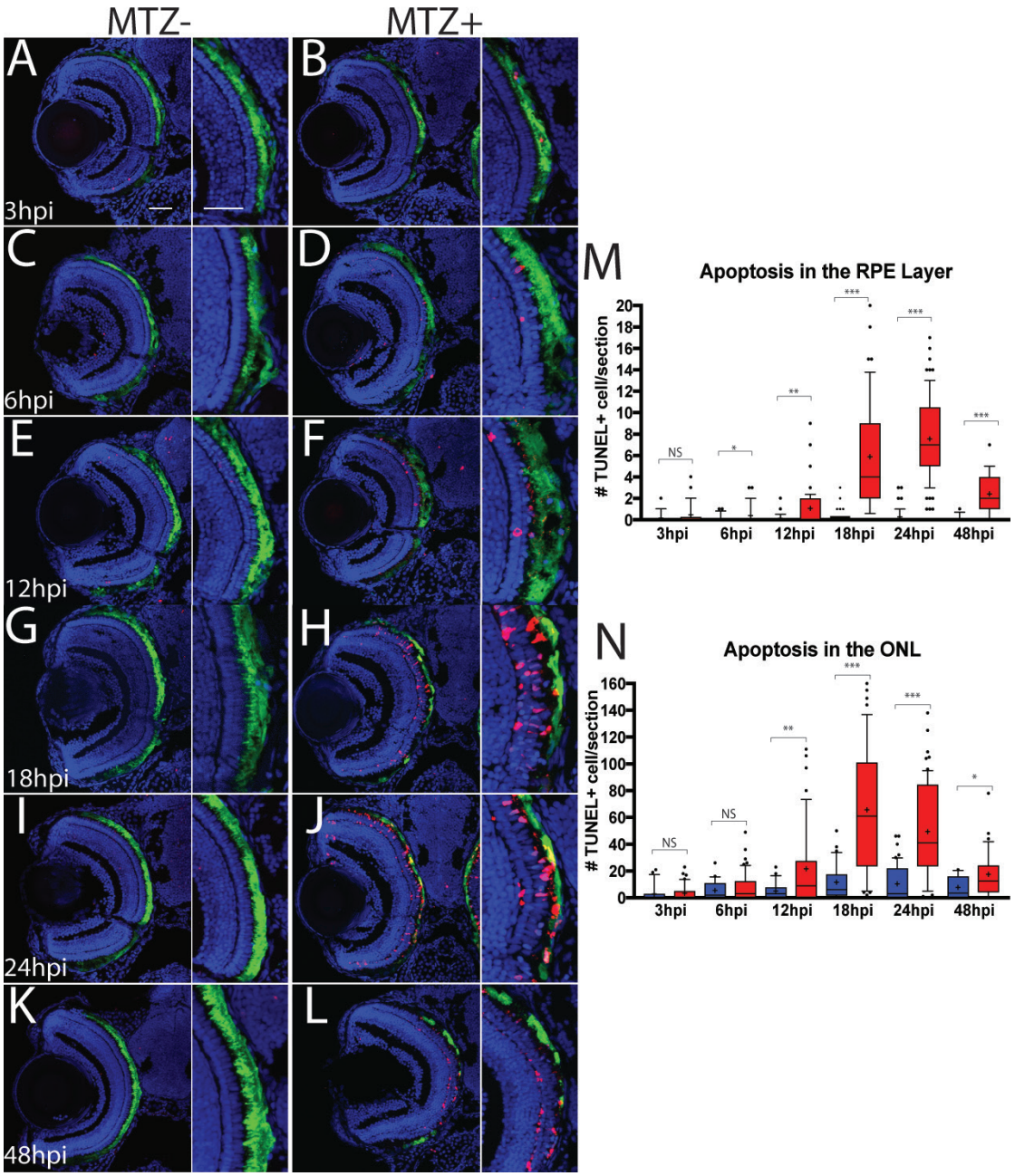

Figure 4.2: Dynamics of apoptosis following RPE ablation. (A-L) Transverse cryosections stained for TUNEL (red). (A,C,E,G,I,K) Unablated and (B,D,F,H,,J,) ablated eyes at various time points following ablation. (M) Quantification of TUNEL+ cells/section in the RPE layer (M) and ONL (N). Red bars are ablated embryos and blue bars are age-matched controls. Significance determined using Mann-Whitney U test. * $p \leq 0.01$, ** $p < 0.001$, *** $p < 0.0001$. Green=GFP, blue=nuclei. Scale bar = 40μm.

We next performed a time course using markers for RPE (ZPR2), cone photoreceptors (ZPR1), and F-actin (phalloidin) to characterize degeneration of the RPE and photoreceptors after RPE ablation (Fig 4.3). In unablated larvae, GFP colocalizes with ZPR2 in the central RPE, confirming that transgene expression is specifically restricted to the RPE. ZPR2 stain also extends further into the periphery to label less-mature RPE closer to the ciliary marginal zone (CMZ) (Fig 4.3A). Between 1 and 2 days post injury (1-2dpi), ZPR2 staining recapitulates the morphological disruption of GFP seen in Figure 4.2J, displaying identical retraction of apical processes and blebbing of the cell body (Fig 4.3D). By 3dpi, both GFP and ZPR2 signal is mostly absent in the central RPE layer, indicating that RPE cell degeneration is complete and RPE cell debris has largely been removed from the injury site (Fig 4.3J). Staining for red/green cone arrestin (ZPR1) revealed that cone photoreceptor morphology becomes disorganized, with a thickening of the cell body and extension of outer segments into the RPE layer (Fig 4.3B,E). This outer segment morphology corresponds to a marked loss of F-actin organization in outer segments. F-actin in POS is normally organized into bundles and extends perpendicularly into the RPE layer in a regular, train-track pattern (Fig 4.3C). F-actin signal in the POS becomes more diffuse, and their orientation becomes less regular (Fig 4.3F). By 3dpi, photoreceptor degeneration in the central retina peaks as well: ZPR1-positive cones are less prevalent and display a more disorganized, diffuse morphology than unablated cones (Fig 4.3K), and POS appear to have degenerated, with a near-total loss of organized F-actin structures extending into the RPE layer (Fig 4.3L).

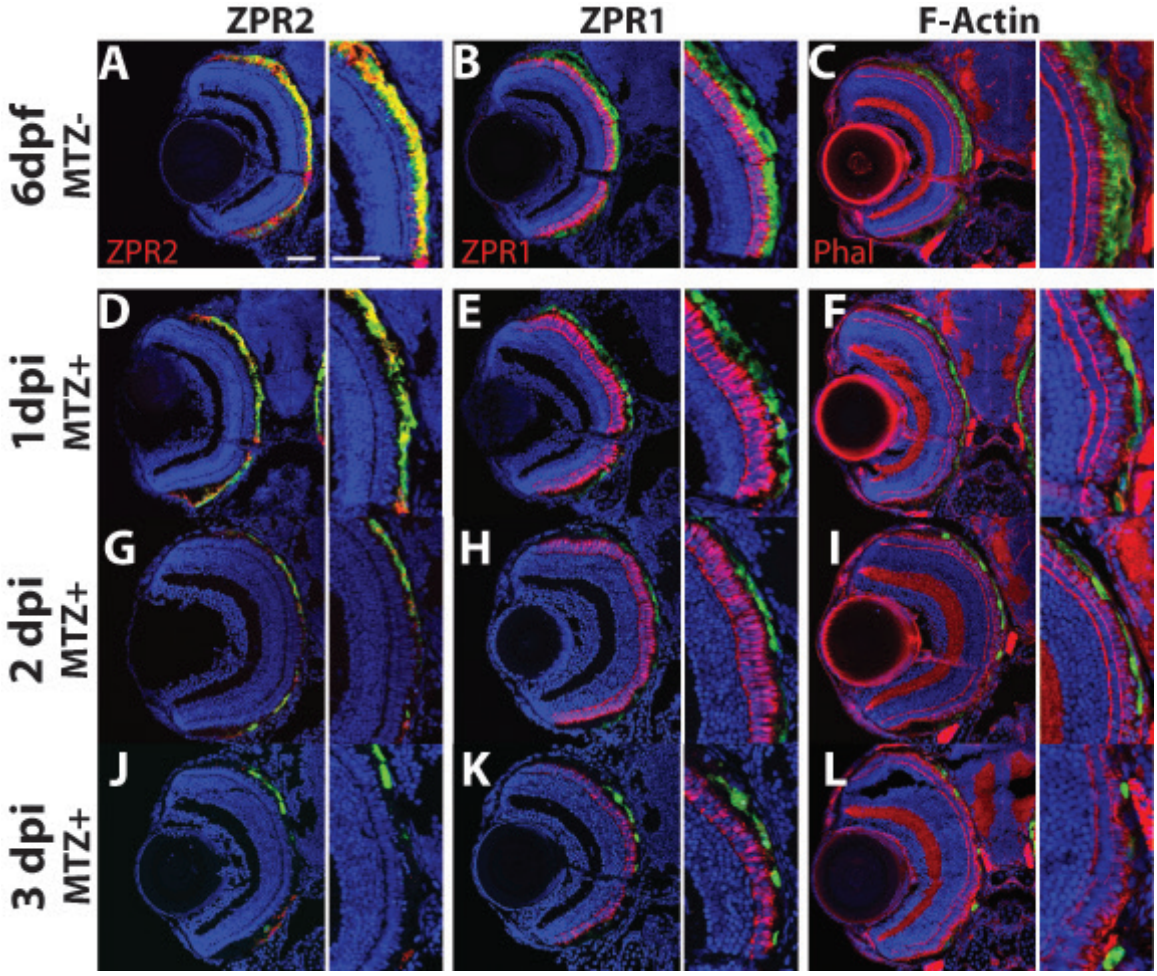

Figure 4.3: Timeline of degeneration following RPE ablation. Transverse sections of unablated 6dpf larvae stained for ZPR2 (A), ZPR1 (B) and F-Actin (C). Ablated larvae stained for ZPR2 (D,G,J), ZPR1 (E,H,K) Phalloidin (F,I,L) at 1,2,3dpi. Green=GFP, blue=nuclei, red=cell stain. Scale bar = 40μm.

To confirm that central RPE cells and POS degenerate at 3dpi, we performed transmission electron microscopy (TEM) and characterized the cellular morphology of the RPE and outer nuclear layer (Fig 4.4). Unablated RPE cells contain pigmented melanosomes (Fig 4.4E, white arrowheads), form tight junctions with adjacent RPE cells (Fig 4.4E, TJ), extend melanosome-containing apical processes to interdigitate with POS (Fig 4.4B), and phagocytose spent POS discs to form OS-containing organelles called phagosomes (Fig 4.4E, white arrow) (Fig 4C,E). The photoreceptor layer is also well organized, with readily identifiable cone outer segments (cOS) and rod outer segments (rOS) extending from properly laminated cone and rod nuclei (Fig 4.4A,B). Analysis of ablated embryos revealed severe degeneration of the RPE (Fig 4.4C,D). Identifiable RPE cells are entirely absent, and the space they once occupied has largely been replaced with a substantial amount of debris—much of it likely consisting of degrading POS—that appears as if it is either freely distributed (Fig 4.4H) or collected in membranous structures which could potentially be macrophages (white arrows, Fig 4.4C,D). The BM underlying ablated RPE becomes significantly thinner than control by 3dpi (Figure 4.4I,K $p<0.0001$) and contains perforations (Fig 4.4I, arrows). Confirming histology (Fig 4.3), the photoreceptor layer exhibits clear signs of degeneration. Most apparent is the reduction in size and integrity of POS, and, as noted above, the aggregation of degenerated POS and other cellular debris in the ablated RPE layer (Fig 4.4C,D, and Fig4.4H, arrow). The orderly stacking of photoreceptor nuclei is generally disrupted in ablated retinae, and rod photoreceptor nuclei no longer correctly localize to the outer plexiform layer (Fig 4.4C). Finally, ribbon synapse (RS) morphology is disrupted and frequently absent in in ablated embryos, suggesting that photoreceptor connectivity to bipolar cells also degrades following RPE ablation (Fig 4.4G,J).

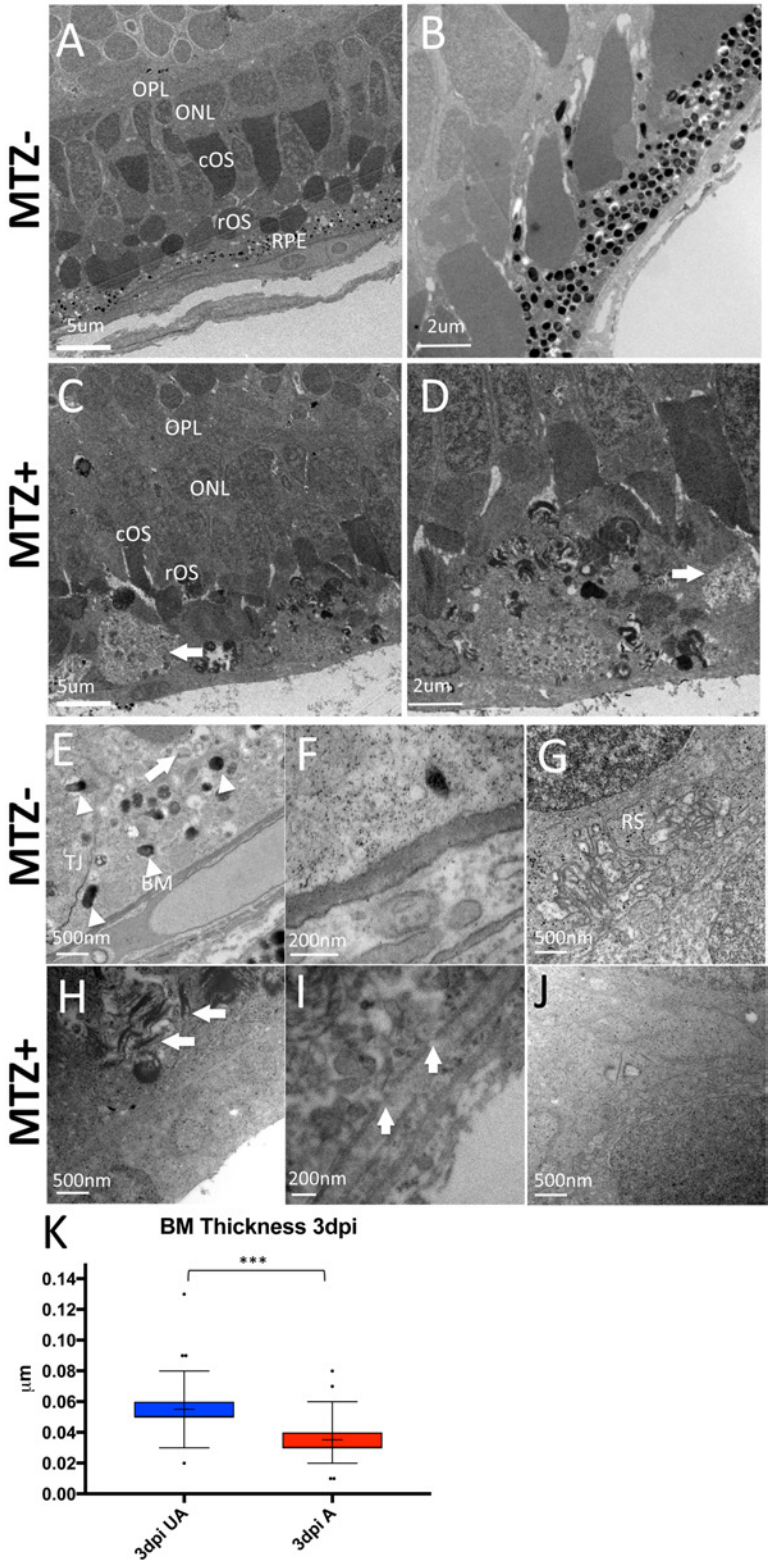
MTZ-
MTZ+
MTZ-
MTZ+
A
B
C
D
E
F
G
H
I
J
K
OPL
ONL
cOS
rOS
RPE
RS
TJ
BM
5um
2um
500nm
200nm
BM Thickness 3dpi
***
µm
0.14
0.12
0.10
0.08
0.06
0.04
0.02
0.00
3dpi UA
3dpi A

Figure 4.4

Figure 4.4: TEM images of central RPE photoreceptors at 3dpi. (A,B,E,F,G) Unablated 8dpf larvae. (C,D,H,I,J) 3dpi larvae. (A,B) Images of unablated RPE and ONL ultrastructure. (C,D) Gross ultrastructure of ablated RPE and ONL. Arrows=membrane-enclosed aggregates of debris. (E,H) magnified images of RPE cells. (E) Arrowheads = mature melanosomes, arrow=phagosome. TJ=tight junction, BM=Bruch's Membrane (H) arrows=free POS debris. Magnification of BM in unablated (F) and ablated (I) larvae. Arrows in (I) mark perforations in BM. Magnified images of ribbon synapses (RS) in unablated (G) and ablated (J) larvae. (K) Quantification of BM thickness. Student's T-test, *** $p<0.0001$.

Finally, we determined whether RPE ablation leads to functional vision defects using the Optokinetic Response assay (Gestri et al., 2012; Huang and Neuhauss, 2008; Neuhauss et al., 1999; Neuhauss, 2003; Scheetz et al., 2017) (Fig 4.5). A cohort of ablated and control larvae were exposed to a rotating full-field visual stimulus at both 1dpi and 2dpi. At 1dpi, ablated larvae appeared to saccade more frequently ($p>0.05$), but a greater percentage of saccades were not of the appropriate direction relative to stimulus (hence, "incorrect.") compared to control ($p=0.018$) (Fig 4.5A), indicating at least a partial compromise in visual system performance. 2dpi ablated larvae exhibited a significant reduction in both total saccade number ($p=0.011$) as well as in stimulus tracking gain ($p=0.0055$) (Fig 4.5B), indicating that vision is disrupted after ablation. By 3dpi, recovery of the OKR occurred, as evidenced by the recovery of the number and correctness of saccades, as well as a recovery of stimulus tracking gain.

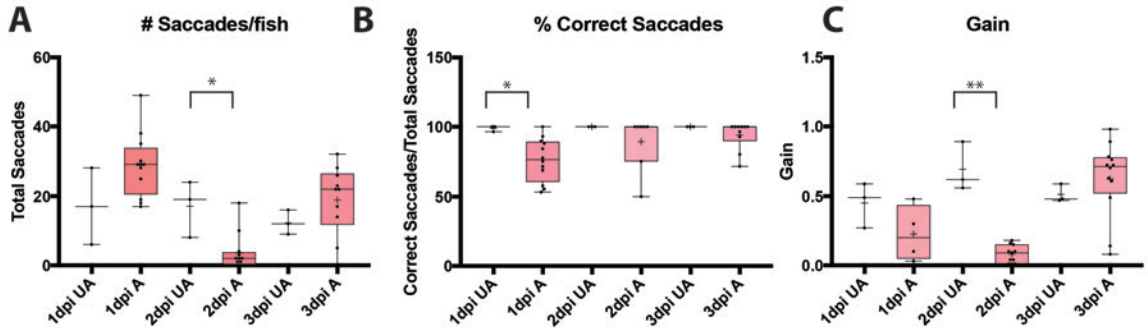

Figure 4.5: RPE ablation leads to vision defects at 1, 2, and 3dpi. (A) Quantification of the total number of saccades per fish. (B) Quantification of the percentage of saccades that were direction-appropriate relative to stimulus direction ("correct"). (C) Quantification of reflex gain. (Mann-Whitney U test, *$P < 0.05$, **$P < 0.005$).

4.2.2 Effective regeneration of the RPE following ablation

We next sought to determine whether zebrafish can regenerate the RPE after acute injury. To characterize the response of RPE cells after ablation, we performed a time course using markers for RPE (ZPR2), cone photoreceptors (ZPR1), and F-actin (phalloidin) at 4, 6, 7, and 14dpi (Fig 4.6). This time series revealed that dim GFP signal, indicating the presence of maturing RPE, reappears in the eye periphery at 4dpi. ZPR2 staining confirms that this GFP signal is confined to RPE cells, and indicates that immature RPE cells extend past GFP+ RPE cells into the injury site (Fig 4.6D, arrows). Although ZPR1 signal in the ONL is still disrupted in the ablation site, morphologically normal ZPR1-positive cones appear in the peripheral retina directly apposed to recovered GFP+ RPE cells (Fig 4.6E, arrow). Similarly, while F-actin-labeled POS remain degenerated in the central retina, POS closer to the periphery (Fig 4.6F) are better organized and extend into the RPE layer (arrow, Fig 4.6F). At 6dpi, this trend continues: morphologically normal GFP/ZPR2+ RPE cells extend further toward the center (Fig 4.6H), and ZPR1 and F-actin staining indicates that photoreceptor recovery continues to occur apace (Fig 4.6I,J). Interestingly, ZPR2-positive, GFP-negative cells form what appear to be multilaminar structures at the advancing tip of the regenerating monolayer (arrows, Fig 4.6G). By 7dpi, the injury site becomes filled in by ZPR2+ cells extending apical processes into the ONL (Fig 4.6J, arrows). Although central photoreceptor cells are still disorganized (Fig 4.6K), there is an improvement in POS architecture and organization (Fig 4.6L). By 14dpi, the RPE is populated by ZPR2/GFP double-positive RPE cells that display proper cell morphology, including extended apical microvilli (Fig 4.6M, arrows). Photoreceptor outer segments recover to the point where they are nearly indistinguishable in pattern from WT (Fig 4.6 N). While cone photoreceptors throughout the retina regain normal morphology and extend into the RPE layer, they have not yet

fully recapitulated normal cone morphology—disorganization persists, particularly in the injury site, where cones do not properly align perpendicularly to the RPE (Fig 4.6N). Finally, at 44dpi, morphologically normal GFP+ RPE populate the central retina and interdigitate with properly-oriented cone photoreceptors (Fig 4.6P,Q).

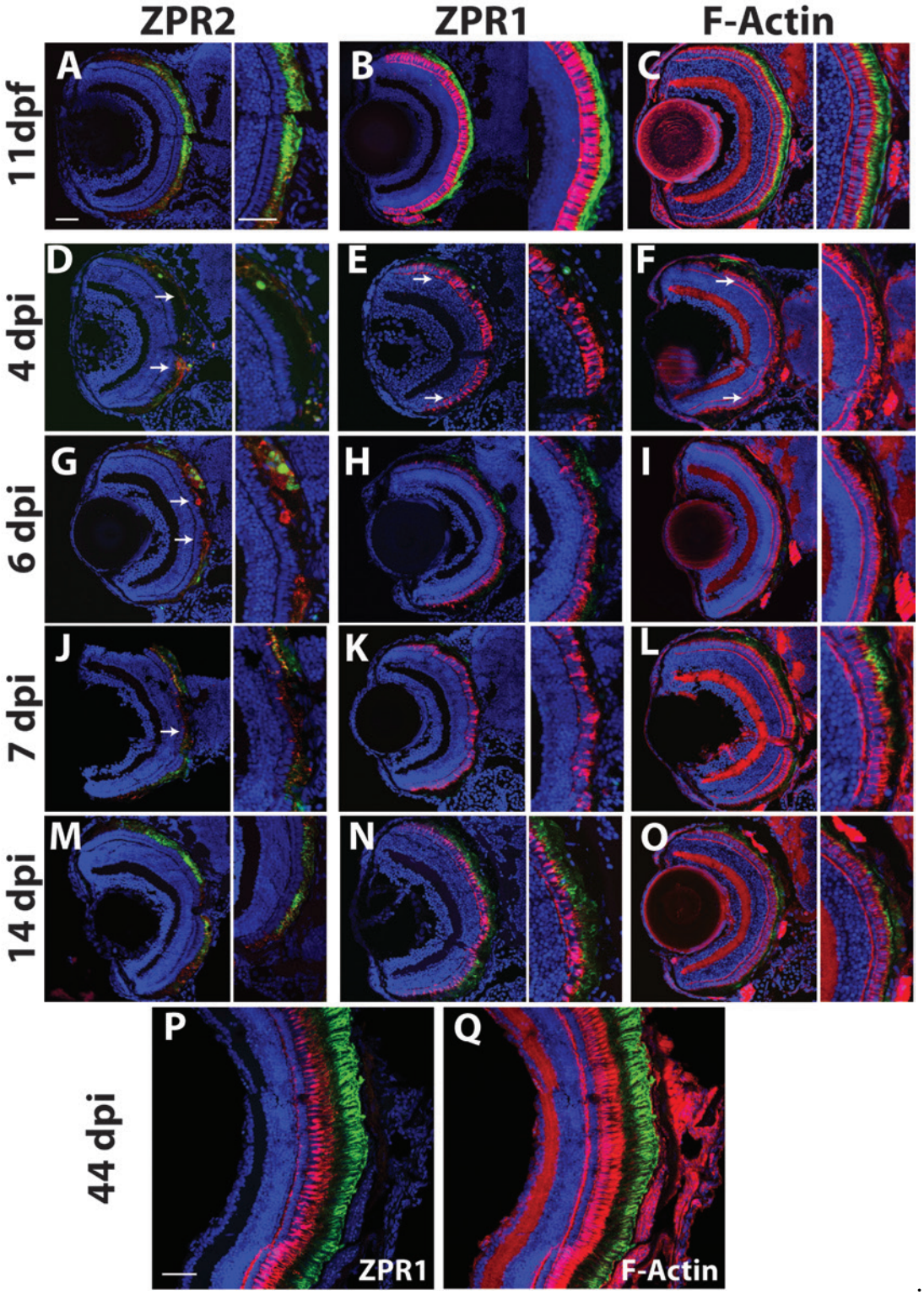
ZPR2
ZPR1
F-Actin
11dpf
4 dpi
6 dpi
7 dpi
14 dpi
44 dpi
A
B
C
D
E
F
G
H
I
J
K
L
M
N
O
P
Q
ZPR1
F-Actin

Figure 4.6

Figure 4.6: Timeline of regeneration following RPE ablation. Transverse sections of unablated 11dpf larvae stained for ZPR2 (A), ZPR1 (B) and F-Actin (C). Ablated eyes stained for ZPR2 (D,G,J,M), ZPR1 (E,H,K,N,P), and Phalloidin (F,I,L,O,Q) at 4, 6, 7, 14, 44dpi Green=GFP, blue=nuclei, red=cell stain. Scale bar = 40μm.

As noted above, variation in the severity of ablation was observed within each treatment group and this likely stemmed from natural variation of transgene expression and ablation efficiency. Even after carefully screening for ablation severity at 2dpi, some variability occurred in the timing of regeneration in each larva (compare Fig 4.6K to L). We hypothesized that these differences are accounted by unavoidable variations in ablation severity and that regeneration proceeds in a periphery-to-center fashion in each case, with milder ablation leading to quicker recovery. To test this hypothesis, we undertook longitudinal OCT analysis of RPE. We performed this analysis on a mixed cohort of mildly- and severely-ablated larvae and studied the pattern and temporal dynamics by which RPE signal returned in each larva over time (Fig 4.7). Compared to unablated embryos (Fig 4.7A), degeneration and subsequent regeneration of the RPE layer was observable in both severely- and mildly- ablated larvae (Fig 4.7B,C, yellow arrows).

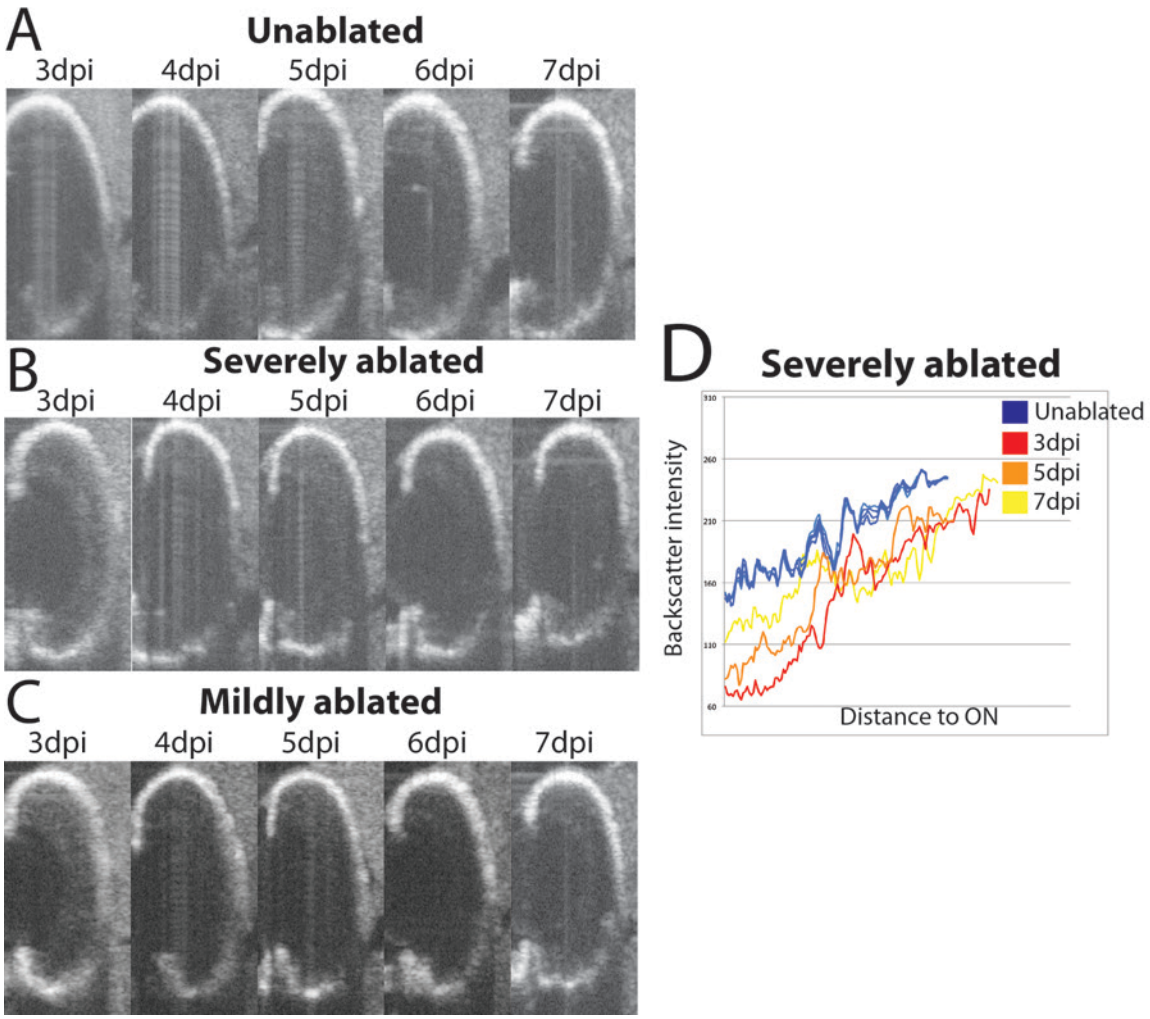

Figure 4.7: Longitudinal analysis of regeneration in mildly- and severely-ablated larvae. (A-C) Example time series of (A) unablated, (B) severely-ablated and (C) mildly ablated larvae. (D) Preliminary quantification of dorsal RPE backscatter in a severely ablated larvae as a proxy for RPE layer integrity.

To assess the morphology of regenerated RPE, we performed transmission electron microscopy (TEM) at 14dpi, when regenerated GFP/ZPR2+ RPE cells reliably populated the injury site and appeared by confocal microscopy to be morphologically normal. At 19dpf, unablated RPE cells contain melanosomes (Fig 4.8A,B,E), form tight junctions with adjacent RPE cells (Fig 4.8E, TJ), extend melanosome-containing apical processes to interdigitate with POS (Fig 4.8B), and phagocytose OS material (Fig 4.8E, white arrow). By 19dpf, the ONL is highly organized: rod nuclei are proximal to the outer plexiform layer and underlie cone nuclei, while cOS and rOS are easily distinguishable and properly localized (Fig 4.8A,B). TEM analysis confirms the presence of regenerated and functional RPE cells at 14dpi. Identifiable RPE cells containing melanosomes and projecting apical processes into the ONL are present throughout the ablated site. These RPE cells also contain phagosomes (Fig 4.8H, arrow) and appear to have repaired a healthy BM (Fig 4.8I,K). Regenerated RPE displays intriguing differences compared to unablated RPE: individual cells contain far more pigmented melanosomes, and their cell body width appears to be increased and more variable. Some recovery of the ONL is discernible: photoreceptor outer segment length has increased throughout the injury site, rod nuclei more frequently appear proximal to the OPL, and OS degeneration is no longer apparent (Fig 4.8C,D). Despite this improvement, the ONL organization has not yet improved to the level seen in unablated retinae. Nonetheless, morphologically normal ribbon synapses appear in the OPL, suggesting that photoreceptor connectivity to bipolar cells has, to some extent, successfully been repaired (Fig 4.8G,J).

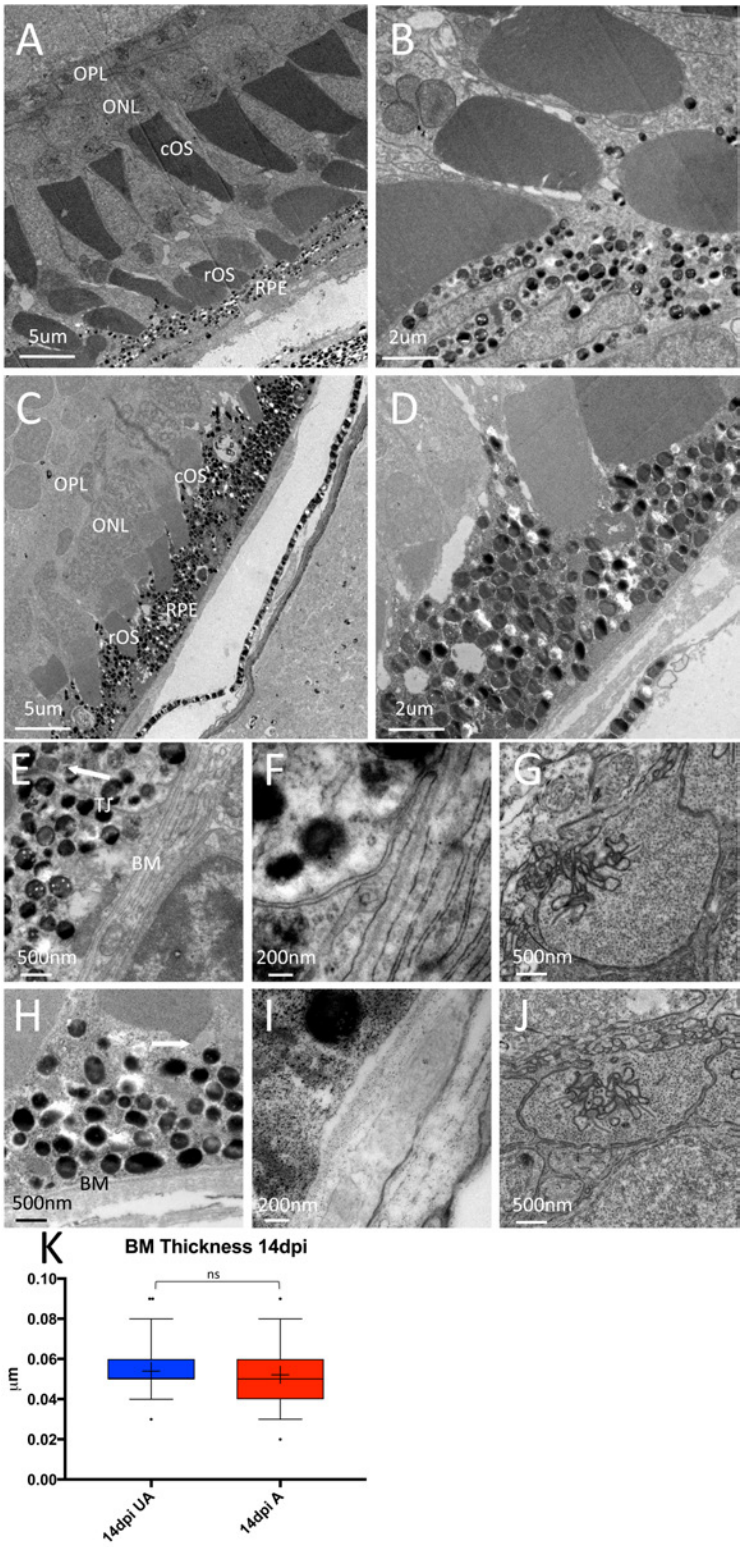
A
OPL
ONL
cOS
rOS
RPE
5um
B
2um
C
OPL
cOS
ONL
RPE
rOS
5um
D
2um
E
TJ
BM
500nm
F
200nm
G
500nm
H
BM
500nm
I
200nm
J
500nm
K
BM Thickness 14dpi
ns
0.10
0.08
0.06
0.04
0.02
0.00
µm
14dpi UA
14dpi A

Figure 4.8

Figure 4.8: TEM images confirm regeneration of central RPE and photoreceptors at 14dpi. (A,B,E,F,G) Unablated 19dpf larvae. (C,D,H,I,J) 14dpi larvae. (A,B) Images of unablated RPE and ONL ultrastructure. (C,D) Gross ultrastructure of ablated RPE and ONL. (E,H) magnified images of RPE cells. (E) Arrow=phagosome. TJ=tight junction, BM=Bruch's Membrane Magnification of BM in unablated (F) and ablated (I) larvae. Magnified images of ribbon synapses (RS) in unablated (G) and ablated (J) larvae. (K) Quantification of BM thickness. Student's T-test, *$p<0.01$.

4.2.3 Proliferative cells enter the injury site and participate in RPE regeneration

Our data thus far indicate that zebrafish are capable of regenerating a functional RPE monolayer after widespread ablation of roughly two-thirds of the original tissue, and over the surprisingly short timespan of 1-2 weeks. This rapidity of regrowth, coupled with the outside-in pattern of recovery, suggests that RPE regeneration is driven at least in part by cell proliferation. During regeneration of different tissues, proliferative cells derive either from a resident pool of progenitor cells, as occurs in blood and skin (Iyengar et al., 2015; Orkin and Zon, 2008), or from differentiated cells forming part of the injured tissue, as is the case during heart or retinal neuron regeneration (Kikuchi et al., 2010; Poss et al., 2002). BM degeneration occurs in the injury site and RPE cell proliferation following injury or loss of BM contact is widely observed (Grierson et al., 1994; Heller and Martin, 2014; Stern and Temple, 2015). Additionally, researchers recently discovered that a subpopulation of differentiated human RPE cells are capable of dedifferentiating into an RPE stem cell that can produce new RPE cells (Salero et al., 2012). For these reasons, we hypothesized that uninjured peripheral RPE cells respond to injury by dedifferentiating and proliferating to replace ablated tissue. To begin to test this hypothesis, we performed BrdU incorporation assays to elucidate the temporal and spatial dynamics by which proliferative cells arrive in the injury site (Figure 9).

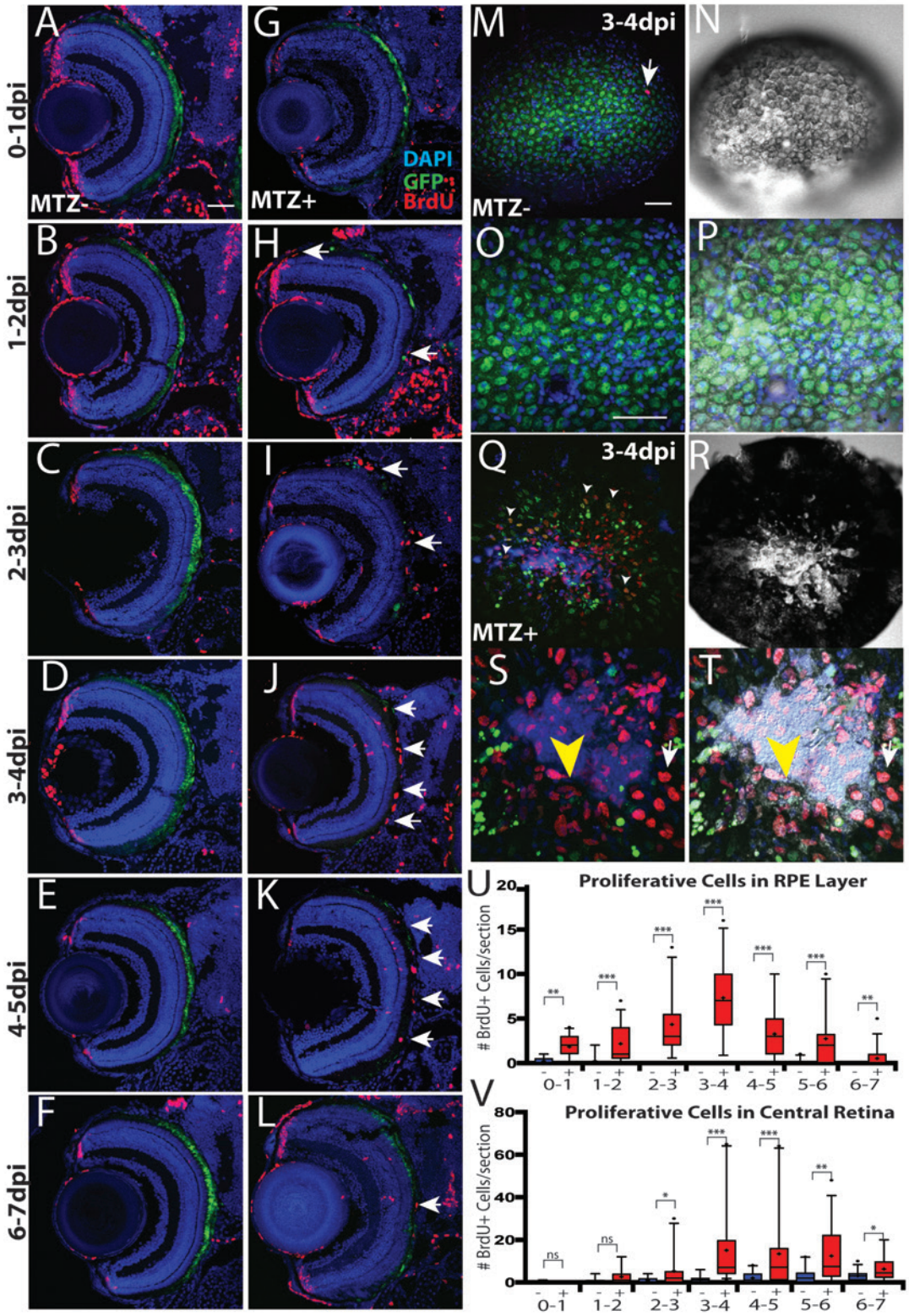
A
G
M
3-4dpi
N
0-1dpi
MTZ-
MTZ+
DAPI
GFP
BrdU
MTZ-
B
H
O
P
1-2dpi
C
I
Q
3-4dpi
R
2-3dpi
MTZ+
D
J
S
T
3-4dpi
E
K
U
Proliferative Cells in RPE Layer
BrdU+ Cells/section
4-5dpi
F
L
V
Proliferative Cells in Central Retina
BrdU+ Cells/section
6-7dpi
0-1
1-2
2-3
3-4
4-5
5-6
6-7

Figure 4.9

Figure 4.9: Proliferative cells enter the injury site during regeneration. (A-L) Transverse retinal sections of unablated (A-F) and ablated (G-L) larvae exposed to 24-hour BrdU pulses at various days post injury. (M-T) *en face* wholemount images of unablated (M-P) and ablated (Q-T) eyes from larvae exposed to BrdU between 3-4dpi. Quantification of total number of BrdU+ cells/section in the RPE (U) and central retina (V). Mann-Whitney U Test, * $p<0.01$, ** $p<0.001$, *** $p<0.0001$. Scale bar = 40μm.

Proliferative cells appear with greater frequency in the RPE layer as early as 0-1dpi. Interestingly, these cells usually appeared in one of two places: in the dorsalmost RPE layer immediately adjacent to the dorsal CMZ and in the ablated central RPE (Fig 4.9, arrows). Between 2-3dpi, the dorsal population of proliferative cells appears both to increase in number and approach the injury site, while more BrdU+ cells appear in the ablated region (Fig 4.9I). The number of proliferative cells in the RPE layer peaks between 3-4dpi (Fig 4.9U), during which time BrdU+ cells are evenly distributed in the central RPE between GFP-expressing regenerated RPE cells in the periphery (note the light GFP signal in peripheral RPE cells beginning in Fig 4.9J). As regeneration proceeds, regenerated GFP+ RPE cells appear closer to the center of the injury site and the number of BrdU+ cells in the RPE layer decreases (Fig 4.9K,L). Interestingly, in transverse sections BrdU+ nuclei seem to be preferentially distributed in actively regenerating regions of the RPE, and rarely persist in regenerated GFP+ areas. To better visualize the distribution of proliferative cells in relation to regenerating tissue, we enucleated eyes from larvae exposed to BrdU during peak proliferation (3-4dpi) and acquired *en face* views of the RPE (Fig 4.9M-O). In unablated eyes, GFP signal labels individual RPE cells throughout the central RPE, and BrdU+ nuclei appeared to be restricted to the overlying choroid (arrow) (Fig 4.9, M-P). Wholemount imaging of BrdU+ nuclei in ablated larvae confirmed that proliferative cells are primarily located in the injury site (Fig 4.9 Q-T). Increased DAPI signal within the injury site is from retinal neurons that were uncovered by removal of overlying RPE tissue. Interestingly, GFP/BrdU double-positive nuclei were also detected, and were chiefly located in the regenerating RPE immediately peripheral to the injury site (white arrowheads, Fig 4.9Q). Meanwhile, the injury site was divided into two zones: the central, unpigmented zone and the transitional zone. In the unpigmented zone, BrdU+ nuclei appear to be proliferative

and display no regularly identifiable RPE morphology. Meanwhile, in the transitional zone, BrdU+ cells are observed in various stages of pigmentation (yellow arrowhead, Fig 4.9T), and also begin to develop the rounded nuclear appearance of differentiated RPE cells (white arrow, Fig 4.9T). Consistent with our findings in TEM, regenerated RPE cells displayed greater pigmentation than in unablated RPE. Finally, we observed BrdU+, Müller glia-derived retinal precursor cells (MGPCs) in the retina, indicating photoreceptor regeneration, which is well studied is also occurring (R. L. Bernardos et al., 2007; Brockerhoff and Fadool, 2011; Kassen et al., 2007; Thummel et al., 2007). We quantified the number of BrdU+ cells in the ONL and found that proliferative cells appear in the ONL at similar times as in the RPE (Fig 4.9V).

These data suggest that proliferative cells initially enter the injury site from the periphery and that after they interact with the ablated region they cease proliferating and differentiate to form new RPE cells. To determine whether cells that proliferate immediately following ablation enter the injury site, we pulsed ablated larvae with BrdU between 0-1dpi, and with EdU at 3dpi before fixation and analysis (Fig 4.10A-B). Transverse sections revealed that at 3dpi, BrdU+ cells appear throughout the injury site (white arrowheads, Fig 4.10B) and that some remain proliferative (BrdU/EdU+, white arrow). Interestingly, preliminary analysis revealed that these EdU/BrdU+ nuclei only appear in the injury site following ablation (Fig 4.10C), and appeared very similar to RPE nuclei. Indeed, some EdU/BrdU+ cells appeared to be lightly pigmented (Fig 4.10B"), further suggesting they may be differentiating into an RPE cell. To determine whether these cells stably integrated into the regenerated RPE, we exposed ablated larvae to BrdU at 18-42hpi and fixed them at 8dpi (Fig 4.10C). Transverse sections revealed the presence of pigmented, GFP+ nuclei in the central RPE (arrows, Fig 4.10D). Together, these data

suggest that proliferative cells enter the RPE soon after injury and ultimately differentiate into the regenerated RPE layer

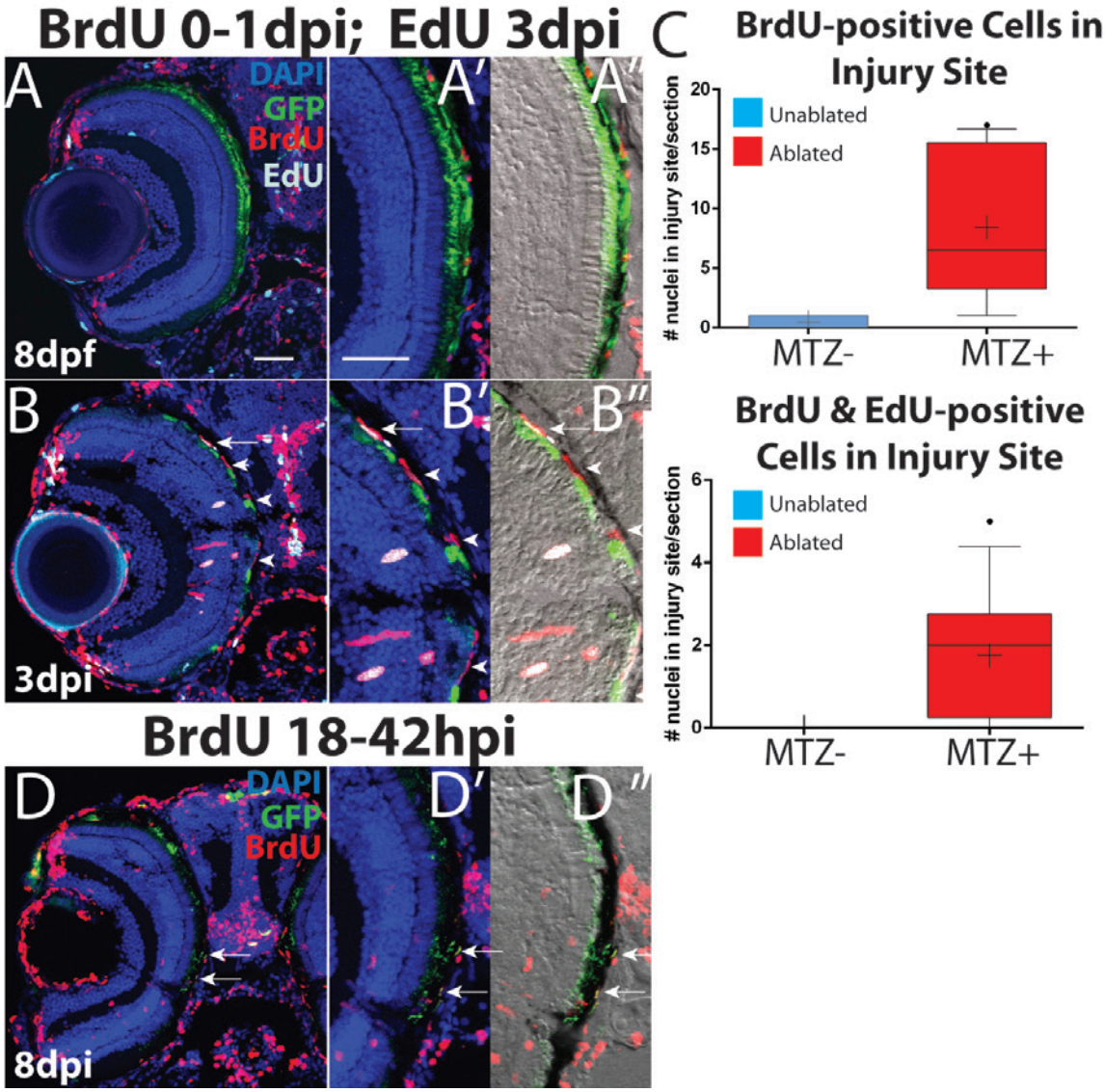

Figure 4.10: Pulse-chase analysis of proliferating cells in the ablated RPE. (A) Transverse sections from unablated larvae exposed to BrdU from 5-6dpf and pulsed with EdU for 2 hours before fixation at 8dpf. (B) Ablated larvae were exposed to BrdU from 0-1dpi and pulsed with EdU for 2 hours before fixation at 3dpi. (A',B',C') Magnified inset of BrdU/EdU. (A",B",C") Magnified inset of BrdU/EdU and DIC. White arrows in (B,B',B") denote proliferative RPE-like cells. White arrowhead indicates unpigmented, previously-proliferative RPE-like cell in the injury site. (C) Preliminary quantification of BrdU/EdU+ and BrdU+ nuclei in the injury site. (D) Larvae exposed to BrdU 18-42hpi and fixed at 8dpi. Scale bar = 40μm.

Finally, we used TEM to investigate the cellular appearance of RPE cells at 3dpi and determine whether RPE cells could be identified extending toward the injury site (Fig 4.11). These analyses revealed the presence of a regenerating RPE layer which extended into the injury site in a pattern remarkably consistent with that seen in Figure 10 (dotted yellow line, Fig 4.11A). A closer examination of the cells revealed similar morphology in regenerating cells to that seen in Figure 9: namely, a peripheral transitional zone consisting of moderately-to-lightly pigmented cells (Fig4.11B) and a lightly-to-unpigmented central zone nearer to the injury site (Fig4.11A,C). In the transitional zone (Fig 4.11B), morphologically normal RPE cells form tight junctions (white arrows) with a lightly pigmented RPE cell (marked by black arrowheads) which contains a cell nucleus that could be one of the proliferative nuclei seen in the pulse-chase experiment (red arrow, compare to Fig 4.11A). Interestingly, this cell also appears to contain a large phagosome, likely consisting of cellular debris from ablated RPE cells (green arrow). At this dorsal region, BM thickness (white arrowhead) is normal. While degenerated POS are present in the ONL, there is also evidence of POS regrowth. At the injury site, the identifiable RPE cell (marked by black arrowheads) does contain a somewhat morphologically-normal nucleus (red arrow) and small number of melanosomes. Otherwise, normal aspects of RPE cell morphology are absent (Fig 4.11C): the BM is so thin that at his magnification it is nearly undetectable (white arrowheads), and the RPE cells are compressed between the choroid and what appear to be large aggregations of debris that may be internalized within macrophages (green arrows). This cell appears to terminate at the black arrow, though we cannot rule out the possibility that it continues either in a different section plane or with less-identifiable morphology.

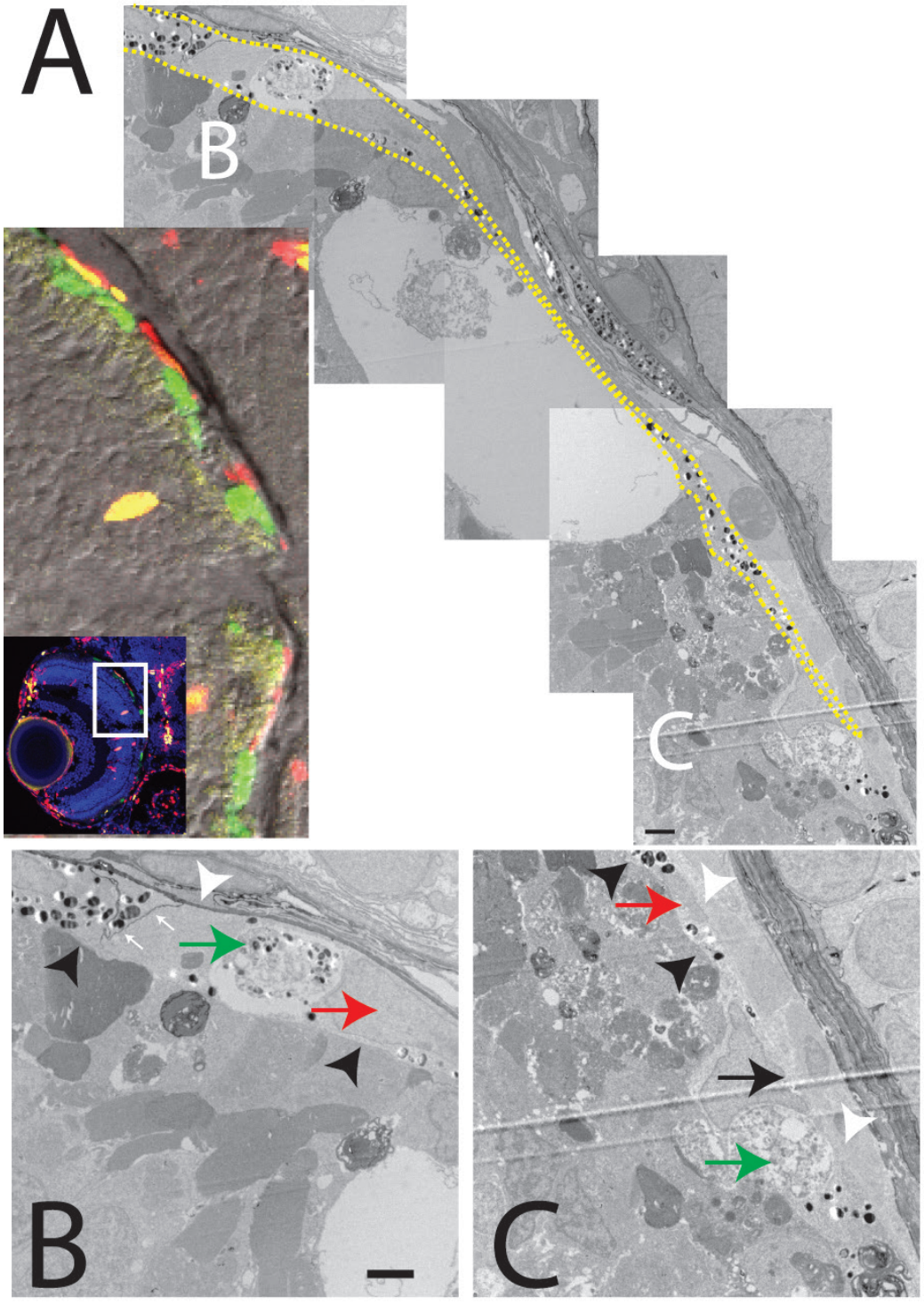

Figure 4.11

Figure 4.11: TEM analysis of regenerating RPE cells (A) Example section from ablated BrdU/EdU pulse-chase larva and overlaid TEM images of the dorsal eye. The regenerating RPE layer is highlighted with a black dotted line. Images in (B) and (C) are magnified views of the panels labeled “A” and “B” in white. (B) Dorsal transition zone. Note pigmented RPE cell on the left side of the image bordering an unpigmented epithelioid cell. (C) Injury site. The furthest discernible tip of the regrowing RPE layer terminates at the third black arrow. Black arrows=apical RPE surface, green arrows=possible GFP+debris, red arrows=putative regenerating RPE cell nuclei, white arrowheads=BM. Scale bar = 2μm.

4.3: DISCUSSION

Despite intense interest in the development of therapies to treat neurodegenerative diseases involving the RPE, very little is known about the process by which RPE cells successfully integrate into damaged tissue in any animal model, and virtually nothing is known about RPE regeneration in zebrafish. In this Chapter, we characterized a novel zebrafish model for AMD in which genetic ablation of mature RPE cells leads to degeneration of underlying photoreceptors. We used this model to show, for the first time, that zebrafish are capable of regenerating the RPE after widespread injury. Finally, we provided evidence suggesting that unablated RPE cells in the periphery respond to ablation by rapidly proliferating and regenerating a functional RPE monolayer in a periphery-central manner.

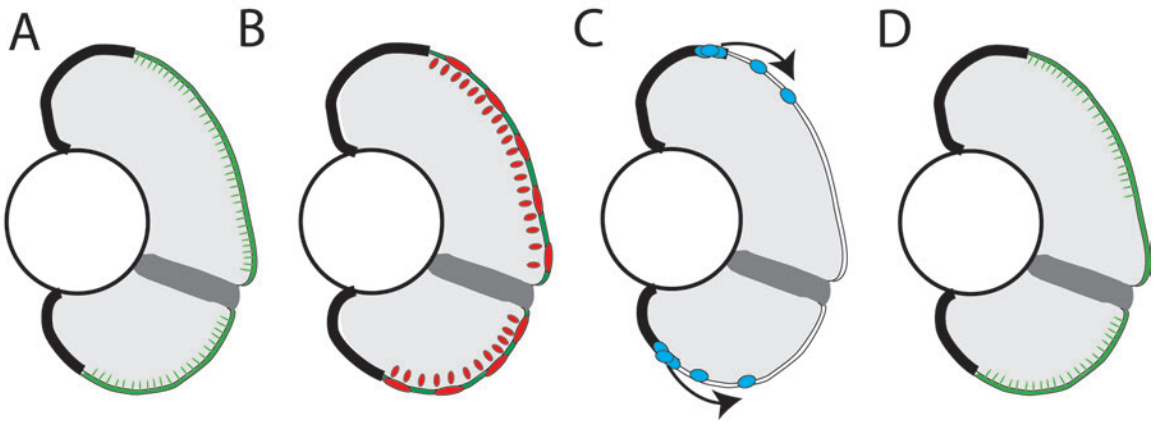

Figure 4.12: Model of RPE regeneration in zebrafish. (A) NfsB-GFP is specifically expressed in mature RPE cells in the central two-thirds of the eye. (B) Ablation leads to apoptosis and degeneration of RPE which is rapidly followed by degeneration of phtoreceptors. (C) A robust proliferative response, which likely arises from unablated RPE cells, occurs and begins to regenerate the injury from the periphery inwards. (D) Successful regeneration of a functional layer is complete by 2wpi.

4.3.1: RPE ablation and photoreceptor degeneration

In our model, nitroreductase-mediated ablation of the RPE in PTU-treated larvae is rapidly followed by severe degeneration of underlying photoreceptors (Fig 4.3-4.4) and loss of vision (Fig 4.5). While the specific causes of AMD in human patients remain unclear, RPE and photoreceptor cell degeneration occurs in large part due to apoptosis (Adler et al., 1999; Dunaief et al., 2002; Portera-Cailliau et al., 1994), though other mechanisms of cell death have been found to be involved with AMD-related degeneration, such as necroptosis (Hanus et al., 2015) and pyroptosis (Tseng et al., 2013; Wang et al., 2016). The nitroreductase system converts MTZ into a potent DNA crosslinking agent that triggers apoptosis in targeted cells (Bridgewater et al., 1995; Knox et al., 1988), mimicking the starting point of AMD degeneration. We confirmed that application of MTZ rapidly leads to the degeneration of all GFP+ RPE cells via apoptosis and found that RPE degeneration was quickly followed by apoptosis and degeneration in the photoreceptor layer (Figs 4.1-2). As photoreceptor degeneration continued, we regularly observed what appear to be delaminated and pyknotic nuclei in the ONL that are not TUNEL+ (e.g. Fig 4.2H). These cells may simply be in advanced stages of apoptotic degeneration such that they are no longer detectible by TUNEL. Alternatively, these cells could be degenerating via an alternate pathway, similar to degeneration seen in AMD patients. Further characterization of the cell death pathways activated in photoreceptors following ablation might yield valuable clues into the interaction between degenerating RPE and photoreceptors in AMD pathogenesis.

To our knowledge, this is the first model that involves the specific genetic ablation of a large contiguous area of RPE. The only other study using genetic ablation of RPE as an injury model expressed diphtheria toxin in a subpopulation of mouse RPE and led to the variable and patchy ablation of 60-80% of total RPE cells and found that

unaffected RPE cells expanded to encompass the area vacated by ablated cells to preserve the RPE monolayer and choriodcapillaris, but were ultimately unable to restore proper photoreceptor health and retinal function (Longbottom et al., 2009). This process did not involve RPE cell proliferation and the authors hypothesized that this was because BM integrity was not compromised by ablation, and this suppressed RPE cell proliferation. Our ablation model creates a more severe lesion, which may explain why we observe such a different response. Indeed, our ablation leads to a significant decrease in BM thickness and integrity (Figure 4.4). That specific RPE ablation leads to BM breakdown and compromise may provide insight into the mechanisms underlying the initiation of CNV at the onset of exudative AMD. During CNV, choroidal endothelial cells penetrate through the BM and grow into the subretinal space, and the question of whether this process is initiated by the degeneration of the choriocapillaris or of RPE remains controversial (Bhutto and Lutty, 2012; Biesemeier et al., 2014; Korte et al., 1984). Our results suggest that the RPE is required for BM maintenance. A logical next step would be to determine if the choroidal vasculature invades the subretinal space following degeneration, as this would provide evidence that RPE degeneration is causative of CNV.

In summary, although our system does not recreate the underlying causes of AMD, it does model the end stages of AMD neurodegeneration and therefore represents a clinically-relevant starting point for studying RPE regeneration.

4.3.2: RPE regeneration

Our model posits that injury-adjacent RPE cells respond to RPE ablation by proliferating and generating RPE progenitor cells which progressively move into the injury site to reform the RPE (Fig 4.12C). We hypothesize that unablated RPE cells

proliferate in response to ablation in the following mechanism: (1) unablated RPE cells in the periphery expand into the subretinal space created after RPE degeneration. (2) Interaction with degenerating BM reduces contact inhibition and initiates proliferation. RPE cell expansion into territory vacated by ablated neighboring RPE is commonly observed (Al-Hussaini et al., 2009; Grierson et al., 1994; Longbottom et al., 2009). Here, we provide evidence indicating that RPE cells immediately proximal to the injury site spread into the space created by ablated tissue (Fig 4.11A), and that BM is degraded within the injury site (Fig 4.4). Loss of BM contact induces RPE proliferation in many models which ultimately leads either to pathology (PVR) or an incomplete attempt at regeneration and formation of structurally abnormal RPE (Anderson et al., 1981; Grierson et al., 1994; Hergott et al., 1993; Hiscott et al., 1999; Stern and Temple, 2015; Wang et al., 2003). This mechanism might also explain why we identified a significant increase in cell proliferation between 0-1dpf and proliferative cells incorporating BrdU at that time point end up in the regenerating RPE (Fig 4.9):

RPE regeneration appears to proceed in a peripheral-inward manner, with new RPE cells first appearing in the periphery and expanding further into the eye over time (Fig 4.6). As this proceeds, regenerating RPE cells form a complex structure comprised of mature RPE in the periphery and immature (ZPR2-positive, GFP-negative) RPE cells at the leading tip (Fig 4.6D,G). These cells are also likely proliferative: they display similar rounded morphology to the BrdU+ cells in the RPE layer during peak proliferation, and RPE layer proliferation peaks around the same time that these structures enter the injury site to repopulate the RPE (Figs 4.6-7, 4.9). We found that these regenerative structures were generally divided into three zones (Fig 4.9Q-T): (1) nonproliferative and morphologically normal GFP+ RPE cells in the periphery, (2) pigmented GFP+/BrdU+ cells (Fig 4.9Q, inset) proximal to the injury site, and (3)

proliferative ZPR2+/GFP-negative cells within the injury site, which are at various early stages of RPE differentiation (Fig 4.6T, yellow arrow). Cells in the second and third transition zones often appeared to be in close proximity to bright GFP+ puncta (Figs 4.6,9), which likely consist of cellular debris generated by ablated GFP+ RPE cells. RPE cells are highly phagocytic (Kevany and Palczewski, 2010; Mazzoni et al., 2014; Strauss, 2005) and it is possible that they internalize cellular debris from within the injury site as they progress inward. Further work is needed to determine whether or not the phagocytosis of cellular debris by regenerating RPE cells occurs, and whether it informs the regenerative response, perhaps by maintaining a proliferative state or directing the differentiation of regenerating RPE cells.

Following ablation, we saw a significant reduction of visual system performance as determined by analysis of the OKR, but were surprised to find recovery of the OKR by 3dpi (Fig 4.5). During our pulse-chase analysis of early proliferating cells following injury, we observed the integration of BrdU+ cells into the photoreceptor layer by 3dpi (Fig 4.10A,B). This suggests that this recovery of OKR may be the result of the integration of photoreceptors from the CMZ. Further experiments will be necessary to determine whether this is the case, or whether this early OKR recovery could be driven by the early regeneration of RPE and photoreceptors in the periphery during the earliest time points of RPE regeneration.

It is important to point out that we have preliminary evidence indicating that RPE ablation elicits a strong immune response involving the invasion of leukocytes into the injury site. We observed highly motile cells containing RPE debris exiting the eye during stages of peak regeneration, and have observed phagocytic cells which may be macrophages in our TEM analysis of ablated larvae (data not shown). If present in the injury site, these macrophages would also likely be BrdU+ and display phagocytic

behavior. Therefore, further work is required to distinguish between phagocytic immune cells and regenerating RPE.

We observed a clear correlation between RPE and photoreceptor regeneration (Fig 4.6). This was not surprising, since photoreceptors and RPE cells depend upon each other for their terminal differentiation during development (Pearson et al., 2005; Strauss, 2005). Interestingly, photoreceptors regenerate after ablation at very similar times as the RPE: peak MG proliferation occurs by 4dpi, and regeneration is considered complete by 14dpi (Bernardos et al., 2007; Qin et al., 2009). This may indicate that RPE cells are capable of regenerating faster than photoreceptors are regenerated. Further supporting that conclusion, we found that RPE regeneration appeared to be accelerated in larvae that were not treated with PTU and therefore had reduced ONL degeneration (data not shown). Taken together, these data indicate that RPE regeneration depends upon interaction with healthy photoreceptors.

While a functional RPE monolayer capable of phagocytosing POS is restored by 14dpi, it displays clear differences from unablated controls (Figure 4.8). Most obvious is an increased density of pigmented melanosomes, which correlates with observations earlier in regeneration (Figure 4.9). This likely occurs because regenerating RPE cells were not inhibited by PTU as they differentiated and therefore were able to pigment to a greater degree than unablated controls, which were exposed to PTU during highly melanogenic developmental time points. We were unable to easily identify tight junctions in our TEM analysis, which could indicate that they have yet fully formed by 14dpi, or be obscured by the densely-packed melanosomes. Regenerated RPE cells also appeared to be slightly hypertrophic and had variable cell body thickness. In contrast, regenerated RPE cells in mammalian models were often hypopigmented and/or formed multilaminar structures (Heriot and Machemer, 1992; Lopez et al., 1995; Priore et al., 1995; Roider et

al., 1992). Hypertrophic RPE is commonly associated with AMD (Bressler 1994), and has been postulated to be the result of limited RPE cell proliferation during failed attempts at endogenous repair of RPE atrophy (Stern et al., 2015; Stern and Temple, 2015). Therefore, RPE hypertrophy at 14dpi may indicate that these cells were recently proliferative. Finally, our TEM analysis of the regenerated RPE also indicates that zebrafish RPE cells are capable of repairing the BM (Fig 4.8). In human, the BM undergoes a series of changes during aging that are thought to underlie AMD pathogenesis and inhibit RPE cell function, and this forms a major barrier in the success of RPE transplant therapies (Binder et al., 2007; Booij et al., 2010). Learning more about the mechanisms underlying BM repair in zebrafish may provide critical insights into improving transplant survival and reintegration.

While we present strong evidence that regenerated RPE cells derive from unablated peripheral RPE cells, we cannot definitively establish the source of regenerated RPE cells without performing lineage tracing experiments. Therefore, other cell populations could be responsible for regenerating new RPE. Indeed, Müller Glia cells, which are responsible for regenerating lost photoreceptors (Fausett and Goldman, 2006; Goldman, 2014), are actively generating MGPCs which, as noted above, are regenerating photoreceptors at identical time points and in regions directly adjacent to the ablated RPE layer (Fig 4.9). While unlikely, it is formally possible that MGPCs could transdifferentiate into RPE cells while they are in the ONL and encounter the ablated RPE layer. Another additional possible source of regenerated RPE cells is the CMZ. The CMZ is a specialized niche of multipotent retinal adult stem cells located in the retinal periphery which generates new retinal neurons throughout the life of the zebrafish (Raymond et al., 2006). The CMZ has also been shown to contribute to retinal regeneration following neuronal injury (Fischer et al., 2014; Raymond et al., 2006;

Stenkamp et al., 2001), and it was recently determined that *rx2+* stem cells in the CMZ generate RPE cells as well as retinal neurons (Reinhardt et al., 2015). While the reported rate at which CMZ stem cells generate new RPE cells during normal development appears to be too slow to account for the speed with which RPE tissue regenerates, we cannot exclude the possibility that *rx2+* stem cells in the CMZ respond to RPE ablation by increasing the rate at which they generate new RPE cells, much as Müller glia do in response to retinal injury. Interestingly, we observed what appeared to be reduced proliferation in the CMZ following RPE ablation (data not shown), which could either suggest that some sort of injury signal suppresses RPE proliferation, or that CMZ responds to RPE ablation by increasing the rate at which it generates RPE cells at the expense of retinal cells. We also find that regenerated RPE cells always first appear in the periphery, quite close to the CMZ (Fig 4.6). To clarify the source of regenerated RPE, and to determine the genetic mechanisms underlying RPE regeneration, it is necessary to develop genetic tools enabling lineage tracing experiments of uninjured RPE. Once these tools are in place and we have identified the source of regenerated RPE, we will be able to isolate cells as they regenerate to determine the genetic and molecular mechanisms driving the remarkable regenerative behavior of zebrafish RPE cells.

In summary, we have generated a novel zebrafish model of AMD wherein the specific ablation of mature RPE cells leads to photoreceptor degeneration, have demonstrated that zebrafish RPE can regenerate, and that RPE regeneration involves a robust proliferative response. Finally, we have provided evidence suggesting that uninjured RPE cells are responsible for regeneration. These data establish a novel zebrafish model of endogenous RPE regeneration that will aid the development of stem cell therapies by enabling the study of the process by which RPE cells integrate with damaged retinal tissue.

Chapter 5: Future Directions

5.1: Summary of work

This dissertation focuses on the development and regeneration of the RPE, which performs critical roles in the development and function of the eye. Rho GTPases are small G-proteins that regulate many cell processes critical for eye development, including cell cycle, cytoskeletal dynamics, polarity and membrane trafficking. In Chapter 2, I generated and validated 10 novel transgenic lines that enable the GAL4-specific modulation of Cdc42, RhoA and Rac1. These lines will useful both to the wider zebrafish community and for the study of optic cup morphogenesis and RPE development/function. In Chapter 3, I characterized two novel zebrafish alleles for oculocutaneous albinism and established a role for N ethyl maleimide-sensitive factor B (nsfb) in regulating the maturation of melanosomes in the RPE. In Age-related Macular Degeneration (AMD), RPE atrophy leads to the death of underlying photoreceptors. No FDA-approved therapy exists which can replace lost RPE. In Chapter 4, I characterized a novel model of AMD in zebrafish whereby specific ablation of the RPE mimics AMD pathology, and show, for the first time, that zebrafish are capable of regenerating the RPE. Further, I provide evidence suggesting that injury-adjacent RPE cells respond to injury by proliferating to generate RPE progenitor cells that form a new RPE layer. These results lay the groundwork for deeper study into (1) the genetic mechanisms underlying RPE regeneration, (2) the interactions between regenerating RPE and its environment, and (3) the role the immune response plays in modulating RPE regeneration. Understanding more about these processes will aid the development of AMD therapies.

5.2: Determining the genetic underpinnings of Retinal Pigment Epithelium Regeneration

In Chapter 4, I presented evidence suggesting that unablated peripheral RPE cells respond to ablation by proliferating and regenerating the RPE. Though these data strongly suggest that RPE-derived cells regenerate the RPE, there are alternative cell populations that could theoretically regenerate the RPE. As discussed in Chapter 4.3.2, two of the likeliest alternative sources of regenerated RPE are *rx2*-positive cells in the CMZ (Reinhardt et al., 2015) and Müller Glia-derived progenitor cells (MGPCs) (Fausett and Goldman, 2006). To determine which population of cells is the source of regenerated RPE, it is necessary perform cre-based lineage tracing experiments.

To achieve this, I have developed a number of transgenic lines and will employ the following lineage tracing strategy: first, a CreER driver line will be crossed with the *ubb:*floxGFP-dsRed transgenic (Mosimann et al., 2011). *rpe65a*:Crimson-t2a-NfsB will be injected into double-transgenic embryos to create patches of MTZ-sensitive Crimson+ RPE clones. After indelibly labeling the mature RPE by stimulating Cre activity with tamoxifen, I will ablate Crimson+ patches of RPE cells by adding metronidazole. After recovery, I will then determine whether dsRed-positive cells enter the injury site and fill in the damage (Figure 5.1A). To indelibly label unablated RPE, I have generated and am currently validating *rpe65a*:GAL4;4xnr:CreER transgenic zebrafish. I have also generated and am attempting to validate *rx2*:GAL4;4xnr:CreER transgenics to label CMZ cells. Finally, we have obtained the Müller glia-specific *gfap*:CreER line (Briona et al., 2015) and will use it to determine whether MGPCs transdifferentiate into RPE cells to regenerate the damage.

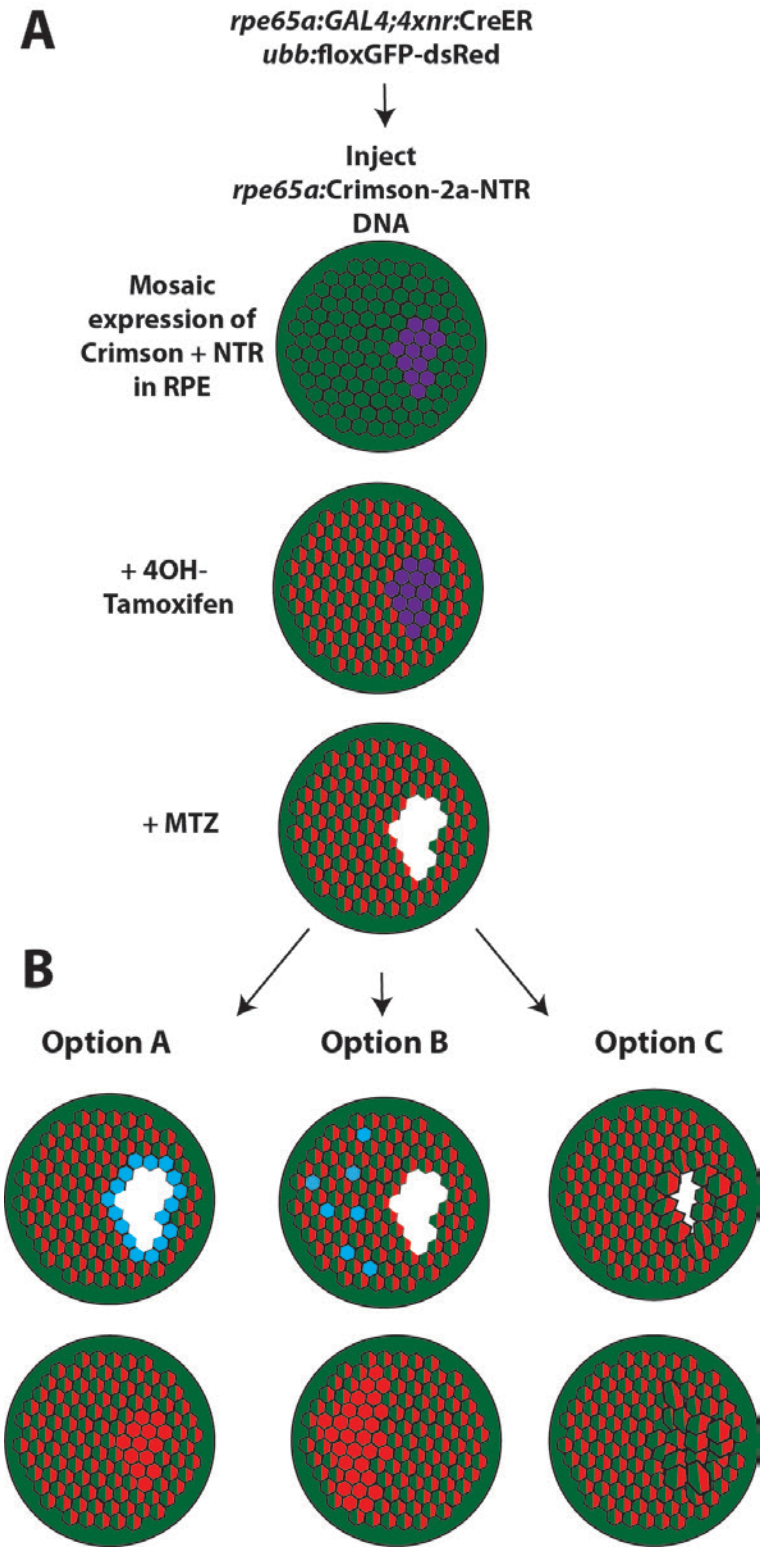
A
rpe65a:GAL4;4xnr:CreER
ubb:floxGFP-dsRed
Inject
rpe65a:Crimson-2a-NTR
DNA
Mosaic
expression of
Crimson + NTR
in RPE
+ 4OH-
Tamoxifen
+ MTZ
B
Option A
Option B
Option C

Figure 5.1

Figure 5.1: Lineage tracing strategy. All cartoons represent an en face view of the RPE. (A) RPE65a: rpe65a:Crimson-2a-NTR will be injected into rpe65a:CreER;ubb:floxGFP-mCherry embryos to create mosaic patches of Crimson-NTR cells in the RPE (purple). Addition of Tamoxifen from 4-5dpf will activate mCherry expression in RPE cells (red/green). Addition of Metronidazole (MTZ) at 5dpf will ablate Crimson-NTR+ RPE cells. (B) Several possible outcomes are possible from this experiment: Option A, RPE cells adjacent to the injury site respond by proliferating (blue), and their daughter cells (red) fill in the injury site. Option B, a subset of RPE cells away from the injury site respond by proliferating (blue). Daughter cell integration into the RPE then enables uninjured RPE cells adjacent to the injury site to fill in lost RPE. Option C, adjacent RPE cells respond to damage by expanding to cover the lesion site (i.e. no proliferative response).

With these tools in hand and the source of RPE cells determined, we would be able to perform live confocal imaging series to finely determine the kinetics of RPE regeneration. After this, we could interrogate the genetic mechanisms underlying RPE regeneration by isolating indelibly labeled cells during regeneration and subjecting them to transcriptomic analysis. Regardless of the cell type responsible for regenerating RPE, gaining insight into the following stages of RPE regeneration would provide maximum benefit for supplementing the study of AMD therapies and regenerative therapy: (1) the period immediately following ablation when RPE ablation-responsive cells are responding to signals to dedifferentiate (0-1dpi), (2) the period of peak proliferation and motility (3-4dpi), and (3) as newly-generated RPE cells functionally mature and interact with the photoreceptor layer (7-8dpi). After these datasets are generated and candidate pathways are elucidated, we would be able to complement traditional candidate validation techniques by modifying our Cre-based transgenics to enable tamoxifen-inducible overexpression of each individual candidate gene within the RPE cell source.

In the event that the above transgenic strategy fails, we could perform transcriptomic analysis by resorting to the dissection of RPE cells from the retina and choroid (Leung et al., 2007; Zhang and Leung, 2010). In Chapter 4, I showed that regenerated RPE cells are more highly pigmented than unablated RPE, likely because they were not PTU-inhibited during melanogenesis (Fig 4.9). We may be able to exploit this finding by coupling RPE dissection with FACS to isolate regenerating RPE cells at all three stages in the following manner: (1) for the injury response: isolating the RPE layer and excluding dying (ablated) cells, (2) for proliferation and motility: isolating the RPE and selecting for highly pigmented, weakly GFP+ (maturing RPE) and lightly pigmented, GFP-negative (functionally maturing RPE) cells, and finally (3) for reintegration: isolating the RPE and selecting all highly pigmented GFP+ cells.

5.3: Elucidating the interaction between the Retinal Pigment Epithelium and surrounding tissue during ablation and regeneration

We were surprised to find that RPE ablation does not lead to photoreceptor degeneration in larvae that had not been treated with PTU (data not shown). PTU is a chemical compound that inhibits tyrosinase activity by binding to its copper-containing active site (Klabunde et al., 1998) and is widely used in the zebrafish community to suppress pigmentation during development (e.g. Das et al., 2003; Higashijima et al., 2000; Stenkamp et al., 1998; Westerfield, 2007). However, PTU has nonspecific effects which disrupt gene expression (Tingaud-Sequeira et al., 2006) and thyroid function (Elsalini and Rohr, 2003). Fish treated with PTU over a similar time frame as our study (1-5dpf) were found to have smaller eyes, likely caused by PTU-mediated inhibition of thyroid hormone synthesis, though retinal cell number and differentiation were unaffected (Li et al., 2012). Alternatively, inhibition of tyrosinase activity by PTU might contribute to photoreceptor degeneration. PTU-mediated inhibition of tyrosinase activity disrupts photoreceptor light adaptation, likely by inhibiting L-DOPA secretion from the RPE (Page-McCaw et al., 2004). A third possibility is that RPE pigmentation is somehow protective to photoreceptors. Learning more about the mechanism by which the photoreceptors are sensitized to RPE ablation in PTU+ larvae—and protected from RPE ablation in PTU- larvae—could yield insights into the process by which RPE degeneration leads to photoreceptor degeneration in AMD and help the development of neuroprotective therapies.

To begin to determine the cause of ONL degeneration, a straightforward first experiment would be to cross our RPE ablation transgenic into zebrafish lacking tyrosinase (*sdy*) (Kelsh et al., 1996) and determining whether photoreceptor degeneration occurs following ablation of PTU- mutant larvae. ONL degeneration would suggest that

inhibition of tyrosinase activity could be causative of photoreceptor degeneration, and the opposite result would indicate either that off-target effects of PTU or a lack of RPE pigmentation sensitizes photoreceptors to RPE ablation. Since tyrosinase is important for proper RPE differentiation and the ablation transgenic makes use of a promoter fragment expressed in mature RPE, transgene expression may be compromised in *sdy* mutants. If that occurs, we could use CRISPRs targeted to tyrosinase (Jao et al., 2013) to create patches of $tyr^{-/-}$ RPE and determine whether photoreceptors proximal to those patches are sensitized to RPE ablation. In concert with these analyses, we could also take a nonbiased approach and perform a pharmaceutical screen for compounds that either rescue ONL degeneration in PTU+ larvae or lead to ONL degeneration in PTU- larvae.

In Chapter 4, I presented evidence suggesting that photoreceptor and RPE regeneration are coordinated (Figure 4.6), and that RPE regeneration may occur more rapidly when the ONL is intact (IE, in PTU- larvae). This leads to several fascinating questions centered on the relationship between photoreceptor and RPE co-regeneration. Firstly, what would happen to RPE cells if photoreceptor regeneration were to be inhibited? The most direct avenue to address this question would be to cross the RPE ablation transgenic into *gfap*:NfsB transgenics (Johnson et al., 2016; Shimizu et al., 2015; Smith et al., 2016) to simultaneously ablate both the RPE and Müller glia and thereby remove the source of regenerate photoreceptors. However, similar to RPE, Müller glia play critical roles in supporting retinal neurons (Goldman, 2014), and retinal health may degrade significantly following the ablation of two important cell populations that normally providing gliotic functions. To avoid this, we could specifically inhibit injury-responsive proliferation of Müller Glia. Electroporation of morpholinos targeting *stat3* have been shown to prevent injury-specific proliferation of Müller Glia (Nelson et al., 2012). Therefore, our first option would be electroporating *stat3* morpholinos into the

larval retina prior to RPE ablation (Teh et al., 2003). Failing that, we could use pharmaceutical inhibitors that have been found to inhibit Müller glia proliferation, such as Jak (Zhao et al., 2014) or the phagocytic inhibitor L-SOP (Bailey et al., 2010). However, these chemicals are nonspecific and therefore could also inhibit RPE regeneration. Finally, a more time-consuming but specific approach would be to assemble a transgenic enabling the expression of dominant negative *stat3* specifically in Müller glia prior to injury. This could be done by obtaining the ubb:floxed-stat3^{DN}-GFP transgenic (Fang et al., 2013) and crossing it into the *gfap*:CreER driver and our RPE ablation line. The resulting triple-transgenic would enable tamoxifen-inducible downregulation of stat3 signaling specifically in the Müller glia concurrently with ablation. Once an effective strategy for inhibiting photoreceptor regeneration is in place, we would be able to determine whether the RPE is capable of regenerating in the absence of healthy or regenerating photoreceptors, or if it ultimately degrades. Answering these questions will provide further insights into the process by which the RPE interacts with the damaged retina.

A related question is: would inducing photoreceptor ablation simultaneously with RPE ablation lead to more rapid regeneration, or change the morphology of regenerated RPE and photoreceptor cells, following a more robust regenerative response from Müller glia? Even in severely ablated fish, we do not see universal degeneration of all photoreceptor cells, and a variable proliferative response from Müller glia. The transgenic tools enabling photoreceptor ablation are readily available (Fraser et al., 2013; Montgomery et al., 2010b; Yoshimatsu et al., 2016) and their assembly would be straightforward. Following ablation of RPE and photoreceptors, we would be able to analyze the process of RPE regeneration to more finely interrogate the relationship between regenerating RPE and photoreceptors.

Finally, in Chapter 4 I determined that BM degeneration occurs following RPE ablation, and that this suggests that RPE degeneration may be causative of CNV. To determine whether CNV occurs after RPE ablation, we have obtained *flk*:mCherry transgenics, which express mCherry in endothelial cells and are seeking to determine whether vasculature invades into the injury site. As a followup to this experiment, it would be interesting to determine whether less severe perturbations of RPE cell function could have lead to BM degeneration and/or CNV. For example, the RPE secretes anti-angiogenic factors such as PEDF (Strauss, 2005), and loss of PEDF signaling has been shown to induce neovascularization (Dawson et al., 1999). Modifying our RPE-specific transgenic such that it leads to sub-acute disruption of RPE function—for example, by inducing the expression of pro-angiogenic factors such as VEGF (Ford et al., 2011) or reducing expression of PEDF—could serve as an excellent tool to interrogate that question.

5.4: Determining the role of the immune response during Retinal Pigment Epithelium regeneration

The immune system plays a critical role in influencing the regenerative response to injury (Kyritsis et al., 2014). In mammals, neuroinflammation following CNS injury is largely detrimental to successful regeneration. For example, mammalian Müller glia respond to inflammation by entering into reactive gliosis during which Müller glia proliferate to form a gliotic scar and secrete factors which accelerate the death of surrounding neurons (Bringmann et al., 2006; Thomas et al., 2015). Conversely, zebrafish Müller glia respond to similar inflammatory cues by dedifferentiating and successfully regenerating the retina (Nelson et al., 2013). Since AMD is thought to arise as a result of chronic inflammation, it is important to determine how regenerating RPE cells interact with the immune system and what effects immune cells have on

regenerating RPE. The adaptive immune system is not operational during the early stages of larval development studied here (5-19dpf), but the innate immune system, including phagocytic leukocytes, is active (Herbomel et al., 2001, 1999; Lam et al., 2004; Traver et al., 2003; Trede et al., 2004). The specific role played by leukocytes during CNS regeneration in zebrafish is not well understood. For example, during regeneration of skin melanocytes and fin, macrophages and neutrophils play integral roles in directing the regenerative response (Ellett et al., 2011; Iyengar et al., 2015; Li et al., 2012; Petrie et al., 2014), and macrophage entry into the retina has been observed following puncture injuries (White et al., 2017). Chronic inflammation and activation of both the innate and adaptive immune system is believed to directly cause RPE degeneration in AMD (Ambati et al., 2014; Gnanaguru et al., 2016; Lim et al., 2012b; Parmeggiani et al., 2012). For these reasons, determining (1) the location and movements of immune cells during regeneration, and (2) their requirement for successful RPE regeneration would undoubtedly provide critical information for the development of clinical treatments to mitigate inflammation in AMD patients.

Transgenics enabling the live imaging of macrophages and neutrophils are easily accessible and will allow the real-time *in vivo* analysis of macrophages (*mpeg1*) (Ellett et al., 2011) and neutrophils (*mpx*) (Renshaw and Loynes, 2006) as they react to RPE ablation and interact with the injury site. These analyses will serve to distinguish between leukocytes and regenerating RPE cells, establish when or if leukocytes ever directly contact regenerating RPE cells, and determine whether the GFP+ puncta near the leading tip of regenerating RPE cells (Fig 4.6,9) is phagocytosed by leukocytes. Complementary to these analyses, we could determine whether leukocytes inhibit or facilitate RPE regeneration. To specifically address the role of macrophages during RPE regeneration, we could obtain macrophage:NfsB transgenics (Ellett et al., 2011) and ablate

macrophages and RPE simultaneously. Additionally, we could treat ablated and regenerating larvae with the glucocorticoid agonist dexamethasone, which inhibits leukocyte invasion into lesions (Tsurufuji et al., 1984) and ablates T cells (Langenau et al., 2004). Together, these analyses would provide novel insight into the how the zebrafish innate immune system could provide a permissive environment for RPE regeneration, and may provide insights which could supplement the development of immunomodulatory therapies during treatment of AMD or implantation of stem cell-derived RPE.

Appendix: Materials and Methods

FISH MAINTENANCE AND HUSBANDRY:

Zebrafish were maintained at 28.5°C on a 14-hour light/10 hour dark cycle. Embryos were obtained from the natural spawning of transgenic or wild-type parents in pairwise crosses. According to established protocols (Westerfield, 1995), embryos were collected and raised at 28.5°C in the dark until they reached appropriate ages for experimentation. *hsp70l:*gal4^{kca4} (Scheer et al., 2001) transgenic embryos were obtained from the Zebrafish International Resource Center (ZIRC) and were propagated by outcrosses to AB-strain wild type fish. *pou4f3:*gal4^{s311t} transgenic (Xiao and Baier, 2007a) embryos were provided by Dr. Chris Chang and propagated by outcrosses to AB-strain fish. *ptf1a:*gal4 transgenic embryos were provided by Dr. Michael Parsons (Johns Hopkins University) and propagated by outcrosses to AB-strain wild-type fish (Parsons et al., 2009). All animals were treated in accordance with provisions established by the University of Texas at Austin and University of Pittsburgh School of Medicine Institutional Animal Care and Use Committees conform to the ARVO Statement for the Use of Animals in Ophthalmic and Vision Research.

The following transgenic lines were generated in this Dissertation: *au66* (*uas*:mCherry-f2a-myc-Cdc42^{WT}), *au67* (*uas*:mCherry-f2a-myc-Cdc42^{T17N}), *au68* (*uas*:mCherry-f2a-myc-Cdc42^{CA}), *au69* (*uas*:mCherry-f2a-myc-Cdc42^{F37A}), *au70* (*uas*:mcherry-f2a-Rac1^{WT}), *au71* (*uas*:mcherry-f2a-Rac1^{DN}), *au72* (*uas*:mcherry-f2a-Rac1^{CA}), *au73* (*uas*:mCherry-f2a-myc-RhoA^{WT}), *au74* (*uas*:mCherry-f2a-myc-RhoA^{DN}),

and *au75* (*uas*:mCherry-f2a-myc-RhoA^{CA}), (Hanovice et al., 2016) and these will be deposited at ZIRC for distribution.

TABLE 1. Primers Used for Construct Assembly

Primer number	Primer name	Sequence
1	Gibson1 attL1-Not1-Kozak-mCherry FWD	GCCAACTTTGTACAAAAAAGCAGGCTTTGCGG CCGCGCCGCCACCATGGTGAG
2	Gibson1 attL2-Not1-Cdc42 REV	GCCAACTTTGTACAAGAAAGCTGGGTCGCCGC GCTCATAGCAGCACACACCTGC
3	Gibson1 attL2-Not1-RhoA REV	GCCAACTTTGTACAAGAAAGCTGGGTCGCGGC CGCTCACAAGACAAGGCAACCAG
4	Gibson1 attL2-Not1-F37A REV	GCCAACTTTGTACAAGAAAGCTGGGTCGCGGC CGCTCATAGCAGCATACACTTGCGTTTC
5	Gibson2 attL1 REV	AAAGCCTGCTTTTTTGTACAAAGTTGGC
6	Gibson2 attL2 FWD	GACCCAGCTTTCTTGTACAAAGTTGGC
7	Linker-Rac1 FWD	ATGTCCAATTTACTGATGCAGGCCATCAAGTGTGT
8	Rac1 p3pA REV	TATCATGTCTGGATCCTTACAACAGCAGGCATTTTCTCTTCC
9	p3pA-GFP FWD	ACAAAGTGGGGGATCCATGGTGAGCAAGGGCGAG
10	2A-Linker REV	CAGTAAATTGGACATGGGCCCTG
11	attB1-GFP-2a-Linker-Rac REV	CCACACACTTGATGGCCTGCATCAGTAAATTGGACAT GGGCCCTGGGTTG
12	GFP2aCdcWT+Kozak+att FWD	GGGGACAAGTTTGTACAAAAAAGCAGGCTTTGGCCGCC ACCATGGTGAGCAAGGGCGAG
13	GFP-2a-Linker Rac FWD	CAACCCAGGGCCCATGTCCAATTTACTGATGCAGGCCAT CAAGTGTGTGG
14	attB2-Rac1 REV	GGGGACCACTTTGTACAAGAAAGCTGGGTCTTACAACAG CAGGCATTTTCTCTTCC

Table A.1: List of primers used for assembly of constructs enabling modulation of Rho GTPase activity.

ASSEMBLY OF CONSTRUCTS:

Constructs encoding human and *Xenopus* Cdc42, Rac1, and RhoA were provided by Dr. John Wallingford (Kieserman and Wallingford, 2009; Nobes and Hall, 1995; Sokol et al., 2001).

Cdc42: To create pME-mcherry-f2a-cdc42^{wt} (pME-mCWT), a pUCIDT-attL1-mcherry-f2a-myc-cdc42^{wt}-attL2 (pUCIDT-mCWT) oligo was purchased from IDT Gene Synthesis and used to create a pME-mCherry-f2a-Cdc42^{WT} via Gateway cloning (Invitrogen). To build pME-mCherry-f2a-myc-Cdc42^{CA} (pME-mCCA), pME-mCherry-f2a-myc-

Cdc42^{DN}(T17N) (pME-mCDN), and pME-mCherry-f2a-myc-Cdc42^{DN}(F37A) (pME-mCF37A), each Cdc42 isoform was PCR amplified from pCS2+cdc42^{XX} plasmids using primers 3 and 4 (Table 1) to create Cdc42^{xx}-attL2 PCR fragments. attL1-mCherry-f2a was PCR amplified from pUCIDT-attL1-mCherry-f2a-Cdc42^{WT}-attL2 using primers 4 and 5 (Table 1) These PCR fragments were then cloned into pME via Gibson Assembly (New England BioLabs).

LR Clonase II Plus was used to carry out all Multisite Gateway assembly reactions using protocols established previously (Kwan et al., 2007). Tg(*uas*:mCherry-f2a-myc-Cdc42^{XX}) was created using Tol2Kit vectors #302 (p3E-pA), #327 (p5E-UAS), #395 (pDestTol2CG) and pME-mCXX.

RhoA: To build pME-mCherry-f2a-myc-RhoA^{WT} (pME-mRhWT), pME-mCherry-f2a-myc-RhoA^{CA} (pME-mRhCA), and pME-mCherry-f2a-myc-RhoA^{DN} (pME-mRhDN), each RhoA isoform was PCR amplified from pCS2+RhoA^{XX} plasmids using primers 5 and 6 (Table 1) to create RhoA^{xx}-attL2 PCR fragments. attL1-mcherry-f2a was PCR amplified from pUCIDT-mCWT using primers 4 and 5 (Table 1) These PCR fragments were then cloned into pME via Gibson Assembly (New England BioLabs).

Tg(uas:mcherry-f2a-myc-RhoA2^{XX}) was created using Tol2Kit vectors #302 (p3E-pA), #327 (p5E-UAS), #395 (pDestTol2CG) and pME-mRhXX.

Rac1: To create pME-gfp-f2a-Rac1^{WT} (pME-gRWT) and pME-gfp-f2a-Rac1^{DN} (pME-gRDN), Rac1WT and Rac1DN were PCR amplified using Vent polymerase (New England Biolabs) using primers 7 and 8 (Table 1). gfp-f2a was amplified from

T2Kactb2:gfp-f2a-creER^{T2} (Wang et al., 2011), a gift from Dr. Michael Parsons, using primers 9 and 10 (Table 1) and cloned into a 3' entry vector via InFusion recombination technology (Clontech). Finally, attB1-egfp-2a-Rac1^{WT}-attB2 and attB1-egfp-2a-Rac1^{DN}-attB2 were amplified via Phusion polymerase using primers 11 and 14 (Table 1) and recombined with pDONR221 to create middle entry vectors pME-gRWT and pME-gRDN. To create pME-gfp-f2a-Rac1^{CA} (pME-gRCA), Rac1CA-attB2 was PCR amplified with Phusion polymerase using primers 11 and 12 (Table 1) and ligated to attB1-gfp-f2a (primers 13 and 14 (Table 1)) via overlap PCR to form attB1-gfp-f2a-Rac1^{XX}-attB2 PCR fragments. These fragments were then cloned into middle entry vectors by BP reaction to create pME-gRCA. Tg(*uas*:mcherry-f2a- Rac1^{XX}) constructs were created using Tol2Kit vectors #302 (p3E-pA), #327 (p5E-UAS), #395 (pDestTol2CG) and pME-gRXX.

All plasmids were sequence confirmed via sequencing on Applied Biosystems 3730 DNA Analyzers at the University of Texas at Austin Institute for Cellular and Molecular Biology DNA Sequencing Facility.

TOL2 TRANSGENESIS:

Capped Tol2 mRNA was synthesized from pCS2FA-transposase using the Ambion mMessage mMachine SP6 *in vitro* transcription kit. Between 50-75pg Tol2 mRNA and between 20-25pg cDNA were microinjected into single-cell embryos. Embryos displaying acceptable levels of mosaic *cmlc2:*egfp expression were raised to adulthood, and outcrossed to screen for founders. F1 embryos displaying ubiquitous *cmlc2:*egfp expression were isolated and reared to generate stable lines.

HEAT SHOCK INDUCTION OF GAL4:

Embryos from *hsp70l*:gal4 outcrosses of transgenic founders were raised in system water supplemented with Phenylthiourea (PTU). Embryos were individually placed in ~120uL system water in PCR tubes and heat shocked for 30 minutes at 39.5°C in a PCR thermocycler. They were then immediately returned to 28.5°C fish medium for recovery and imaging on either a Leica MZ16F or a Zeiss Axio Zoom V16 fluorescent stereoscope.

WESTERN BLOT ANALYSIS:

Heat shocked and dechorionated embryos were collected at 3dpf. To deyolk embryos, a borosilicate injection needle was used to mechanically disrupt yolks. Embryos were next washed in deyolking buffer without calcium (Link et al., 2006), spun at 300rcf and washed in wash buffer (110mM NaCl, 3.5mM KCl, 2.7mM $CaCl_2$, 10mM Tris/Cl) containing Complete Mini protease inhibitor mixture (Roche Diagnostics). Deyolked embryos were lysed with modified LeMeer's Lysis Buffer (50mM Tris pH 7.5, 150mM NaCl, 1mM EDTA, 1% IGEPAL, 0.1% sodium deoxycholate) supplemented with Complete Mini protease inhibitor cocktail (Lemeer et al., 2007) before being centrifuged at low speed and sonicated by a Sonic Dismembranator Model 300 (Fisher Scientific). Using manufacturer's protocol, protein samples were gel electrophoresed using 4-12% Bis-Tris gel and transferred onto PVDF membrane (Invitrogen NuPage system). Blots

were incubated 1:5000 anti-myc (abcam ab9106), followed by 1:5000 horse anti-mouse HRP secondary (Cell Signaling Technology 7076). Blots were imaged via the Super Signal West Femto visualization system (Life Sciences) on an ImageQuant LAS4000 machine (GE Life Sciences). Following imaging of myc antibody labeling, blots were stripped for 15 minutes in Restore Western Blot Stripping Buffer (Thermo Scientific 21059) and reprobed with 1:5000 anti-actin (calbiochem cp01).

IMMUNOHISTOCHEMISTRY OF RETINAL SECTIONS:

Embryos were fixed in 4% paraformaldehyde overnight at 4°C, sucrose-protected, and embedded in OCT tissue-freezing medium (TBS, Inc.) before being sectioned at 14μm on a Leica CM1850 crysotat. Sections were rehydrated in 1XPBS for 5 minutes, and blocked in 5% normal goat serum in PBS for 2 hours at room temperature. Antigen presentation before BrdU imaging, sections were treated with 4N HCl for 8 minutes at 37 degrees. Sections were stained with 1:500 TOPRO or 1:500 DAPI (Life Technologies) for 9 minutes at room temperature, washed 3X with PBS, and mounted with Vectashield (Vector Laboratories). Images were obtained with a 63X objective on a Leica SP5 and/or a 40X objective on an Olympus FV1200 confocal microscope. Antibodies used in this study include BrdU (Rac1 (Milipore, 05-389), ZPR2 (ZIRC), ZPR1 (ZIRC), phalloidin (Thermo Fisher), and myc (Abcam, ab9106). Phalloidin (Thermo Fisher, A22284) was used at a 1:33 dilution. TUNEL (Roche #12145792910, Mannheim, Germany) and Click-It EdU staining (Thermo Fisher, C10618) were performed according to manufacturer's instructions.

SNP MAPPING AND GENOTYPING:

Heterozygous *au18* carriers in an AB background were outcrossed with wild type TU fish to generate a polymorphic mapping line. 200 homozygous mutant embryos from four parental mapping pairs were collected, genomic DNA was isolated (DNeasy Blood & Tissue Kit; Qiagen, Valencia CA, USA) and 1μg was utilized in whole-genome sequencing at the University of Texas Genomic Sequencing and Analysis Facility. On an Illumina HiSeq 2000 machine (Illumina San Diego, CA, USA), 82 million paired-end 100-bp sequences were generated for an average genome coverage of 10.9X. To identify putative mutations, sequencing reads were analyzed via the MegaMapper single nucleotide polymorphism (SNP)-mapping pipeline(Obholzer et al., 2012). cDNA sequencing was performed to confirm the putative *nsfb* mutation. To genotype $nsfb^{c893t}$, we utilized dCAPS Finder 2.0(Neff et al., 2002) to analyze the genomic sequence of nsfb proximal to the SNP and generate the following primers: *forward* 5'-agattttgaacaaatacgtgggaggat-3' and *reverse* 5'-tgactgttgacagaggaacc-3'. These primers amplify a 260bp product with a *MboI* restriction site present in wild-type gDNA, but not in $nsfb^{c893t}$. Amplicons from gDNA generated from individual embryos were digested with *MboI* and run on 3% agarose gel to distinguish wild-type (260bp) from $nsfb^{c893t}$ (234bp) bands.

IN SITU HYBRIDIZATION:

In situ hybridizations were performed as described(Jowett and Lettice, 1994; Thisse and Thisse, 2008). For *nsfb* probe synthesis, a partial cDNA fragment of the coding sequence of *nsfb* was cloned by RT-PCR using primers, 5'-agagaccgccaaatgtcagg-3 and' 5'-ctaaaaagccacatgtttatcagggc-3'.

PHYLOGENETIC ANALYSIS:

Protein sequences of nsf were obtained from Ensembl release 80 (http://www.ensembl.org)(Flicek et al., 2014), the Saccharomyces genome database (SGD project, http://www.yeastgenome.org)(Engel et al., 2014), the WormBase website (http://www.wormbase.org, release WS248)(Yook et al., 2012), and from FlyBase (http://flybase.org) (Marygold et al., 2013). These sequences are yeast nsf (SEC18, YBR080C), Drosophila Nsf1 (FBgn0000346) and Nsf2 (FBgn0266464), *C. elegans* NSF (WBGene00003818), *Xenopus* NSF (ENSXETG00000031364), Zebrafish nsfa (ENSDARG00000007654) and nsfb (ENSDARG00000038991), mouse nsf (ENSMUSG00000034187), chimpanzee nsf (ENSPTRG00000009320), and human NSF (NSG00000073969), with yeast AAA-protein ORC1 as an outgroup (YML065W). A phylogenetic tree was generated via Geneious alignment (Geneious version 7.1.5, http://www.geneious.com)(Kearse et al., 2012), and Bootstrapped 1,000 times for statistical analysis.

QUANTITATIVE POLYMERASE CHAIN REACTION:

qPCR was performed on wild type, *au18*, and *au13* embryos at 48 hours post fertilization. Ten embryos were collected per each biological replicate (n=3), and mRNA was extracted with Trizol Reagent (Life Technologies, Carlsbad, CA) according to the manufacturer's protocol and potential genomic DNA contaminants were digested with RNAse-free DNAse I (Roche Diagnostics, Mannheim Germany) before being reverse transcribed into cDNA with the iScript Reverse Transcriptase Kit (Bio-Rad, Hercules, CA). Real time quantitative PCR was conducted on five technical replicates per biological replicate using SYBR Green and a Via 7 Real-Time PCR System (Life Technologies, Carlsbad, CA).

act2b, was used as the reference gene, using primers provided as a generous gift by Johann Eberhart (University of Texas at Austin): *forward*: 5'-cgagcaggagatgggaacc-3' and *reverse:* 5'-caacggaaacgctcattgc-3', which produce an amplicon of 128bp. Primers for *nsfb* were as follows: *forward:* 5'-ggagctttcttggaggctttca-3' and *reverse:* 5'-cgctctgtcctttcacctgtt-3', which amplify 68bp(Kurrasch et al., 2009). Fold change in *nsfb* transcript expression between *au18*, *au13* and WT was calculated using the relative gene quantification method(Livak and Schmittgen, 2001).

HISTOLOGY:

Embryos were fixed in fresh 4% glutaraldehyde, 2% paraformaldehyde overnight at room temperature, stained in 2% OsO_4 and 2% potassium ferrocyanide and 2% uranyl acetate, and microwave-embedded with a modified reduced-viscosity Spurr-Quetol-651 resin using a BDMA accelerator (Electron Microscopy Services, Hatfield, PA) via a 30, 50, 75, 100, and 100% resin/acetone infiltration series. Samples were sectioned using a Leica Ultracut UC7 ultramicrotome at a thickness of 1μm, stained with 1% toluidine blue, 1% borax, and imaged on a Leica DM2500 at 400X and 1,000X magnification.

TRANSMISSION ELECTRON MICROSCOPY:

Samples were embedded as above and a Leica Ultracut UC7 ultramicrotome at a thickness of 70nm. These sections were imaged on a FEI Tecnai transmission electron microscope. Reference images were acquired at 390X magnification to locate the optic nerve and ultrastructure of the RPE. Images (n=3) of the RPE were collected from 3 regions of the RPE: dorsal, central, and ventral, from n = 3 fish at 11,500X magnification. Central RPE was defined as RPE contained within the region 10-30° clockwise from a line connecting the middle of the optic nerve head and the lens core. Dorsal RPE was defined as the region included between 80-100° clockwise and ventral RPE between 30-40° counterclockwise. Images were rotated to orient the RPE on a horizontal line, and the number, size, and maturity of melanosomes were analyzed using Image J Software. In RPE-ablated larvae, the injury site was defined as the dorsal region extending between the optic nerve head and the intersection of the choroid and brain, as this correlated with the area of highest

transgene expression. To quantify BM thickness, n=3 images were taken from 3 larvae at each group at 20,500X magnification. From each image, the thickness of BM was measured 3 times using Image J Software.

STATISTICAL ANALYSIS:

Levene's test found was used to test whether the homoscedasticity assumption is satisfied in all datasets. To determine whether there was a significant difference between sibling and mutant data during each time point, as well as the change over time of each variable within an individual group, the nonparametric Kruskal-Wallis test was applied, and Mann-Whitney U was performed for pairwise comparisons of nonparametric datasets. In parametric datasets, Student's T-test was applied for pairwise comparisons. Analyses were completed using GraphPad Prism version 6.0f for Mac (GraphPad Software, San Diego California USA, www.graphpad.com).

RECORDING AND ANALYZING LARVAL OKR:

Stimulation and recording of OKR in zebrafish was performed as described in Scheetz *et al* (Scheetz et al., 2017), using equipment generously shared by members of the Burton lab (University of Pittsburgh). Briefly, larvae were immobilized in 3% methylcellulose, oriented dorsal up and exposed to a full field rotating stimulus projected onto a screen (#NP100, NEC, Itasca, Illinois) that encompassed 180 degrees of the stimulated eye's field of vision. Responses were captured using infrared light (880nm; #BL34-880, Spectrum, Montague, MI) through a Flea3 Camera (#FLU-U3-13Y3M-C, Point Grey Research, Richmond, BC, Canada) that was mounted (10447367, Leica) on a

on a dissecting microscope (#S8 APO, Leica Microsystems, Wetzlar, Germany). Videos were recorded by FlyCapture software (Point Grey) and analyzed using custom MATLAB scripts (University of Pittsburgh) (Scheetz et al., 2017).

OCT IMAGING:

Ablated larvae were immobilized dorsal up in 3% methylcellulose and imaged by under near-infrared light (~840nm; Bioptigen Spectral Domain Ophthalmic Imaging System) and analyzed by the associated software (InVivoVue; Bioptigen, Research Triangle Park, NC). After imaging, larvae were rinsed out of methylcellulose and transferred into petri dishes to recover.

References

Abramowitz, J., Turner, W.A., Chavin, W., Taylor, J.D., 1977. Trysinase positive oculocutaneous albinism in the goldfish, Carassius auratus l., and ultrastructural and biochemical study of the eye. Cell Tissue Res. 182, 409–419.

Abrams, E.W., Mullins, M.C., 2010. Early zebrafish development: It's in the maternal genes. Curr. Opin. Genet. Dev. 19, 396–403.

Adamis, A.P., Shima, D.T., Yeo, K.T., Yeo, T.K., Brown, L.F., Berse, B., Damore, P.A., Folkman, J., 1993. Synthesis and Secretion of Vascular Permeability Factor/Vascular Endothelial Growth Factor by Human Retinal Pigment Epithelial Cells. Biochem. Biophys. Res. Commun. 193, 631–638.

Adams, A., Johnson, D., Longnecker, R., Sloat, B., Pringle, J., 1990. CDC42 and CDC43, two additional genes involved in budding and the establishment of cell polarity in the yeast Saccharomyces cerevisiae. J. Cell … 111, 131–142.

Adler, R., Curcio, C.A., Hicks, D., Price, D., Wong, F., 1999. Cell death in age-related macular degeneration. Mol.Vis. 5, 31.

Agathocleous, M., Harris, W. a, 2009. From progenitors to differentiated cells in the vertebrate retina. Annu. Rev. Cell Dev. Biol. 25, 45–69.

Akitake, C.M., Macurak, M., Halpern, M.E., Goll, M.G., 2011. Transgenerational analysis of transcriptional silencing in zebrafish. Dev. Biol. 352, 191–201.

Al-Hussaini, H., Schneiders, M., Lundh, P., Jeffery, G., 2009. Drusen are associated with local and distant disruptions to human retinal pigment epithelium cells. Exp. Eye Res. 88, 610–612.

Algvere, P., Gouras, P., Dafgard Kopp, E., 1999. Long-term outcome of RPE allografts in non-immunosuppressed patients with AMD. Eur. J. Ophthalmol. 9, 217–30.

Algvere, P. V., Berglin, L., Gouras, P., Sheng, Y., 1994. Transplantation of fetal retinal pigment epithelium in age-related macular degeneration with subfoveal neovascularization. Graefe's Arch. Clin. Exp. Ophthalmol. 232, 707–716.

Algvere, P. V, 1997. Clinical possibilities in retinal pigment epithelial transplantations. Acta Ophthalmol. Scand. 75, 1.

Ambati, J., Atkins, J.P., Gelfand, B.D., 2014. Immunology of age-related macular degeneration. Natl. Rev. Immunol. 13, 438–451.

Amores, a, Force, a, Yan, Y.L., Joly, L., Amemiya, C., Fritz, a, Ho, R.K., Langeland, J., Prince, V., Wang, Y.L., Westerfield, M., Ekker, M., Postlethwait, J.H., 1998. Zebrafish hox clusters and vertebrate genome evolution. Science 282, 1711–1714.

Amsterdam, A., Nissen, R.M., Sun, Z., Swindell, E.C., Farrington, S., Hopkins, N., 2004. Identification of 315 genes essential for early zebrafish development. Proc. Natl. Acad. Sci. U. S. A. 101, 12792–12797.

Ancans, J., Tobin, D.J., Hoogduijn, M.J., Smit, N.P., Wakamatsu, K., Thody, A.J., 2001. Melanosomal pH controls rate of melanogenesis, eumelanin/phaeomelanin ratio and

melanosome maturation in melanocytes and melanoma cells. Exp. Cell Res. 268, 26–35.
Anderson, D.H., Stern, W.H., Fisher, S.K., Erickson, P. a, Borgula, G. a, 1981. The onset of pigment epithelial proliferation after retinal detachment. Invest. Ophthalmol. Vis. Sci. 21, 10–16.
Aoki, H., Hara, A., Nakagawa, S., Motohashi, T., Hirano, M., Takahashi, Y., Kunisada, T., 2006. Embryonic stem cells that differentiate into RPE cell precursors in vitro develop into RPE cell monolayers in vivo. Exp. Eye Res. 82, 265–74.
Araki, M., Takano, T., Uemonsa, T., Nakane, Y., Tsudzuki, M., Kaneko, T., 2002. Epithelia-mesenchyme interaction plays an essential role in transdifferentiation of retinal pigment epithelium of silver mutant quail: localization of FGF and related molecules and aberrant migration pattern of neural crest cells during eye rudiment forma. Dev. Biol. 244, 358–71.
Bahadoran, P., Aberdam, E., Mantoux, F., Buscà, R., Bille, K., Yalman, N., De Saint-Basile, G., Casaroli-Marano, R., Ortonne, J.P., Ballotti, R., 2001. Rab27a: A key to melanosome transport in human melanocytes. J. Cell Biol. 152, 843–849.
Bailey, T.J., El-Hodiri, H., Zhang, L., Shah, R., Mathers, P.H., Jamrich, M., 2004. Regulation of development by Rx genes. Int. J. Dev. Biol. 48, 761–770.
Bailey, T.J., Fossum, S.L., Fimbel, S.M., Montgomery, J.E., Hyde, D.R., 2010. The inhibitor of phagocytosis, O-phospho-L-serine, suppresses Muller glia proliferation and cone cell regeneration in the light-damaged zebrafish retina. Exp. Eye Res. 91, 601–612.
Bakall, B., Marmorstein, L.Y., Hoppe, G., Peachey, N.S., Wadelius, C., Marmorstein, A.D., 2003. Expression and localization of bestrophin during normal mouse development. Invest Ophthalmol.Vis.Sci 44, 3622–3628.
Banerjee, a., Barry, V. a., DasGupta, B.R., Martin, T.F.J., 1996. N-Ethylmaleimide-sensitive Factor Acts at a Prefusion ATP-dependent Step in Ca2+-activated Exocytosis. J. Biol. Chem. 271, 20223–20226.
Bankhead, E.J., Colasanto, M.P., Dyorich, K.M., Jamrich, M., Murtaugh, L.C., Fuhrmann, S., 2015. Multiple requirements of the focal dermal hypoplasia gene porcupine during ocular morphogenesis. Am. J. Pathol. 185, 197–213.
Barbosa-Sabanero, K., Hoffmann, A., Judge, C., Lightcap, N., Tsonis, P.A., Del Rio-Tsonis, K., 2012. Lens and retina regeneration: new perspectives from model organisms. Biochem. J. 447, 321–334.
Bashaw, G.J., Klein, R., 2010. Signaling from axon guidance receptors. Cold Spring Harb. Perspect. Biol. 2, a001941.
Becker, T., Wullimann, M.F., Becker, C.G., Bernhardt, R.R., Schachner, M., 1997. Axonal regrowth after spinal cord transection in adult zebrafish. J. Comp. Neurol. 377, 577–595.
Bernardos, R., Barthel, L., Meyers, J., Bernardos, R.L., Barthel, L.K., Meyers, J.R., Raymond, P.A., 2007. Late-Stage Neuronal Progenitors in the Retina Are Radial Muller Glia That Function as Retinal Stem Cells Late-Stage Neuronal Progenitors in the Retina Are Radial Mu ¨ ller Glia That Function as Retinal Stem Cells.

Bernardos, R.L., Barthel, L.K., Meyers, J.R., Raymond, P. a, 2007. Late-stage neuronal progenitors in the retina are radial Müller glia that function as retinal stem cells. J. Neurosci. 27, 7028–40.

Betz, H., 1994. The N-ethylmaleimide-sensitive fusion protein (NSF) is preferentially expressed in the nervous system. FEBS Lett. 347, 55–58.

Bhutto, I., Lutty, G., 2012. Understanding age-related macular degeneration (AMD): relationships between the photoreceptor/retinal pigment epithelium/Bruch's membrane/choriocapillaris complex. Mol. Aspects Med. 33, 295–317.

Bibliowicz, J., Tittle, R., Gross, J., 2011. Towards a better understanding of human eye disease: insights from the zebrafish, danio rerio. Prog. Mol. Biol. ….

Biesemeier, A., Taubitz, T., Julien, S., Yoeruek, E., 2014. Neurobiology of Aging Choriocapillaris breakdown precedes retinal degeneration in age-related macular degeneration q. Neurobiol. Aging 35, 2562–2573.

Binder, S., Stanzel, B. V., Krebs, I., Glittenberg, C., 2007. Transplantation of the RPE in AMD. Prog. Retin. Eye Res. 26, 516–554.

Bird, a. C., Bressler, N.M., Bressler, S.B., Chisholm, I.H., Coscas, G., Davis, M.D., de Jong, P.T.V.M., Klaver, C.C.W., Klein, B.E.K., Klein, R., Mitchell, P., Sarks, J.P., Sarks, S.H., Soubrane, G., Taylor, H.R., Vingerling, J.R., 1995. An international classification and grading system for age-related maculopathy and age-related macular degeneration. Surv. Ophthalmol. 39, 367–374.

Blenkinsop, T.A., Salero, E., Stern, J.H., Temple, S., 2013. The culture and maintenance of functional retinal pigment epithelial monolayers from adult human eye. In: Methods in Molecular Biology: Second Edition. pp. 45–65.

Block, M.R., Glick, B.S., Wilcox, C. a, Wieland, F.T., Rothman, J.E., 1988. Purification of an N-ethylmaleimide-sensitive protein catalyzing vesicular transport. Proc. Natl. Acad. Sci. U. S. A. 85, 7852–6.

Boguski, M., McCormick, F., 1993. Proteins regulating Ras and its relatives. Nature 366.

Booij, J.C., Baas, D.C., Beisekeeva, J., Gorgels, T.G.M.F., Bergen, A.A.B., 2010. The dynamic nature of Bruch's membrane. Prog. Retin. Eye Res. 29, 1–18.

Bosco, E.E., Mulloy, J.C., Zheng, Y., 2009. Rac1 GTPase: a "Rac" of all trades. Cell. Mol. Life Sci. 66, 370–4.

Bovolenta, P., Mallamaci, a, Briata, P., Corte, G., Boncinelli, E., 1997. Implication of OTX2 in pigment epithelium determination and neural retina differentiation. J. Neurosci. 17, 4243–4252.

Brand, A., Perrimon, N., 1993. Targeted gene expression as a means of altering cell fates and generating dominant phenotypes. Development 415, 401–415.

Bridgewater, J.A., Springer, C.J., Knox, R.J., Minton, N.P., Michael, N.P., Collins, M.K., 1995. Expression of the bacterial nitroreductase enzyme in mammalian cells renders them selectively sensitive to killing by the prodrug CB1954. Eur. J. Cancer 31, 2362–2370.

Bringmann, A., Pannicke, T., Grosche, J., Francke, M., Wiedemann, P., Skatchkov, S.N., Osborne, N.N., Reichenbach, A., 2006. Müller cells in the healthy and diseased retina. Prog. Retin. Eye Res. 25, 397–424.

Briona, L.K., Poulain, F.E., Mosimann, C., Dorsky, R.I., 2015. Wnt/ß-catenin signaling is required for radial glial neurogenesis following spinal cord injury. Dev. Biol. 403, 15–21.
Brockerhoff, S.E., Fadool, J.M., 2011. Genetics of photoreceptor degeneration and regeneration in zebrafish. Cell. Mol. Life Sci. 68, 651–659.
Brown, K.E., Keller, P.J., Ramialison, M., Rembold, M., Stelzer, E.H.K., Loosli, F., Wittbrodt Joachim, J., 2010. Nlcam modulates midline convergence during anterior neural plate morphogenesis. Dev. Biol. 339, 14–25.
Carido, M., Zhu, Y., Postel, K., Benkner, B., Cimalla, P., Karl, M.O., Kurth, T., Paquet-Durand, F., Koch, E., Munch, T., Tanaka, E.M., Ader, M., 2014. Charactrization of a mouse model with complete RPE loss and its use for RPE cell transplantation. Invest. Ophthalmol. Vis. Sci. 49.
Carr, A.-J., Vugler, A. a, Hikita, S.T., Lawrence, J.M., Gias, C., Chen, L.L., Buchholz, D.E., Ahmado, A., Semo, M., Smart, M.J.K., Hasan, S., da Cruz, L., Johnson, L. V, Clegg, D.O., Coffey, P.J., 2009. Protective effects of human iPS-derived retinal pigment epithelium cell transplantation in the retinal dystrophic rat. PLoS One 4, e8152.
Casco-Robles, M.M., Islam, M.R., Inami, W., Tanaka, H.V., Kunahong, A., Yasumuro, H., Hanzawa, S., Casco-Robles, R.M., Toyama, F., Maruo, F., Chiba, C., 2016. Turning the fate of reprogramming cells from retinal disorder to regeneration by Pax6 in newts. Sci. Rep. 6, 33761.
Cavodeassi, F., Carreira-Barbosa, F., Young, R.M., Concha, M.L., Allende, M.L., Houart, C., Tada, M., Wilson, S.W., 2005. Early stages of zebrafish eye formation require the coordinated activity of Wnt11, Fz5, and the Wnt/B-catenin pathway. Neuron 47, 43–56.
Cavodeassi, F., Ivanovitch, K., Wilson, S.W., 2013. Eph/Ephrin signalling maintains eye field segregation from adjacent neural plate territories during forebrain morphogenesis. Development 140, 4193–202.
Chan, H.Y., V, S., Xing, X., Kraus, P., Yap, S.P., Ng, P., Lim, S.L., Lufkin, T., 2011. Comparison of IRES and F2A-based locus-specific multicistronic expression in stable mouse lines. PLoS One 6, e28885.
Chauhan, B.K., Disanza, A., Choi, S.-Y., Faber, S.C., Lou, M., Beggs, H.E., Scita, G., Zheng, Y., Lang, R. a, 2009. Cdc42- and IRSp53-dependent contractile filopodia tether presumptive lens and retina to coordinate epithelial invagination. Development 136, 3657–67.
Chen, F., Ma, L., Parrini, M., Mao, X., Lopez, M., 2000. Cdc42 is required for PIP 2-induced actin polymerization and early development but not for cell viability. Curr. Biol. 758–765.
Chen, Y., Stump, R.J.W., Lovicu, F.J., McAvoy, J.W., 2006. A role for Wnt/planar cell polarity signaling during lens fiber cell differentiation? Semin. Cell Dev. Biol. 17, 712–725.
Chew, E.Y., Clemons, T., Sangiovanni, J.P., Danis, R., Domalpally, A., McBee, W., Sperduto, R., Ferris, F.L., 2012. The age-related eye disease study 2 (AREDS2):

Study design and baseline characteristics (AREDS2 Report Number 1). Ophthalmology 119, 2282–2289.
Chew, T.W., Liu, X.J., Liu, L., Spitsbergen, J.M., Gong, Z., Low, B.C., 2014. Crosstalk of Ras and Rho: activation of RhoA abates Kras-induced liver tumorigenesis in transgenic zebrafish models. Oncogene 33, 2717–27.
Chiba, C., 2014. The retinal pigment epithelium: An important player of retinal disorders and regeneration. Exp. Eye Res. 123, 107–114.
Chiba, C., Hoshino, A., Nakamura, K., Susaki, K., Yamano, Y., Kaneko, Y., Kuwata, O., Maruo, F., Saito, T., 2006. Visual cycle protein RPE65 persists in new retinal cells during retinal regeneration of adult newt. J. Comp. Neurol. 495, 391–407.
Choe, C.P., Collazo, A., Trinh, L. a, Pan, L., Moens, C.B., Crump, J.G., 2013. Wnt-dependent epithelial transitions drive pharyngeal pouch formation. Dev. Cell 24, 296–309.
Choe, S.-K., Nakamura, M., Ladam, F., Etheridge, L., Sagerström, C.G., 2012. A Gal4/UAS system for conditional transgene expression in rhombomere 4 of the zebrafish hindbrain. Dev. Dyn. 241, 1125–32.
Choudhary, P., Booth, H., Gutteridge, A., Surmacz, B., Louca, I., Steer, J., Kerbey, J., Whiting, P.J., 2016. Directing differentiation of pluripotent stem cells toward retinal pigment epithelium lineage. Stem Cells Transl. Med. 6, 490–501.
Chow, R.L., Lang, R.A., 2001. Early eye development in vertebrates. Annu. Rev. Cell Dev. Biol. 17, 255–296.
Chuang, J.C., Mathers, P.H., Raymond, P.A., 1999. Expression of three Rx homeobox genes in embryonic and adult zebrafish. Mech. Dev. 84, 195–198.
Chuang, J.C., Raymond, P.A., 2001. Zebrafish Genes rx1 and rx2 Help Define the Region of Forebrain That Gives Rise to Retina. Dev. Biol. 30, 13–30.
Cleary, P.E., Ryan, S.J., 1979a. Experimental posterior penetrating eye injury in the rabbit. I. Method of production and natural history. Br. J. Ophthalmol. 63, 306–11.
Cleary, P.E., Ryan, S.J., 1979b. Experimental posterior penetrating eye injury in the rabbit. II. Histology of wound, vitreous, and retina. Br. J. Ophthalmol. 63, 312–321.
Collery, R.F., Volberding, P.J., Bostrom, J.R., Link, B.A., Besharse, J.C., 2016. Loss of Zebrafish Mfrp Causes Nanophthalmia, Hyperopia, and Accumulation of Subretinal Macrophages. Investig. Opthalmology Vis. Sci. 57, 6805.
Crabb, J.W., Miyagi, M., Gu, X., Shadrach, K., West, K.A., Sakaguchi, H., Kamei, M., Hasan, A., Yan, L., Rayborn, M.E., Salomon, R.G., Hollyfield, J.G., 2002. Drusen proteome analysis: an approach to the etiology of age-related macular degeneration. Proc. Natl. Acad. Sci. U. S. A. 99, 14682–7.
Cruz, P.M.D., Yasumura, D., Weir, J., Matthes, M.T., Abderrahim, H., Lavail, M.M., Vollrath, D., 2000. Mutation of the receptor tyrosine kinase gene Mertk in the retinal dystrophic RCS rat. Hum. Mol. Genet. 9, 645–652.
Curado, S., Anderson, R.M., Jungblut, B., Mumm, J., Schroeter, E., Stainier, D.Y.R., 2007. Conditional Targeted Cell Ablation in Zebrafish : A New Tool for Regeneration Studies 1025–1035.
Curcio, C.A., Medeiros, N.E., Millican, C.L., 1996. Photoreceptor loss in age-related

macular degeneration. Investig. Ophthalmol. Vis. Sci. 37, 1236–1249.
Daly, C.M.S., Willer, J., Gregg, R., Gross, J.M., 2013. snow white, a zebrafish model of Hermansky-Pudlak Syndrome type 5. Genetics 195, 481–94.
Danno, H., Michiue, T., Hitachi, K., Yukita, A., Ishiura, S., Asashima, M., 2008. Molecular links among the causative genes for ocular malformation: Otx2 and Sox2 coregulate Rax expression. Proc. Natl. Acad. Sci. 105, 5408–5413.
Das, T., Payer, B., Cayouette, M., Harris, W.A., 2003. In vivo time-lapse imaging of cell divisions during neurogenesis in the developing zebrafish retina. Neuron 37, 597–609.
Davis, R.J., Blenkinsop, T.A., Campbell, M., Borden, S.M., Charniga, C.J., Lederman, P.L., Frye, A.M., Aguilar, V., Zhao, C., Naimark, M., Kiehl, T.R., Temple, S., Stern, J.H., 2016. Human RPE Stem Cell-Derived RPE Preserves Photoreceptors in the Royal College of Surgeons Rat: Method for Quantifying the Area of Photoreceptor Sparing. J. Ocul. Pharmacol. 32, 304–309.
Dawson, D.W., Volpert, O. V, Gillis, P., Crawford, S.E., Xu, H., Benedict, W., Bouck, N.P., 1999. Pigment epithelium-derived factor: a potent inhibitor of angiogenesis. Science (80-.). 285, 245–248.
Dessinioti, C., Stratigos, A.J., Rigopoulos, D., Katsambas, A.D., 2009. A review of genetic disorders of hypopigmentation: Lessons learned from the biology of melanocytes. Exp. Dermatol. 18, 741–749.
Disanza, A., Mantoani, S., Hertzog, M., Gerboth, S., Frittoli, E., Steffen, A., Berhoerster, K., Kreienkamp, H.-J., Milanesi, F., Di Fiore, P.P., Ciliberto, A., Stradal, T.E.B., Scita, G., 2006. Regulation of cell shape by Cdc42 is mediated by the synergic actin-bundling activity of the Eps8-IRSp53 complex. Nat. Cell Biol. 8, 1337–1347.
Donnelly, M., Luke, G., 2001. Analysis of the aphthovirus 2A/2B polyprotein "cleavage"mechanism indicates not a proteolytic reaction, but a novel translational effect: a putative ribosomal "skip." J. Gen. … 1013–1025.
Dunaief, J.L., Dentchev, T., Ying, G.-S., Milam, A.H., 2002. The role of apoptosis in age-related macular degeneration. Arch. Ophthalmol. (Chicago, Ill. 1960) 120, 1435–42.
Edwards, R.B., Adler, a J., 1994. Exchange of retinol between IRBP and CRBP. Exp. Eye Res.
Ellenbroek, S.I.J., Collard, J.G., 2007. Rho GTPases: functions and association with cancer. Clin. Exp. Metastasis 24, 657–72.
Ellett, F., Pase, L., Hayman, J.W., Andrianopoulos, A., Lieschke, G.J., 2011. Mpeg1 Promoter Transgenes Direct Macrophage-Lineage Expression in Zebrafish. Blood 117, e49–e56.
Elsalini, O.A., Rohr, K.B., 2003. Phenylthiourea disrupts thyroid function in developing zebrafish. Dev. Genes Evol. 212, 593–598.
Engel, S.R., Dietrich, F.S., Fisk, D.G., Binkley, G., Balakrishnan, R., Costanzo, M.C., Dwight, S.S., Hitz, B.C., Karra, K., Nash, R.S., Weng, S., Wong, E.D., Lloyd, P., Skrzypek, M.S., Miyasato, S.R., Simison, M., Cherry, J.M., 2014. The reference genome sequence of Saccharomyces cerevisiae: then and now. G3 (Bethesda). 4,

389–98.
England, S.J., Blanchard, G.B., Mahadevan, L., Adams, R.J., 2006. A dynamic fate map of the forebrain shows how vertebrate eyes form and explains two causes of cyclopia. Development 133, 4613–7.
Erickson, J.W., Cerione, R. a, 2001. Multiple roles for Cdc42 in cell regulation. Curr. Opin. Cell Biol. 13, 153–157.
Etienne-Manneville, S., Hall, A., 2002. Rho GTPases in cell biology. Nature 420, 629–635.
Fang, Y., Gupta, V., Karra, R., Holdway, J.E., Kikuchi, K., Poss, K.D., 2013. Translational profiling of cardiomyocytes identifies an early Jak1/Stat3 injury response required for zebrafish heart regeneration. Proc. Natl. Acad. Sci. U. S. A. 110, 13416–21.
Fausett, B. V, Goldman, D., 2006. A role for alpha1 tubulin-expressing Müller glia in regeneration of the injured zebrafish retina. J. Neurosci. 26, 6303–13.
Fischer, A.J., Bosse, J.L., El-Hodiri, H.M., 2014. Reprint of: The ciliary marginal zone (CMZ) in development and regeneration of the vertebrate eye. Exp. Eye Res. 123, 115–120.
Fischer, J., Giniger, E., Maniatis, T., Ptashne, M., 1988. GAL4 activates transcription in Drosophila. Nature 332, 853–856.
Flicek, P., Amode, M.R., Barrell, D., Beal, K., Billis, K., Brent, S., Carvalho-Silva, D., Clapham, P., Coates, G., Fitzgerald, S., Gil, L., Girón, C.G., Gordon, L., Hourlier, T., Hunt, S., Johnson, N., Juettemann, T., Kähäri, A.K., Keenan, S., Kulesha, E., Martin, F.J., Maurel, T., McLaren, W.M., Murphy, D.N., Nag, R., Overduin, B., Pignatelli, M., Pritchard, B., Pritchard, E., Riat, H.S., Ruffier, M., Sheppard, D., Taylor, K., Thormann, A., Trevanion, S.J., Vullo, A., Wilder, S.P., Wilson, M., Zadissa, A., Aken, B.L., Birney, E., Cunningham, F., Harrow, J., Herrero, J., Hubbard, T.J.P., Kinsella, R., Muffato, M., Parker, A., Spudich, G., Yates, A., Zerbino, D.R., Searle, S.M.J., 2014. Ensembl 2014. Nucleic Acids Res. 42, 749–755.
Ford, K.M., Saint-Geniez, M., Walshe, T., Zahr, A., D'Amore, P.A., 2011. Expression and role of VEGF in the adult retinal pigment epithelium. Investig. Ophthalmol. Vis. Sci. 52, 9478–9487.
Fraser, B., DuVal, M.G., Wang, H., Allison, W.T., 2013. Regeneration of cone photoreceptors when cell ablation is primarily restricted to a particular cone subtype. PLoS One 8, e55410.
Fricke, C., Lee, J.S., Geiger-Rudolph, S., Bonhoeffer, F., Chien, C.B., 2001. Astray, a Zebrafish Roundabout Homolog Required for Retinal Axon Guidance. Science 292, 507–510.
Fuhrmann, S., 2010. Eye Morphogenesis and Patterning of the Optic Vesicle. Curr. Top. Dev. Biol. 93, 61–84.
Fuhrmann, S., Levine, E.M., Reh, T. a, 2000. Extraocular mesenchyme patterns the optic vesicle during early eye development in the embryonic chick. Development 127, 4599–609.

Fuhrmann, S., Zou, C., Levine, E.M., 2014. Retinal pigment epithelium development, plasticity, and tissue homeostasis. Exp. Eye Res. 123, 141–150.
Fujimura, N., Taketo, M.M., Mori, M., Korinek, V., Kozmik, Z., 2009. Spatial and temporal regulation of Wnt/??-catenin signaling is essential for development of the retinal pigment epithelium. Dev. Biol. 334, 31–45.
Gabriel, J., Trivedi, C., Maurer, C., 2012. Layer-Specific Targeting of Direction Selective Neurons in the Zebrafish Optic Tectum. Neuron 76, 1147–1160.
Gamm, D.M., Melvan, J.N., Shearer, R.L., Pinilla, I., Sabat, G., Svendsen, C.N., Wright, L.S., 2008. A novel serum-free method for culturing human prenatal retinal pigment epithelial cells. Investig. Ophthalmol. Vis. Sci. 49, 788–799.
Gargiulo, A., Bonetti, C., Montefusco, S., Neglia, S., Di Vicino, U., Marrocco, E., Corte, M. Della, Domenici, L., Auricchio, A., Surace, E.M., 2009. AAV-mediated tyrosinase gene transfer restores melanogenesis and retinal function in a model of oculo-cutaneous albinism type I (OCA1). Mol. Ther. 17, 1347–1354.
Gargiulo, A., Testa, F., Rossi, S., Di Iorio, V., Fecarotta, S., de Berardinis, T., Iovine, A., Magli, A., Signorini, S., Fazzi, E., Galantuomo, M.S., Fossarello, M., Montefusco, S., Ciccodicola, A., Neri, A., Macaluso, C., Simonelli, F., Surace, E.M., 2011. Molecular and clinical characterization of albinism in a large cohort of Italian patients. Invest. Ophthalmol. Vis. Sci. 52, 1281–1289.
Gestri, G., Link, B., Neuhauss, S., 2012. The Visual System of Zebrafish and its Use to Model Human Retinal Diseases. Dev. … 72, 302–327.
Gnanaguru, G., Choi, A.R., Amarnani, D., D'Amore, P.A., 2016. Oxidized Lipoprotein Uptake Through the CD36 Receptor Activates the NLRP3 Inflammasome in Human Retinal Pigment Epithelial Cells. Investig. Opthalmology Vis. Sci. 57, 4704.
Goldman, D., 2014. Müller glial cell reprogramming and retina regeneration. Nat. Rev. Neurosci. 15, 431–42.
Goll, M.G., Anderson, R., Stainier, D.Y.R., Spradling, A.C., Halpern, M.E., 2009. Transcriptional silencing and reactivation in transgenic zebrafish. Genetics 182, 747–55.
Golling, G., Amsterdam, A., Sun, Z., Antonelli, M., Maldonado, E., Chen, W., Burgess, S., Haldi, M., Artzt, K., Farrington, S., Lin, S.-Y., Nissen, R.M., Hopkins, N., 2002. Insertional mutagenesis in zebrafish rapidly identifies genes essential for early vertebrate development. Nat. Genet. 31, 135–140.
Gonzalez-Fernandez, F., 2003. Interphotoreceptor retinoid-binding protein - An old gene for new eyes. Vision Res. 43, 3021–3036.
Govek, E., Newey, S., Aelst, L. Van, 2005. The role of the Rho GTPases in neuronal development. Genes Dev. 1–49.
Graw, J., 2003. The genetic and molecular basis of congenital eye defects. Nat Rev Genet 4, 876–888.
Grierson, I., Hiscott, P., Hogg, P., Robey, H., 1994. Development, repair and regeneration of the retinal pigment epithelium. Eye 8, 255–262.
Griscelli, C., Durandy, a, Guy-Grand, D., Daguillard, F., Herzog, C., Prunieras, M., 1978. A syndrome associating partial albinism and immunodeficiency. Am. J. Med.

65, 691–702.
Grønskov, K., Ek, J., Brondum-Nielsen, K., 2007. Oculocutaneous albinism. Orphanet J. Rare Dis. 2, 43.
Grønskov, K., Ek, J., Sand, A., Scheller, R., Bygum, A., Brixen, K., Brondum-Nielsen, K., Rosenberg, T., 2009. Birth prevalence and mutation spectrum in Danish patients with autosomal recessive albinism. Investig. Ophthalmol. Vis. Sci. 50, 1058–1064.
Gross, J., Perkins, B., 2008. Zebrafish mutants as models for congenital ocular disorders in humans. Mol. Reprod. Dev. 555, 547–555.
Haffter, P., Granato, M., Brand, M., Mullins, M.C., Hammerschmidt, M., Kane, D. a, Odenthal, J., van Eeden, F.J., Jiang, Y.J., Heisenberg, C.P., Kelsh, R.N., Furutani-Seiki, M., Vogelsang, E., Beuchle, D., Schach, U., Fabian, C., Nüsslein-Volhard, C., 1996. The identification of genes with unique and essential functions in the development of the zebrafish, Danio rerio. Development 123, 1–36.
Hall, A., 1998. Rho GTPases and the Actin Cytoskeleton. Science (80-.). 279, 509–514.
Hamel, C.P., Tsilou, E., Pfeffer, B. a, Hooks, J.J., Detrick, B., Redmond, T.M., 1993. Molecular cloning and expression of RPE65, a novel retinal pigment epithelium-specific microsomal protein that is post-transcriptionally regulated in vitro. J. Biol. Chem. 268, 15751–7.
Hanovice, N.J., McMains, E., Gross, J.M., 2016. A GAL4-inducible transgenic toolkit for the in vivo modulation of Rho GTPase activity in zebrafish. Dev. Dyn. 844–853.
Hanus, J., Anderson, C., Wang, S., 2015. RPE necroptosis in response to oxidative stress and in AMD. Ageing Res. Rev. 24, 286–298.
Hartsock, A., Lee, C., Arnold, V., Gross, J.M., 2014. In vivo analysis of hyaloid vasculature morphogenesis in zebrafish: A role for the lens in maturation and maintenance of the hyaloid. Dev. Biol. 1–13.
Haruta, M., 2004. In Vitro and In Vivo Characterization of Pigment Epithelial Cells Differentiated from Primate Embryonic Stem Cells. Invest. Ophthalmol. Vis. Sci. 45, 1020–1025.
Haynes, T., Del Rio-Tsonis, K., 2004. Retina repair, stem cells and beyond. Curr. Neurovasc. Res. 1, 231–239.
Heasman, S.J., Ridley, A.J., 2008. Mammalian Rho GTPases: new insights into their functions from in vivo studies. Nat. Rev. Mol. Cell Biol. 9, 690–701.
Heermann, S., Schütz, L., Lemke, S., Krieglstein, K., Wittbrodt, J., 2015. Eye morphogenesis driven by epithelial flow into the optic cup facilitated by modulation of bone morphogenetic protein. Elife 4, 1–17.
Heller, J.P., Martin, K.R., 2014. Enhancing RPE Cell-Based Therapy Outcomes for AMD: The Role of Bruch's Membrane. Transl. Vis. Sci. Technol. 3, 11.
Herbomel, P., Thisse, B., Thisse, C., 1999. Ontogeny and behaviour of early macrophages in the zebrafish embryo. Development 126, 3735–45.
Herbomel, P., Thisse, B., Thisse, C., 2001. Zebrafish early macrophages colonize cephalic mesenchyme and developing brain, retina, and epidermis through a M-CSF receptor-dependent invasive process. Dev. Biol. 238, 274–88.
Hergott, G.J., Nagai, H., Kalnins, V.I., 1993. Inhibition of retinal pigment epithelial cell

migration and proliferation with monoclonal antibodies against the beta 1 integrin subunit during wound healing in organ culture. Invest Ophthalmol Vis Sci 34, 2761–2768.
Heriot, W., Machemer, R., 1992. Pigment epithelial repair. Graefe's Arch. Clin. Exp. … 91–100.
Hertwig, P., 1942. Neue Mutationen und Koppelungsgruppen bei der Hausmaus. Z. Indukt. Abstamm. Vererbungsl. 80, 220–246.
Heynen, S.R., Meneau, I., Caprara, C., Samardzija, M., Imsand, C., Levine, E.M., Grimm, C., 2013. CDC42 is required for tissue lamination and cell survival in the mouse retina. PLoS One 8, e53806.
Higashijima, S., Hotta, Y., Okamoto, H., 2000. Visualization of cranial motor neurons in live transgenic zebrafish expressing green fluorescent protein under the control of the islet-1 promoter/enhancer. J. Neurosci. 20, 206–18.
Hill, R.E., Favor, J., Hogan, B.L., Ton, C.C., Saunders, G.F., Hanson, I.M., Prosser, J., Jordan, T., Hastie, N.D., van Heyningen, V., 1991. Mouse small eye results from mutations in a paired-like homeobox-containing gene. Nature 354, 522–525.
Hiscott, P., Sheridan, C., Magee, R.M., Grierson, I., 1999. Matrix and the retinal pigment epithelium in proliferative retinal disease. Prog. Retin. Eye Res. 18, 167–90.
Hodgkinson, C.A., Moore, K.J., Nakayama, A., Steingrímsson, E., Copeland, N.G., Jenkins, N.A., Arnheiter, H., 1993. Mutations at the mouse microphthalmia locus are associated with defects in a gene encoding a novel basic-helix-loop-helix-zipper protein. Cell 74, 395–404.
Hsu, C.C., Hou, M.F., Hong, J.R., Wu, J.L., Her, G.M., 2010. Inducible male infertility by targeted cell ablation in zebrafish testis. Mar. Biotechnol. 12, 466–478.
Hsu, C.L., Muerdter, C.P., Knickerbocker, A.D., Walsh, R.M., Zepeda-Rivera, M. a, Depner, K.H., Sangesland, M., Cisneros, T.B., Kim, J.Y., Sanchez-Vazquez, P., Cherezova, L., Regan, R.D., Bahrami, N.M., Gray, E. a, Chan, A.Y., Chen, T., Rao, M.Y., Hille, M.B., 2012. Cdc42 GTPase and Rac1 GTPase act downstream of p120 catenin and require GTP exchange during gastrulation of zebrafish mesoderm. Dev. Dyn. 241, 1545–61.
Hu, J., Bok, D., 2001. A cell culture medium that supports the differentiation of human retinal pigment epithelium into functionally polarized monolayers. Mol. Vis. 7, 14–19.
Huang, Y.-Y., Neuhauss, S.C.F., 2008. The optokinetic response in zebrafish and its applications. Technology 13, 1899–1916.
Huizing, M., Helip-wooley, A., Westbroek, W., Gunay-aygun, M., Gahl, W. a, 2008. Disorders of lysosome-related organelle biogenesis: clinical and molecular genetics. Annu Rev Genomics Hum Genet. 2008 9, 359–386.
Hussain, N.K., Jenna, S., Glogauer, M., Quinn, C.C., Wasiak, S., Guipponi, M., Antonarakis, S.E., Kay, B.K., Stossel, T.P., Lamarche-Vane, N., McPherson, P.S., 2001. Endocytic protein intersectin-l regulates actin assembly via Cdc42 and N-WASP. Nat. Cell Biol. 3, 927–932.
Hutton, S.M., Spritz, R. a, 2008. Comprehensive analysis of oculocutaneous albinism

among non-Hispanic caucasians shows that OCA1 is the most prevalent OCA type. J. Invest. Dermatol. 128, 2442–2450.
Idelson, M., Alper, R., Obolensky, A., Ben-Shushan, E., Hemo, I., Yachimovich-Cohen, N., Khaner, H., Smith, Y., Wiser, O., Gropp, M., Cohen, M. a, Even-Ram, S., Berman-Zaken, Y., Matzrafi, L., Rechavi, G., Banin, E., Reubinoff, B., 2009. Directed differentiation of human embryonic stem cells into functional retinal pigment epithelium cells. Cell Stem Cell 5, 396–408.
Imai, C., Sugai, T., Iritani, S., Niizato, K., Nakamura, R., Makifuchi, T., Kakita, A., Takahashi, H., Nawa, H., 2001. A quantitative study on the expression of synapsin II and N-ethylmaleimide-sensitive fusion protein in schizophrenic patients. Neurosci. Lett. 305, 185–188.
Ivanovitch, K., Cavodeassi, F., Wilson, S.W., 2013. Precocious Acquisition of Neuroepithelial Character in the Eye Field Underlies the Onset of Eye Morphogenesis. Dev. Cell 27, 293–305.
Iyengar, S., Kasheta, M., Ceol, C.J., 2015. Poised Regeneration of Zebrafish Melanocytes Involves Direct Differentiation and Concurrent Replenishment of Tissue-Resident Progenitor Cells. Dev. Cell 33, 631–643.
Jablonski, M.M., Tombran-Tink, J., Mrazek, D.A., Iannaccone, A., 2000. Pigment epithelium-derived factor supports normal development of photoreceptor neurons and opsin expression after retinal pigment epithelium removal. J. Neurosci. 20, 7149–7157.
Jackson, B., Peyrollier, K., Pedersen, E., Basse, A., Karlsson, R., Wang, Z., Lefever, T., Ochsenbein, A.M., Schmidt, G., Aktories, K., Stanley, A., Quondamatteo, F., Ladwein, M., Rottner, K., van Hengel, J., Brakebusch, C., 2011. RhoA is dispensable for skin development, but crucial for contraction and directed migration of keratinocytes. Mol. Biol. Cell 22, 593–605.
Jaffe, A.B., Hall, A., 2005. Rho GTPases: biochemistry and biology. Annu. Rev. Cell Dev. Biol. 21, 247–69.
Jahn, R., Scheller, R.H., 2006. SNAREs--engines for membrane fusion. Nat. Rev. Mol. Cell Biol. 7, 631–643.
James, A., Lee, C., Williams, A.M., Angileri, K., Lathrop, K.L., Gross, J.M., 2016. The hyaloid vasculature facilitates basement membrane breakdown during choroid fissure closure in the zebrafish eye. Dev. Biol. 419, 262–272.
Jao, L.-E., Wente, S.R., Chen, W., 2013. Efficient multiplex biallelic zebrafish genome editing using a CRISPR nuclease system. Proc. Natl. Acad. Sci. U. S. A. 110, 13904–9.
Jeffery, G., 1997. The albino retina: An abnormality that provides insight into normal retinal development. Trends Neurosci. 20, 165–169.
Jeffery, G., 1998. The retinal pigment epithelium as a developmental regulator of the neural retina. Eye (Lond). 12 (Pt 3b, 499–503.
Jiang, L., Hamasaki, D., 1994. Corneal electroretinographic function rescued by normal retinal pigment epithelial grafts in retinal degenerative Royal College of Surgeons rats. Invest. Ophthalmol. Vis. Sci. 35, 4300–4309.

Jin, M., Guan, C., Jiang, Y., Chen, G., Zhao, C., Cui, K., Song, Y., Wu, C., Poo, M., Yuan, X., 2005. Ca2+-dependent regulation of rho GTPases triggers turning of nerve growth cones. J. Neurosci. 25, 2338–47.

Johnson, K., Barragan, J., Bashiruddin, S., Smith, C.J., Tyrrell, C., Parsons, M.J., Doris, R., Kucenas, S., Downes, G.B., Velez, C.M., Schneider, C., Sakai, C., Pathak, N., Anderson, K., Stein, R., Devoto, S.H., Mumm, J.S., Barresi, M.J.F., 2016. Gfap-positive radial glial cells are an essential progenitor population for later-born neurons and glia in the zebrafish spinal cord. Glia 64, 1170–1189.

Jowett, T., Lettice, L., 1994. Whole-mount in situ hybridizationon zebrafish embryos using a mixture of digoxigenin- and fluorescein-labelled probes. Trends Genet.

Jung, I., Leem, G., 2013. Glioma is formed by active Akt1 and promoted by active Rac1 in transgenic zebrafish. Neuro. Oncol. 1–15.

Kaarbø, M., Crane, D.I., Murrell, W.G., 2003. RhoA is highly up-regulated in the process of early heart development of the chick and important for normal embryogenesis. Dev. Dyn. 227, 35–47.

Kamao, H., Mandai, M., Ohashi, W., Hirami, Y., Kurimoto, Y., Kiryu, J., Takahashi, M., Young RW, D., B., Bressler NM, Bressler SB, SL., F., Rosenfeld PJ, Brown DM, Heier JS, Algvere PV, Berglin L, Gouras P, Y., S., Binder S, Stolba U, Krebs I, Falkner-Radler CI, Krebs I, Glittenberg C, Takahashi K, Tanabe K, Ohnuki M, Tezel TH, LV., D.P., Bhatt NS, Newsome DA, Fenech T, Lee CJ, Huie P, Leng T, Stanzel BV, Liu Z, Brinken R, Diniz B, Thomas P, Thomas B, Oganesian A, Gabrielian K, Ernest JT, Yang J, Yamato M, Kohno C, Kamao H, Mandai M, Okamoto S, Kanemura H, Go JM, Shikamura M, Sheng Y, Gouras P, Cao H, Yaji N, Yamato M, Yang J, Nakagawa M, Koyanagi M, Tanabe K, Okita K, Matsumura Y, Sato Y, Hirami Y, Osakada F, Takahashi K, Kamao H, Mandai M, Wakamiya S, Schwartz DS, Hubschman J-P, Heilwell G, Van Meurs JC, PR., V.D.B., 2017. Evaluation of the Surgical Device and Procedure for Extracellular Matrix–Scaffold–Supported Human iPSC–Derived Retinal Pigment Epithelium Cell Sheet Transplantation. Investig. Opthalmology Vis. Sci. 58, 211.

Kamao, H., Mandai, M., Okamoto, S., Sakai, N., Suga, A., Sugita, S., Kiryu, J., Takahashi, M., 2014. Characterization of human induced pluripotent stem cell-derived retinal pigment epithelium cell sheets aiming for clinical application. Stem Cell Reports 2, 205–218.

Kardash, E., Reichman-Fried, M., Maître, J.-L., Boldajipour, B., Papusheva, E., Messerschmidt, E.-M., Heisenberg, C.-P., Raz, E., 2010. A role for Rho GTPases and cell-cell adhesion in single-cell motility in vivo. Nat. Cell Biol. 12, 47-53–11.

Kassen, S.C., Ramanan, V., Montgomery, J.E., Burket, C.T., Liu, C., Vihtelic, T.S., Hyde, D.R., 2007. Time Course Analysis of Gene Expression During Light-Induced Photoreceptor Cell Death and Regeneration in albino Zebrafish.

Kausar, T., Bhatti, M., Ali, M., Shaikh, R., Ahmed, Z., 2013. OCA5, a novel locus for non-syndromic oculocutaneous albinism, maps to chromosome 4q24. Clin. Genet. 84, 91–93.

Kearse, M., Moir, R., Wilson, A., Stones-Havas, S., Cheung, M., Sturrock, S., Buxton,

S., Cooper, A., Markowitz, S., Duran, C., Thierer, T., Ashton, B., Meintjes, P., Drummond, A., 2012. Geneious Basic: An integrated and extendable desktop software platform for the organization and analysis of sequence data. Bioinformatics 28, 1647–1649.

Kelsh, R.N., Brand, M., Jiang, Y.J., Heisenberg, C.P., Lin, S., Haffter, P., Odenthal, J., Mullins, M.C., van Eeden, F.J., Furutani-Seiki, M., Granato, M., Hammerschmidt, M., Kane, D. a, Warga, R.M., Beuchle, D., Vogelsang, L., Nüsslein-Volhard, C., 1996. Zebrafish pigmentation mutations and the processes of neural crest development. Development 123, 369–389.

Kennedy, B.N., Stearns, G.W., Smyth, V. a, Ramamurthy, V., van Eeden, F., Ankoudinova, I., Raible, D., Hurley, J.B., Brockerhoff, S.E., 2004. Zebrafish rx3 and mab21l2 are required during eye morphogenesis. Dev. Biol. 270, 336–49.

Kevany, B., Palczewski, K., 2010. Phagocytosis of retinal rod and cone photoreceptors. Physiology 25, 8–15.

Kieserman, E.K., Wallingford, J.B., 2009. In vivo imaging reveals a role for Cdc42 in spindle positioning and planar orientation of cell divisions during vertebrate neural tube closure. J. Cell Sci. 122, 2481–2490.

Kikuchi, K., Holdway, J.E., Werdich, A. a, Anderson, R.M., Fang, Y., Egnaczyk, G.F., Evans, T., Macrae, C. a, Stainier, D.Y.R., Poss, K.D., 2010. Primary contribution to zebrafish heart regeneration by gata4(+) cardiomyocytes. Nature 464, 601–5.

Kim, G.-H., Her, J.-H., Han, J.-K., 2008. Ryk cooperates with Frizzled 7 to promote Wnt11-mediated endocytosis and is essential for Xenopus laevis convergent extension movements. J. Cell Biol. 182, 1073–82.

Kimmel, C.B., Ballard, W.W., Kimmel, S.R., Ullmann, B., Schilling, T.F., 1995. Stages of embryonic development of the zebrafish. Dev. Dyn. an Off. public 203, 253–310.

Kizil, C., Kaslin, J., Kroehne, V., Brand, M., 2012. Adult neurogenesis and brain regeneration in zebrafish. Dev. Neurobiol. 72, 429–461.

Klabunde, T., Eicken, C., Sacchettini, J.C., Krebs, B., 1998. Crystal structure of a plant catechol oxidase containing a dicopper center. Nat. Struct. Biol. 5, 1084–1090.

Klein, R., Chou, C.-F., Klein, B.E.K., Zhang, X., Meuer, S.M., Saaddine, J.B., 2011. Prevalence of age-related macular degeneration in the US population. Epidemiology 129, 75–80.

Knox, R.J., Friedlos, F., Jarman, M., Roberts, J.J., 1988. A new cytotoxic, DNA interstrand crosslinking agent, 5-(aziridin-1-yl)-4-hydroxylamino-2-nitrobenzamide, is formed from 5-(aziridin-1-yl)-2,4-dinitrobenzamide (CB 1954) by a nitroreductase enzyme in walker carcinoma cells. Biochem. Pharmacol. 37, 4661–4669.

Korner, A., Pawelek, J., 1982. Mammalian tyrosinase catalyzes three reactions in the biosynthesis of melanin. Science (80-.). 17, 1163–1165.

Korte, G.E., Reppucci, V., Henkind, P., 1984. RPE destruction causes choriocapillary atrophy. Invest. Ophthalmol. Vis. Sci. 25, 1135–45.

Krauss, J., Geiger-Rudolph, S., Koch, I., Nüsslein-Volhard, C., Irion, U., 2014. A dominant mutation in tyrp1A leads to melanophore death in zebrafish. Pigment Cell

Melanoma Res.
Krohne, T.U., Westenskow, P.D., Kurihara, T., Friedlander, D.F., Lehmann, M., Dorsey, A.L., Li, W., Zhu, S., Schultz, A., Wang, J., Siuzdak, G., Ding, S., Friedlander, M., 2012. Generation of retinal pigment epithelial cells from small molecules and OCT4 reprogrammed human induced pluripotent stem cells. Stem Cells Transl. Med. 1, 96–109.
Kroschewski, R., Hall, a, Mellman, I., 1999. Cdc42 controls secretory and endocytic transport to the basolateral plasma membrane of MDCK cells. Nat. Cell Biol. 1, 8–13.
Kuksa, V., Imanishi, Y., Batten, M., Palczewski, K., Moise, A.R., 2003. Retinoid cycle in the vertebrate retina: Experimental approaches and mechanisms of isomerization. Vision Res. 43, 2959–2981.
Kurrasch, D.M., Nevin, L.M., Wong, J.S., Baier, H., Ingraham, H. a, 2009. Neuroendocrine transcriptional programs adapt dynamically to the supply and demand for neuropeptides as revealed in NSF mutant zebrafish. Neural Dev. 4, 22.
Kwan, K.M., Fujimoto, E., Grabher, C., Mangum, B.D., Hardy, M.E., Campbell, D.S., Parant, J.M., Yost, H.J., Kanki, J.P., Chien, C.-B., 2007. The Tol2kit: a multisite gateway-based construction kit for Tol2 transposon transgenesis constructs. Dev. Dyn. 236, 3088–99.
Kwan, K.M., Otsuna, H., Kidokoro, H., Carney, K.R., Saijoh, Y., Chien, C.-B., 2012. A complex choreography of cell movements shapes the vertebrate eye. Development 139, 359–372.
Kyritsis, N., Kizil, C., Brand, M., 2014. Neuroinflammation and central nervous system regeneration in vertebrates. Trends Cell Biol. 24, 128–135.
Lagutin, O. V., Zhu, C.C., Kobayashi, D., Topczewski, J., Shimamura, K., Puelles, L., Russell, H.R.C., McKinnon, P.J., Solnica-Krezel, L., Oliver, G., 2003. Six3 repression of Wnt signaling in the anterior neuroectoderm is essential for vertebrate forebrain development. Genes Dev. 17, 368–379.
Lai, S.-L., Chang, C.-N., Wang, P.-J., Lee, S.-J., 2005. Rho mediates cytokinesis and epiboly via ROCK in zebrafish. Mol. Reprod. Dev. 71, 186–96.
Lam, S.H., Chua, H.L., Gong, Z., Lam, T.J., Sin, Y.M., 2004. Development and maturation of the immune system in zebrafish, Danio rerio: A gene expression profiling, in situ hybridization and immunological study. Dev. Comp. Immunol. 28, 9–28.
Lamason, R.L., Mohideen, M.P.K., Mest, J.R., Wong, A.C., Norton, H.L., Aros, M.C., Jurynec, M.J., Mao, X., Humphreville, V.R., Humbert, J.E., Sinha, S., Moore, J.L., Jagadeeswaran, P., Zhao, W., Ning, G., Makalowska, I., McKeigue, P.M., O'donnell, D., Kittles, R., Parra, E.J., Mangini, N.J., Grunwald, D.J., Shriver, M.D., Canfield, V.A., Cheng, K.C., 2005. SLC24A5, a putative cation exchanger, affects pigmentation in zebrafish and humans. Science 310, 1782–1786.
Lane, B.M., Lister, J. a, 2012. Otx but not Mitf transcription factors are required for zebrafish retinal pigment epithelium development. PLoS One 7, e49357.
Langenau, D.M., Ferrando, A.A., Traver, D., Kutok, J.L., Hezel, J.-P.P.D., Kanki, J.P.,

Zon, L.I., Look, a T., Trede, N.S., 2004. In vivo tracking of T cell development, ablation, and engraftment in transgenic zebrafish. Proc Natl Acad Sci U S A 101, 7369–7374.
Lawrence, J., Sauvé, Y., Keegan, D., 2000. Schwann cell grafting into the retina of the dystrophic RCS rat limits functional deterioration. Invest. Ophthalmol. Vis. Sci. 41, 518–528.
Leach, L.L., Clegg, D.O., 2015. Concise Review: Making Stem Cells Retinal: Methods for Deriving Retinal Pigment Epithelium and Implications for Patients with Ocular Disease. Stem Cells 33, 2363–2373.
Lee, J., Cox, B.D., Daly, C.M.S., Lee, C., Nuckels, R.J., Tittle, R.K., Uribe, R. a, Gross, J.M., 2012. An ENU mutagenesis screen in zebrafish for visual system mutants identifies a novel splice-acceptor site mutation in patched2 that results in Colobomas. Invest. Ophthalmol. Vis. Sci. 53, 8214–21.
Lee, J., Gross, J.M., 2007. Laminin B1 and y1 containing laminins are essential for basement membrane integrity in the zebrafish eye. Investig. Ophthalmol. Vis. Sci. 48, 2483–2490.
Lee, J., Willer, J.R., Willer, G.B., Smith, K., Gregg, R.G., Gross, J.M., 2008. Zebrafish blowout provides genetic evidence for Patched1 mediated negative regulation of Hedghog signaling within the proximal optic vesicle of the vertebrate eye. Dev. Biol. 319, 10–22.
Lee, Y.N., Malbon, C.C., Wang, H.Y., 2004. Ga13 signals via p115RhoGEF cascades regulating JNK1 and primitive endoderm formation. J. Biol. Chem. 279, 54896–54904.
Lemeer, S., Ruijtenbeek, R., Pinkse, M.W.H., Jopling, C., Heck, A.J.R., den Hertog, J., Slijper, M., 2007. Endogenous phosphotyrosine signaling in zebrafish embryos. Mol. Cell. Proteomics 6, 2088–99.
Leung, Y.F., Ma, P., Dowling, J.E., 2007. Gene expression profiling of zebrafish embryonic retinal pigment epithelium in vivo. Investig. Ophthalmol. Vis. Sci. 48, 881–890.
Levin, A. V, Stroh, E., 2011. Albinism for the busy clinician. J. AAPOS 15, 59–66.
Li, H., Tierney, C., Wen, L., Wu, J.Y., Rao, Y., 1997. A single morphogenetic field gives rise to two retina primordia under the influence of the prechordal plate. Development 124, 603–15.
Li, L., Yan, B., Shi, Y.Q., Zhang, W.Q., Wen, Z.L., 2012. Live imaging reveals differing roles of macrophages and neutrophils during zebrafish tail fin regeneration. J. Biol. Chem. 287, 25353–25360.
Li, X., Montgomery, J., Cheng, W., Noh, J.H., Hyde, D.R., Li, L., 2012. Pineal photoreceptor cells are required for maintaining the circadian rhythms of behavioral visual sensitivity in zebrafish. PLoS One 7, e40508.
Li, Y., Allende, M.L., Finkelstein, R., Weinberg, E.S., 1994. Expression of two zebrafish orthodenticle-related genes in the embryonic brain. Mech. Dev. 48, 229–244.
Li, Z., Joseph, N.M., Easter, S.S., 2000. The morphogenesis of the zebrafish eye, including a fate map of the optic vesicle. Dev. Dyn. 218, 175–188.

Li, Z., Ptak, D., Zhang, L., Walls, E.K., Zhong, W., Leung, Y.F., 2012. Phenylthiourea specifically reduces zebrafish eye size. PLoS One 7, 1–14.
Lieschke, G.J., Currie, P.D., 2007. Animal models of human disease: zebrafish swim into view. Nat. Rev. Genet. 8, 353–67.
Lim, L.S., Mitchell, P., Seddon, J.M., Holz, F.G., Wong, T.Y., 2012a. Age-related macular degeneration. Lancet 379, 1728–38.
Lim, L.S., Mitchell, P., Seddon, J.M., Holz, F.G., Wong, T.Y., 2012b. Age-related macular degeneration. Lancet 379, 1728–38.
Link, V., Shevchenko, A., Heisenberg, C.-P., 2006. Proteomics of early zebrafish embryos. BMC Dev. Biol. 6, 1.
Lister, J.A., Lane, B.M., Nguyen, A., Lunney, K., 2011. Embryonic expression of zebrafish MiT family genes Tfe3b, Tfeb, and Tfec. Dev. Dyn. 240, 2529–2538.
Little, C.W., Cox, C., Wyatt, J., del Cerro, C., del Cerro, M., 1998. Correlates of photoreceptor rescue by transplantation of human fetal RPE in the RCS rat. Exp. Neurol. 149, 151–60.
Livak, K.J., Schmittgen, T.D., 2001. Analysis of relative gene expression data using real-time quantitative PCR and the 2(-Delta Delta C(T)) Method. Methods San Diego Calif 25, 402–408.
Longbottom, R., Fruttiger, M., Douglas, R.H., Martinez-Barbera, J.P., Greenwood, J., Moss, S.E., 2009. Genetic ablation of retinal pigment epithelial cells reveals the adaptive response of the epithelium and impact on photoreceptors. Proc. Natl. Acad. Sci. U. S. A. 106, 18728–33.
Loosli, F., Winkler, S., Burgtorf, C., Wurmbach, E., Ansorge, W., Henrich, T., Grabher, C., Arendt, D., Carl, M., Krone, a, Grzebisz, E., Wittbrodt, J., 2001. Medaka eyeless is the key factor linking retinal determination and eye growth. Development 128, 4035–4044.
Lopes, V.S., Wasmeier, C., Seabra, M.C., Futter, C.E., 2007. Melanosome Maturation Defect in Rab38-deficient Retinal Pigment Epithelium Results in Instability of Immature Melanosomes during Transient Melanogenesis. Mol. Biol. Cell 19, 3914–3927.
Lopez, P.F., Yan, Q., Kohen, L., Rao, N.A., Spee, C., Black, J., Oganesian, A., 1995. Retinal Pigment Epithelial Wound Healing In Vivo. JAMA Ophthalmol. 113, 1437–1446.
Lopez, R., Gouras, P., Kjeldbye, H., 1989. Transplanted retinal pigment epithelium modifies the retinal degeneration in the RCS rat. Invest. Ophthalmol. Vis. Sci. 30, 586–588.
Lowery, L.A., Sive, H., 2004. Strategies of vertebrate neurulation and a re-evaluation of teleost neural tube formation. Mech. Dev. 121, 1189–1197.
Luo, L., 2002. Actin cytoskeleton regulation in neuronal morphogenesis and structural plasticity. Annu. Rev. Cell Dev. Biol. 18, 601–35.
Luo, L., Hensch, T., Ackerman, L., Barbel, S., 1996. Differential effects of the Rac GTPase on Purkinje cell axons and dendritic trunks and spines. Nature 379, 837–840.

Luz-Madrigal, A., Grajales-Esquivel, E., McCorkle, A., DiLorenzo, A.M., Barbosa-Sabanero, K., Tsonis, P. a, Del Rio-Tsonis, K., 2014. Reprogramming of the chick retinal pigmented epithelium after retinal injury. BMC Biol. 12, 28.

Macdonald, R., Barth, K. a, Xu, Q., Holder, N., Mikkola, I., Wilson, S.W., 1995. Midline signalling is required for Pax gene regulation and patterning of the eyes. Development 121, 3267–3278.

Machalińska, A., Kawa, M.P., Pius-Sadowska, E., Rogińska, D., Kłos, P., Baumert, B., Wiszniewska, B., Machaliński, B., 2013. Endogenous regeneration of damaged retinal pigment epithelium following low dose sodium iodate administration: an insight into the role of glial cells in retinal repair. Exp. Eye Res. 112, 68–78.

Machemer, R., Horn, D. Van, Aaberg, T., 1978. Pigment epithelial proliferation in human retinal detachment with massive periretinal proliferation. Am. J. … 85, 181–191.

Machemer, R., Laqua, H., 1975. Pigment Epithelium Proliferation in Retinal Detachment (Massive Periretinal Proliferation). Am. J. Ophthalmol. 80, 1–23.

Maddala, R., Chauhan, B.K., Walker, C., Zheng, Y., Robinson, M.L., Lang, R.A., Rao, P. V., 2011. Rac1 GTPase-deficient mouse lens exhibits defects in shape, suture formation, fiber cell migration and survival. Dev. Biol. 360, 30–43.

Maddala, R., Deng, P.-F., Costello, J.M., Wawrousek, E.F., Zigler, J.S., Rao, V.P., 2004. Impaired cytoskeletal organization and membrane integrity in lens fibers of a Rho GTPase functional knockout transgenic mouse. Lab. Invest. 84, 679–692.

Magdaleno, S., Jensen, P., Brumwell, C.L., Seal, A., Lehman, K., Asbury, A., Cheung, T., Cornelius, T., Batten, D.M., Eden, C., Norland, S.M., Rice, D.S., Dosooye, N., Shakya, S., Mehta, P., Curran, T., 2006. BGEM: An in situ hybridization database of gene expression in the embryonic and adult mouse nervous system. PLoS Biol. 4, 497–500.

Maminishkis, A., Chen, S., Jalickee, S., Banzon, T., Shi, G., Wang, F.E., Ehalt, T., Hammer, J.A., Miller, S.S., 2006. Confluent monolayers of cultured human fetal retinal pigment epithelium exhibit morphology and physiology of native tissue. Invest. Ophthalmol. Vis. Sci. 47, 3612–24.

Martínez-Morales, J.R., Dolez, V., Rodrigo, I., Zaccarini, R., Leconte, L., Bovolenta, P., Saule, S., 2003. OTX2 activates the molecular network underlying retina pigment epithelium differentiation. J. Biol. Chem. 278, 21721–31.

Martínez-Morales, J.R., Rodrigo, I., Bovolenta, P., 2004. Eye development: a view from the retina pigmented epithelium. Bioessays 26, 766–77.

Martins, R. a P., Pearson, R. a, 2008. Control of cell proliferation by neurotransmitters in the developing vertebrate retina. Brain Res. 1192, 37–60.

Marygold, S.J., Leyland, P.C., Seal, R.L., Goodman, J.L., Strelets, V.B., Wilson, R.J., Ashburner, M., Drysdale, R., De Grey, A., Gelbart, W., Broll, K., Crosby, L., Dos Santos, G., Emmert, D., Falls, K., Gramates, L.S., Matthews, B., Russo, S., Schroeder, A., St. Pierre, S., Zhou, P., Zytkovicz, M., Brown, N.H., Adryan, B., Attrill, H., Costa, M., Field, H., Marigold, S., McQuilton, P., Millburn, G., Ponting, L., Osumi-Sutherland, D., Stefancsik, R., Tweedie, S., Kaufman, T., Matthews, K., Goodmen, J., Grumbling, G., Strelts, V., Thurmond, J., Wong, J.D., Werner-

Washburne, M., Cripps, R., Platero, H., 2013. FlyBase: Improvements to the bibliography. Nucleic Acids Res. 41, 751–757.
Mathers, P.H., Grinberg, a, Mahon, K. a, Jamrich, M., 1997. The Rx homeobox gene is essential for vertebrate eye development. Nature 387, 603–607.
May, a P., Whiteheart, S.W., Weis, W.I., 2001. Unraveling the mechanism of the vesicle transport ATPase NSF, the N-ethylmaleimide-sensitive factor. J. Biol. Chem. 276, 21991–4.
Mazzitello, K.I., Arizmendi, C.M., Family, F., Grossniklaus, H.E., 2009. Formation and growth of lipofuscin in the retinal pigment epithelium cells. Phys Rev E Stat Nonlin Soft Amtter Phys. 80.
Mazzoni, F., Safa, H., Finnemann, S.C., 2014. Understanding photoreceptor outer segment phagocytosis: Use and utility of RPE cells in culture. Exp. Eye Res. 126, 51–60.
Melançon, P., Glick, B., Malhotra, V., 1987. Involvement of GTP-binding "G" proteins in transport through the Golgi stack. Cell 51, 1053–1062.
Mercier, P., Simeone, A., Cotelli, F., Boncinelli, E., 1995. Expression pattern of two otx genes suggests a role in specifying anterior body structures in zebrafish. Int. J. Dev. Biol. 39, 559–573.
Meyer, J.S., Katz, M.L., Maruniak, J. a, Kirk, M.D., 2006. Embryonic Stem Cell-Derived Neural Progenitors Incorporate into Degenerating Retina and Enhance Survival of Host Photoreceptors. Stem Cells 24, 274–283.
Miesfeld, J.B., Gestri, G., Clark, B.S., Flinn, M. a., Poole, R.J., Bader, J.R., Besharse, J.C., Wilson, S.W., Link, B. a., 2015. Yap and Taz regulate retinal pigment epithelial cell fate. Development 3021–3032.
Mizota, A., Adachi-Usami, E., 1997. Functional recovery of retina after sodium iodate injection in mice. Vision Res. 37, 1859–1865.
Mo, W., Nicolson, T., 2011. Both pre- and postsynaptic activity of Nsf prevents degeneration of hair-cell synapses. PLoS One 6, e27146.
Montgomery, J.E., Parsons, M.J., Hyde, D.R., 2010a. A novel model of retinal ablation demonstrates that the extent of rod cell death regulates the origin of the regenerated zebrafish rod photoreceptors. J. Comp. Neurol. 518, 800–14.
Montgomery, J.E., Parsons, M.J., Hyde, D.R., 2010b. A novel model of retinal ablation demonstrates that the extent of rod cell death regulates the origin of the regenerated zebrafish rod photoreceptors. J. Comp. Neurol. 518, 800–14.
Montoliu, L., Grønskov, K., Wei, A.H., Martínez-García, M., Fernández, A., Arveiler, B., Morice-Picard, F., Riazuddin, S., Suzuki, T., Ahmed, Z.M., Rosenberg, T., Li, W., 2014. Increasing the complexity: New genes and new types of albinism. Pigment Cell Melanoma Res. 27, 11–18.
Moore, K.B., Mood, K., Daar, I.O., Moody, S.A., 2004. Morphogenetic movements underlying eye field formation require interactions between the FGF and ephrinB1 signaling pathways. Dev. Cell 6, 55–67.
Mosimann, C., Kaufman, C.K., Li, P., Pugach, E.K., Tamplin, O.J., Zon, L.I., 2011. Ubiquitous transgene expression and Cre-based recombination driven by the

ubiquitin promoter in zebrafish. Development 138, 169–77.
Muccioli, M., Qaisi, D., Herman, K., Plageman, T.F., 2016. Lens placode planar cell polarity is dependent on Cdc42-mediated junctional contraction inhibition. Dev. Biol. 1–12.
Müller, F., Rohrer, H., Vogel-Höpker, A., 2007. Bone morphogenetic proteins specify the retinal pigment epithelium in the chick embryo. Development 134, 3483–3493.
Murray, M., 1953. The effects of administration of sodium iodate to man and animals. Bull. World Health Organ. 9, 211–216.
Nagai, T., Tanaka-Ishikawa, M., Aikawa, R., Ishihara, H., Zhu, W., Yazaki, Y., Nagai, R., Komuro, I., 2003. Cdc42 plays a critical role in assembly of sarcomere units in series of cardiac myocytes. Biochem. Biophys. Res. Commun. 305, 806–810.
Nagashima, M., Barthel, L.K., Raymond, P. a, 2013. A self-renewing division of zebrafish Muller glial cells generates neuronal progenitors that require N-cadherin to regenerate retinal neurons. Development 140, 4510–21.
Nagiec, E.E., Bernstein, A., Whiteheart, S.W., 1995. Each Domain of the N - Ethylmaleimide-sensitive Fusion Protein Contributes to Its Transport Activity *. J. Biol. Chem. 270, 29182–29188.
Navarro, R.E., Ramos-Balderas, J.L., Guerrero, I., Pelcastre, V., Maldonado, E., 2008. Pigment dilution mutants from fish models with connection to lysosome-related organelles and vesicular traffic genes. Zebrafish 5, 309–318.
Neff, M.M., Neff, J.D., Chory, J., Pepper, A.E., 1998. dCAPS, a simple technique for the genetic analysis of single nucleotide polymorphisms: Experimental applications in Arabidopsis thaliana genetics. Plant J. 14, 387–392.
Neff, M.M., Turk, E., Kalishman, M., 2002. Web-based primer design for single nucleotide polymorphism analysis. Trends Genet. 18, 613–615.
Negi, A., Marmor, M., 1984. Healing of photocoagulation lesions affects the rate of subretinal fluid resorption. Ophthalmology 91, 1678–1683.
Nelson, C.M., Ackerman, K.M., O'Hayer, P., Bailey, T.J., Gorsuch, R. a., Hyde, D.R., 2013. Tumor Necrosis Factor-Alpha Is Produced by Dying Retinal Neurons and Is Required for Muller Glia Proliferation during Zebrafish Retinal Regeneration. J. Neurosci. 33, 6524–6539.
Nelson, C.M., Gorsuch, R. a, Bailey, T.J., Ackerman, K.M., Kassen, S.C., Hyde, D.R., 2012. Stat3 defines three populations of müller glia and is required for initiating maximal müller glia proliferation in the regenerating zebrafish retina. J. Comp. Neurol. 520, 4294–311.
Neuhauss, S.C., Biehlmaier, O., Seeliger, M.W., Das, T., Kohler, K., Harris, W. a, Baier, H., 1999. Genetic disorders of vision revealed by a behavioral screen of 400 essential loci in zebrafish. J. Neurosci. 19, 8603–8615.
Neuhauss, S.C.F., 2003. Behavioral genetic approaches to visual system development and function in zebrafish. J. Neurobiol. 54, 148–60.
Ng, A., Uribe, R. a, Yieh, L., Nuckels, R., Gross, J.M., 2009. Zebrafish mutations in gart and paics identify crucial roles for de novo purine synthesis in vertebrate pigmentation and ocular development. Development 136, 2601–2611.

Nguyen, M., Arnheiter, H., 2000. Signaling and transcriptional regulation in early mammalian eye development: a link between FGF and MITF. Development 127, 3581–91.
Nilsson, S.E., Knave, B., Persson, H.E., 1977. Changes in ultrastructure and function of the sheep pigment epithelium and retina induced by sodium iodate. III. Delayed effects. Acta Ophthalmol. 55, 1027–43.
Nobes, C.D., Hall, A., 1995. Rho, Rac, and Cdc42 GTPases regulate the assembly of multimolecular focal complexes associated with actin stress fibers, lamellipodia, and filopodia. Cell 81, 53–62.
Nuckels, R.J., Ng, A., Darland, T., Gross, J.M., 2009. The vacuolar-ATPase complex regulates retinoblast proliferation and survival, photoreceptor morphogenesis, and pigmentation in the zebrafish eye. Invest. Ophthalmol. Vis. Sci. 50, 893–905.
Obholzer, N., Swinburne, I. a, Schwab, E., Nechiporuk, A. V, Nicolson, T., Megason, S.G., 2012. Rapid positional cloning of zebrafish mutations by linkage and homozygosity mapping using whole-genome sequencing. Development 139, 4280–90.
Odenthal, J., Rossnagel, K., Haffter, P., Kelsh, R.N., Vogelsang, E., Brand, M., van Eeden, F.J., Furutani-Seiki, M., Granato, M., Hammerschmidt, M., Heisenberg, C.P., Jiang, Y.J., Kane, D. a, Mullins, M.C., Nüsslein-Volhard, C., 1996. Mutations affecting xanthophore pigmentation in the zebrafish, Danio rerio. Development 123, 391–398.
Oetting, W.S., King, R. a., 1999. Molecular basis of albinism: Mutations and polymorphisms of pigmentation genes associated with albinism. Hum. Mutat. 13, 99–115.
Olson, M., Ashworth, A., Hall, A., 1995. An essential role for Rho, Rac, and Cdc42 GTPases in cell cycle progression through G1. Science (80-.). 269, 1270–1272.
Olson, M.D., 1979. Investigative Ophthalmology & Visual Science chick : an electron microscopic study. Invest. Ophthalmol. Vis. Sci. 18, 329–338.
Onojafe, I.F., Adams, D.R., Simeonov, D.R., Zhang, J., Chan, C., Bernardini, I.M., Sergeev, Y. V, Dolinska, M.B., Alur, R.P., Brilliant, M.H., Gahl, W.A., Brooks, B.P., 2011. Nitisinone improves eye and skin pigmentation defects in a mouse model of oculocutaneous albinism 121.
Orkin, S.H., Zon, L.I., 2008. Hematopoiesis: An Evolving Paradigm for Stem Cell Biology. Cell 132, 631–644.
Orlow, S.J., Brilliant, M.H., 1999. The pink-eyed dilution locus controls the biogenesis of melanosomes and levels of melanosomal proteins in the eye. Exp. Eye Res. 68, 147–154.
Ornitz, D.M., Moreadith, R.W., Leder, P., 1991. Binary system for regulating transgene expression in mice : Targeting int-2 gene expression with yeast GAL4 / UAS control elements 88, 698–702.
Page-McCaw, P.S., Chung, S.C., Muto, A., Roeser, T., Staub, W., Finger-Baier, K.C., Korenbrot, J.I., Baier, H., 2004. Retinal network adaptation to bright light requires tyrosinase. Nat. Neurosci. 7, 1329–1336.

Papan, C., Campos-Ortega, J., 1994. On the formation of the neural keel and neural tube in the zebrafish Danio (Brachydanio) rerio. Roux's Arch. Dev. Biol. 203, 178–186.
Parmeggiani, F., Romano, M.R., Costagliola, C., Semeraro, F., Incorvaia, C., D'Angelo, S., Perri, P., De Palma, P., De Nadai, K., Sebastiani, A., 2012. Mechanism of inflammation in age-related macular degeneration. Mediators Inflamm. 2012.
Parsons, M.J., Pisharath, H., Yusuff, S., Moore, J.C., Siekmann, A.F., Lawson, N., Leach, S.D., 2009. Notch-responsive cells initiate the secondary transition in larval zebrafish pancreas. Mech. Dev. 126, 898–912.
Pearson, R. a, Dale, N., Llaudet, E., Mobbs, P., 2005. ATP released via gap junction hemichannels from the pigment epithelium regulates neural retinal progenitor proliferation. Neuron 46, 731–44.
Penzes, P., Johnson, R.C., Alam, M.R., Kambampati, V., Mains, R.E., Eipper, B.A., 2000. An Isoform of Kalirin , a Brain-specific GDP / GTP Exchange Factor , Is Enriched in the Postsynaptic Density Fraction *. J. Biol. Chem. 275, 6395–6403.
Petrie, T. a, Strand, N.S., Tsung-Yang, C., Rabinowitz, J.S., Moon, R.T., 2014. Macrophages modulate adult zebrafish tail fin regeneration. Development 141, 2581–91.
Peyman, G., Blinder, K., Alturki, W., Nelson, N., Desai, U., 1991. A technique for retinal pigment epithelium transplantation for age-related macular degeneration secondary to extensive subfoveal scarring. Ophthalmic Surg. 22, 102–108.
Phillips, H.M., Murdoch, J.N., Chaudhry, B., Copp, A.J., Henderson, D.J., 2005. Vangl2 acts via RhoA signaling to regulate polarized cell movements during development of the proximal outflow tract. Circ. Res. 96, 292–299.
Piekny, A., Werner, M., Glotzer, M., 2005. Cytokinesis: Welcome to the Rho zone. Trends Cell Biol.
Pinilla, I., Cuenca, N., Martínez-Navarrete, G., Lund, R.D., Sauvé, Y., 2009. Intraretinal processing following photoreceptor rescue by non-retinal cells. Vision Res. 49, 2067–77.
Pisharath, H., Rhee, J.M., Swanson, M. a, Leach, S.D., Parsons, M.J., 2007. Targeted ablation of beta cells in the embryonic zebrafish pancreas using E. coli nitroreductase. Mech. Dev. 124, 218–29.
Portera-Cailliau, C., Sung, C.H., Nathans, J., Adler, R., 1994. Apoptotic photoreceptor cell death in mouse models of retinitis pigmentosa. Proc. Natl. Acad. Sci. U. S. A. 91, 974–8.
Poss, K., Wilson, L., Keating, M., 2002. Heart regeneration in zebrafish. Science (80-.). 298, 2188–2190.
Priore, L.V. Del, Mosinger-ogilvie, J., Kaplan, H.J., Jones, Z., Valentino, T.L., Mosinger-Ogilvie, J., Swinn, M., 1995. Debridement of the Pig Retinal Pigment Epithelium In Vivo. JAMA Opthalmology 113, 939–944.
Puri, N., Gardner, J.M., Brilliant, M.H., 2000. Aberrant pH of melanosomes in pink-eyed dilution (p) mutant melanocytes. J. Invest. Dermatol. 115, 607–613.
Qin, Z., Barthel, L.K., Raymond, P.A., 2009. Genetic evidence for shared mechanisms of epimorphic regeneration in zebrafish. PNAS 106, 9310–9315.

Quinn, J.C., West, J.D., Hill, R.E., 1996. Multiple functions for Pax6 in mouse eye and nasal development. Genes Dev. 10, 435–446.
Raftopoulou, M., Hall, A., 2004. Cell migration: Rho GTPases lead the way. Dev. Biol. 265, 23–32.
Raviv, S., Bharti, K., Rencus-Lazar, S., Cohen-Tayar, Y., Schyr, R., Evantal, N., Meshorer, E., Zilberberg, A., Idelson, M., Reubinoff, B., Grebe, R., Rosin-Arbesfeld, R., Lauderdale, J., Lutty, G., Arnheiter, H., Ashery-Padan, R., 2014. PAX6 Regulates Melanogenesis in the Retinal Pigmented Epithelium through Feed-Forward Regulatory Interactions with MITF. PLoS Genet. 10.
Raymond, P. a, Barthel, L.K., Curran, G. a, 1995. Developmental patterning of rod and cone photoreceptors in embryonic zebrafish. J. Comp. Neurol. 359, 537–50.
Raymond, P., Barthel, L.K., Bernardos, R.L., Perkowski, J.J., 2006. Molecular characterization of retinal stem cells and their niches in adult zebrafish. BMC Dev. Biol. 6, 36.
Redmond, T.M., Yu, S., Lee, E., Bok, D., Hamasaki, D., Chen, N., Goletz, P., Ma, J.X., Crouch, R.K., Pfeifer, K., 1998. Rpe65 is necessary for production of 11-cis-vitamin A in the retinal visual cycle. Nat. Genet. 20, 344–351.
Reinhardt, R., Centanin, L., Tavhelidse, T., Inoue, D., Wittbrodt, B., Concordet, J., Martinez-morales, J.R., Wittbrodt, J., 2015. Sox 2, Tlx, Gli 3, and Her 9 converge on Rx 2 to define retinal stem cells in vivo. EMBO J. 1–17.
Reinisalo, M., Putula, J., Mannermaa, E., Urtti, A., Honkakoski, P., 2012. Regulation of the human tyrosinase gene in retinal pigment epithelium cells: the significance of transcription factor orthodenticle homeobox 2 and its polymorphic binding site. Mol. Vis. 18, 38–54.
Rembold, M., Loosli, F., Adams, R.J., Wittbrodt, J., 2006. Individual cell migration serves as the driving force for optic vesicle evagination. Science 313, 1130–4.
Renshaw, S., Loynes, C., 2006. A transgenic zebrafish model of neutrophilic inflammation. Blood… 108, 3976–3978.
Resnikoff, S., 2008. Global magnitude of visual impairment caused by uncorrected refractive errors in 2004. Bull. World Health Organ. 86, 63–70.
Ridley, A., Paterson, H., Johnston, C., 1992. The Small GTP-Binding Protein rac Regulates Growth Factor-Induced Membrane. Cell 70, 401–410.
Rofagha, S., Bhisitkul, R.B., Boyer, D.S., Sadda, S.R., Zhang, K., 2013. Seven-year outcomes in ranibizumab-treated patients in ANCHOR, MARINA, and HORIZON: A multicenter cohort study (SEVEN-UP). Ophthalmology 120, 2292–2299.
Roider, J., Michaud, N.A., Flotte, T.J., 1992. Response of the retinal pigment epithelium to selective photocoagulation. Arch. Ophthalmol. 110, 1786–1792.
Rojas-Muñoz, A., Dahm, R., Nüsslein-Volhard, C., 2005. Chokh/Rx3 Specifies the Retinal Pigment Epithelium Fate Independently of Eye Morphogenesis. Dev. Biol. 288, 348–62.
Ruchhoeft, M., Ohnuma, S., 1999. The neuronal architecture of Xenopus retinal ganglion cells is sculpted by rho-family GTPases in vivo. J. … 19, 8454–8463.
Sah, V.P., Minamisawa, S., Tam, S.P., Wu, T.H., Dorn, G.W., Ross, J., Chien, K.R.,

Brown, J.H., 1999. Cardiac-specific overexpression of RhoA results in sinus and atrioventricular nodal dysfunction and contractile failure. J. Clin. Invest. 103, 1627–1634.
Sahai, E., Marshall, C.J., 2002. RHO-GTPases and cancer. Nat. Rev. Cancer 2, 133–42.
Sakaguchi, D.S., Janick, L.M., Reh, T.A., 1997. Basic fibroblast growth factor (FGF-2) induced transdifferentiation of retinal pigment epithelium: Generation of retinal neurons and glia. Dev. Dyn. 209, 387–398.
Sakurai-Yageta, M., Recchi, C., Le Dez, G., Sibarita, J.B., Daviet, L., Camonis, J., D'Souza-Schorey, C., Chavrier, P., 2008. The interaction of IQGAP1 with the exocyst complex is required for tumor cell invasion downstream of Cdc42 and RhoA. J. Cell Biol. 181, 985–998.
Salas-Vidal, E., Meijer, A.H., Cheng, X., Spaink, H.P., 2005. Genomic annotation and expression analysis of the zebrafish Rho small GTPase family during development and bacterial infection. Genomics 86, 25–37.
Salero, E., Blenkinsop, T.A., Corneo, B., Harris, A., Rabin, D., Stern, J.H., Temple, S., 2012. Adult human RPE can be activated into a multipotent stem cell that produces mesenchymal derivatives. Cell Stem Cell 10, 88–95.
Scheer, N., 1999. Use of the Gal4-UAS technique for targeted gene expression in the zebrafish. Mech. Dev. 80, 153–158.
Scheer, N., Groth, A., Hans, S., Campos-Ortega, J., 2001. An instructive function for Notch in promoting gliogenesis in the zebrafish retina. Development 1107, 1099–1107.
Scheetz, S.D., Shao, E., Zhou, Y., Cario, C.L., Bai, Q., Burton, E.A., 2017. An open-source technique to analyze optokinetic reflex responses in larval zebrafish : validation for developmental and chemical biology. J. Physiol. Submitted.
Schmitt, E.A., Dowling, J.E., 1994. Early-eye morphogenesis in the zebrafish, Brachydanio rerio. J. Comp. Neurol. 344, 532–542.
Schmitt, E. a, Dowling, J.E., 1999. Early retinal development in the zebrafish, Danio rerio: light and electron microscopic analyses. J. Comp. Neurol. 404, 515–36.
Schwartz, S.D., Hubschman, J.-P., Heilwell, G., Franco-Cardenas, V., Pan, C.K., Ostrick, R.M., Mickunas, E., Gay, R., Klimanskaya, I., Lanza, R., 2012. Embryonic stem cell trials for macular degeneration: a preliminary report. Lancet 379, 713–20.
Seiji, M., Fitzpatrick, T.B., Simpson, R.T., Birbeck, M.S.., 1963a. Chemical composition and terminology of specialized organlles (melanosomes and melanin granules) in mammalian mlanocytes. Nature 197, 1082–1084.
Seiji, M., Shimao, K., Birbeck, M.S.C., Fitzpatrick, T.B., 1963b. Subcellular localization of melanin biosynthesis. Ann. N. Y. Acad. Sci. 100, 497–533.
Shaner, N.C., Campbell, R.E., Steinbach, P. a, Giepmans, B.N.G., Palmer, A.E., Tsien, R.Y., 2004. Improved monomeric red, orange and yellow fluorescent proteins derived from Discosoma sp. red fluorescent protein. Nat. Biotechnol. 22, 1567–72.
Shim, S.H., Kim, G., Lee, R.D., 2017. Survival of Transplanted Human Embryonic Stem Cell-Derived Retinal Pigment Epithelial Cells in a Human Recipient for 22 Months. JAMA Ophthalmol. 135, 287–290.

Shimizu, Y., Ito, Y., Tanaka, H., Ohshima, T., 2015. Radial glial cell-specific ablation in the adult Zebrafish brain. Genesis 53, 431–439.
Sitaram, A., Marks, M.S., 2012. Mechanisms of protein delivery to melanosomes in pigment cells. Physiology (Bethesda). 27, 85–99.
Smith, C.J., Johnson, K., Welsh, T.G., Barresi, M.J.F., Kucenas, S., 2016. Radial glia inhibit peripheral glial infiltration into the spinal cord at motor exit point transition zones. Glia 64, 1138–1153.
Sokol, S.Y., Li, Z., Sacks, D.B., 2001. The effect of IQGAP1 on Xenopus embryonic ectoderm requires Cdc42. J. Biol. Chem. 276, 48425–30.
Spence, J., Madhavan, M., Ewing, J., Jones, D., Lehman, B., Del Rio-Tsonis, K., 2004. The hedgehog pathway is a modulator of retina regeneration. Development 131, 4607–4621.
Spence, J.R., Madhavan, M., Aycinena, J.-C., Del Rio-Tsonis, K., 2007. Retina regeneration in the chick embryo is not induced by spontaneous Mitf downregulation but requires FGF/FGFR/MEK/Erk dependent upregulation of Pax6. Mol. Vis. 13, 57–65.
Srinivas, B.P., Woo, J., Leong, W.Y., Roy, S., 2007. A conserved molecular pathway mediates myoblast fusion in insects and vertebrates. Nat. Genet. 39, 781–6.
Steinfeld, J., Steinfeld, I., Coronato, N., Hampel, M.-L., Layer, P.G., Araki, M., Vogel-Höpker, A., 2013. RPE specification in the chick is mediated by surface ectoderm-derived BMP and Wnt signalling. Development 140, 4959–69.
Stenkamp, D.L., Cunningham, L.L., Raymond, P. a, Gonzalez-Fernandez, F., 1998. Novel expression pattern of interphotoreceptor retinoid-binding protein (IRBP) in the adult and developing zebrafish retina and RPE. Mol. Vis. 4, 26.
Stenkamp, D.L., Powers, M.K., Carney, L.H., Cameron, D.A., 2001. Evidence for two distinct mechanisms evidence for neurogenesis and cellular pattern formation in regenerated goldfish retinas. J. Comp. Neurol. 431, 363–381.
Stern, J., Eveleth, D., Masula, J., Temple, S., 2015. Slow progression of exudative age related macular degeneration associated with hypertrophy of the retinal pigment epithelium 1–8.
Stern, J., Temple, S., 2015. Retinal pigment epithelial cell proliferation. Exp. Biol. Med. 240, 1079–1086.
Strauss, O., 2005. The retinal pigment epithelium in visual function. Physiol. Rev. 845–881.
Streilein, J.W., Ma, N., Wenkel, H., Ng, T.F., Zamiri, P., 2002. Immunobiology and privilege of neuronal retina and pigment epithelium transplants. Vision Res. 42, 487–95.
Streisinger, G., Walker, C., Dower, N., Knauber, D., Singer, F., 1981. Production of clones of homozygous diploid zebra fish (Brachydanio rerio). Nature 291, 293–296.
Sugihara, K., Nakatsuji, N., Nakamura, K., 1998. Rac1 is required for the formation of three germ layers during gastrulation. Oncogene 17, 3427–3433.
Sumida, M., Hong, R., Tagayas, M., 1994. Role of two nucleotide-binding regions in an N-ethylmaleimide-sensitive factor involved in vesicle-mediated protein transport. J.

Biol. Chem. 269, 20636–20641.
Surace, E.M., Domenici, L., Cortese, K., Cotugno, G., Di Vicino, U., Venturi, C., Cellerino, A., Marigo, V., Tacchetti, C., Ballabio, A., Auricchio, A., 2005. Amelioration of both functional and morphological abnormalities in the retina of a mouse model of ocular albinism following AAV-mediated gene transfer. Mol. Ther. 12, 652–658.
Susaki, K., Chiba, C., 2007. MEK mediates in vitro neural transdifferentiation of the adult newt retinal pigment epithelium cells: Is FGF2 an induction factor? Pigment Cell Res. 20, 364–379.
Szymczak, A.L., Workman, C.J., Wang, Y., Vignali, K.M., Dilioglou, S., Vanin, E.F., Vignali, D. a a, 2004. Correction of multi-gene deficiency in vivo using a single "self-cleaving" 2A peptide-based retroviral vector. Nat. Biotechnol. 22, 589–94.
Tachibana, M., 2000. MITF: A Stream Flowing for Pigment Cells. Pigment Cell Res. 13, 230–240.
Tagaya, M., Wilson, D.W., Brunner, M., Arango, N., Rothman, J.E., 1993. Domain structure of an N-ethylmaleimide-sensitive fusion protein involved in vesicular transport. J. Biol. Chem. 268, 2662–2666.
Takai, Y., Sasaki, T., Matozaki, T., 2001. Small GTP-binding proteins. Physiol. Rev. 81.
Takei, Y., Ozanics, V., 1975. Origin and development of Bruch's membrane in monkey fetuses: an electron microscopic study. Invest. Ophthalmol. 14, 903–916.
Teh, C., Chong, S.W., Korzh, V., 2003. DNA delivery into anterior neural tube of zebrafish embryos by electroporation. Biotechniques 35, 950–954.
Thisse, C., Thisse, B., 2008. High-resolution in situ hybridization to whole-mount zebrafish embryos. Nat. Protoc. 3, 59–69.
Thomas, J.L., Ranski, A.H., Morgan, G.W., Thummel, R., 2015. Reactive Gliosis in the Adult Zebrafish Retina. Exp. Eye Res.
Thummel, R., Kassen, S., Montgomery, J., Enright, J., Hyde, D.R., 2007. Inhibition of Muller Glial Cell Division Blocks Regeneration of the Light-Damaged Zebrafish Retina. Dev. Neurobiol. 392–408.
Thummel, R., Kassen, S.C., Enright, J.M., Nelson, C.M., Jacob, E., Hyde, D.R., 2009. Characterization of Muller glia and neuronal progenitors during adult zebrafish retinal regeneration 87, 433–444.
Tingaud-Sequeira, A., Forgue, J., Andre, M., Babin, P.J., 2006. Epidermal transient down-regulation of retinol-binding protein 4 and mirror expression of apolipoprotein Eb and estrogen receptor 2a during zebrafish fin and scale development. Dev. Dyn. 235, 3071–3079.
Toyofuku, K., Valencia, J.C., Kushimoto, T., Costin, G., Virador, V.M., Vieira, W.D., Ferrans, V.J., Hearing, V.J., 2002. The Etiology of Oculocutaneous Albinism (OCA) Type II : The Pink Protein Modulates the Processing and Transport of Tyrosinase 1, 217–224.
Traver, D., Herbomel, P., Patton, E.E., Murphey, R.D., Yoder, J.A., Litman, G.W., Catic, A., Amemiya, C.T., Zon, L.I., Trede, N.S., 2003. The Zebrafish as a Model Organism to Study Development of the Immune System. Adv. Immunol. 81, 254–

330.
Trede, N.S., Langenau, D.M., Traver, D., Look, A.T., Zon, L.I., 2004. The use of zebrafish to understand immunity. Immunity 20, 367–379.
Tseng, W.A., Thein, T., Kinnunen, K., Lashkari, K., Gregory, M.S., D 'amore, P.A., Ksander, B.R., 2013. NLRP3 Inflammasome Activation in Retinal Pigment Epithelial Cells by Lysosomal Destabilization: Implications for Age-Related Macular Degeneration. Retin. Cell Biol. 54, 110–120.
Tso, M.O., 1973. Photic maculopathy in rhesus monkey. A light and electron microscopic study. Invest. Ophthalmol. 12, 17–34.
Tsurufuji, S., Kurihara, A., Ojima, F., 1984. Mechanisms of Anti-inflammatory Action of Dexamethasone : Blockade by Hydrocortisone Mesylate and Actinomycin D of the Inhibitory Eftect of Dexamethasone on Leukocyte Infiltration in Inflammatory Sites. J. Pharmacol. Exp. Ther. 229, 237–243.
Turner, W.A., Taylor, J.D., Tchen, T.T., 1975. Melanosome Formation in the Goldfish: the Role of Multivesicular Bodies. J. Ultrastruct. Res. 51, 16–31.
Uygun, B., Sharma, N., Yarmush, M., 2009. Retinal pigment epithelium differentiation of stem cells: current status and challenges. Crit. Rev. Biomed. 37, 355–375.
Varga, Z.M., Wegner, J., Westerfield, M., 1999. Anterior movement of ventral diencephalic precursors separates the primordial eye field in the neural plate and requires cyclops. Development 126, 5533–46.
Vavvas, D.G., Daniels, A.B., Kapsala, Z.G., Goldfarb, J.W., Ganotakis, E., Loewenstein, J.I., Young, L.H., Gragoudas, E.S., Eliott, D., Kim, I.K., Tsilimbaris, M.K., Miller, J.W., 2016. Regression of Some High-risk Features of Age-related Macular Degeneration (AMD) in Patients Receiving Intensive Statin Treatment. EBioMedicine 5, 198–203.
Videira, I.F.D.S., Moura, D.F.L., Magina, S., 2013. Mechanisms regulating melanogenesis. An. Bras. Dermatol. 88, 76–83.
Visel, A., Thaller, C., Eichele, G., 2004. GenePaint.org: an atlas of gene expression patterns in the mouse embryo. Nucleic Acids Res. 32, D552–D556.
Vogel, P., Read, R.W., Read, W., Vance, R.B., Platt, K.A., Troughton, K., Rice, D.S., 2008. Ocular Albinism and Hypopigmentation Defects in Slc24a5 -/- Mice. Vet. Pathol. 45, 264–279.
Wang, H., Ninomiya, Y., Sugino, I.K., Zarbin, M.A., 2003. Retinal pigment epithelium wound healing in human Bruch's membrane explants. Investig. Ophthalmol. Vis. Sci. 44, 2199–2210.
Wang, Y., Hanus, J., Abu-Asab, M., Shen, D., Ogilvy, A., Ou, J., Chu, X., Shi, G., Li, W., Wang, S., Chan, C.-C., 2016. NLRP3 Upregulation in Retinal Pigment Epithelium in Age-Related Macular Degeneration. Int. J. Mol. Sci. 17, 73.
Wang, Y., Rovira, M., Yusuff, S., Parsons, M.J., 2011. Genetic inducible fate mapping in larval zebrafish reveals origins of adult insulin-producing β-cells. Development 138, 609–17.
Wasmeier, C., Romao, M., Plowright, L., Bennett, D.C., Raposo, G., Seabra, M.C., 2006. Rab38 and Rab32 control post-Golgi trafficking of melanogenic enzymes. J. Cell

Biol. 175, 271–281.
Watabe, H., Valencia, J.C., Yasumoto, K.I., Kushimoto, T., Ando, H., Muller, J., Vieira, W.D., Mizoguchi, M., Appella, E., Hearing, V.J., 2004. Regulation of Tyrosinase Processing and Trafficking by Organellar pH and by Proteasome Activity. J. Biol. Chem. 279, 7971–7981.
Wei, A.-H., Zang, D.-J., Zhang, Z., Liu, X.-Z., He, X., Yang, L., Wang, Y., Zhou, Z.-Y., Zhang, M.-R., Dai, L.-L., Yang, X.-M., Li, W., 2013. Exome sequencing identifies SLC24A5 as a candidate gene for nonsyndromic oculocutaneous albinism. J. Invest. Dermatol. 133, 1834–40.
Wei, M.L., 2006. Hermansky-Pudlak syndrome: A disease of protein trafficking and organelle function. Pigment Cell Res. 19, 19–42.
Weingeist, T., Kobris, J., Watzke, R., 1982. Histopathology of Best's Macular Dystrophy. Clin. Case Reports 100, 1108–1114.
Westenskow, P., Piccolo, S., Fuhrmann, S., 2009. Beta-catenin controls differentiation of the retinal pigment epithelium in the mouse optic cup by regulating Mitf and Otx2 expression. Development 136, 2505–10.
Westerfield, M., 2007. The Zebrafish Book, 5th Edition; A guide for the laboratory use of zebrafish (Danio rerio)., Eugene, University of Oregon Press. University of Oregon Press.
White, D.T., Mumm, J.S., 2013. The Nitroreductase System of Inducible Targeted Ablation Facilitates Cell-specific Regenerative Studies in Zebrafish. Methods.
White, D.T., Sengupta, S., Saxena, M.T., Xu, Q., Hanes, J., Ding, D., Ji, H., Mumm, J.S., 2017. Immunomodulation-accelerated neuronal regeneration following selective rod photoreceptor cell ablation in the zebrafish retina. Proc. Natl. Acad. Sci. 201617721.
White, Y. a R., Woods, D.C., Wood, A.W., 2011. A transgenic zebrafish model of targeted oocyte ablation and de novo oogenesis. Dev. Dyn. 240, 1929–37.
Whiteheart, S.W., Rossnagel, K., Buhrow, S. a, Brunner, M., Jaenicke, R., Rothman, J.E., 1994. N-ethylmaleimide-sensitive fusion protein: a trimeric ATPase whose hydrolysis of ATP is required for membrane fusion. J. Cell Biol. 126, 945–54.
Wong, W., Faulkner-Jones, B., 2000. Rapid dendritic remodeling in the developing retina: dependence on neurotransmission and reciprocal regulation by Rac and Rho. J. … 20, 5024–5036.
Wong, W.L., Su, X., Li, X., Cheung, C.M.G., Klein, R., Cheng, C.Y., Wong, T.Y., 2014. Global prevalence of age-related macular degeneration and disease burden projection for 2020 and 2040: A systematic review and meta-analysis. Lancet Glob. Heal. 2, e106–e116.
Woods, I.G., Lyons, D. a, Voas, M.G., Pogoda, H.-M., Talbot, W.S., 2006. Nsf Is Essential for Organization of Myelinated Axons in Zebrafish. Curr. Biol. 16, 636–48.
Wykoff, C.C., Brown, D.M., Maldonado, M.E., Croft, D.E., 2014. Aflibercept treatment for patients with exudative age-related macular degeneration who were incomplete responders to multiple ranibizumab injections (TURF trial). Br. J. Ophthalmol. 98, 951–5.

Xiang, S., Vanhoutte, D., 2011. RhoA protects the mouse heart against ischemia/reperfusion injury. J. … 121, 3269–3276.
Xiao, T., Baier, H., 2007a. Lamina-specific axonal projections in the zebrafish tectum require the type IV collagen Dragnet. Nat. Neurosci. 10, 1529–1537.
Xiao, T., Baier, H., 2007b. Lamina-specific axonal projections in the zebrafish tectum require the type IV collagen Dragnet 10, 1529–1537.
Xiao, T., Roeser, T., Staub, W., Baier, H., 2005. A GFP-based genetic screen reveals mutations that disrupt the architecture of the zebrafish retinotectal projection. Development 132, 2955–2967.
Xu, X., Shuen, W.H., Chen, C., Goudevenou, K., Jones, P., Sablitzky, F., 2014. Swap70b is required for convergent and extension cell movement during zebrafish gastrulation linking Wnt11 signalling and RhoA effector function. Dev. Biol. 386, 191–203.
Yasumoto, K., Yokoyama, K., Shibata, K., Tomita, Y., Shibahara, S., 1994. Microphthalmia-associated transcription factor as a regulator for melanocyte-specific transcription of the human tyrosinase gene. Mol. Cell. Biol. 14, 8058–70.
Yeh, C.-M., Liu, Y.-C., Chang, C.-J., Lai, S.-L., Hsiao, C.-D., Lee, S.-J., 2011. Ptenb mediates gastrulation cell movements via Cdc42/AKT1 in zebrafish. PLoS One 6, e18702.
Yook, K., Harris, T.W., Bieri, T., Cabunoc, A., Chan, J., Chen, W.J., Davis, P., De La Cruz, N., Duong, A., Fang, R., Ganesan, U., Grove, C., Howe, K., Kadam, S., Kishore, R., Lee, R., Li, Y., Muller, H.M., Nakamura, C., Nash, B., Ozersky, P., Paulini, M., Raciti, D., Rangarajan, A., Schindelman, G., Shi, X., Schwarz, E.M., Tuli, M.A., Van Auken, K., Wang, D., Wang, X., Williams, G., Hodgkin, J., Berriman, M., Durbin, R., Kersey, P., Spieth, J., Stein, L., Sternberg, P.W., 2012. WormBase 2012: More genomes, more data, new website. Nucleic Acids Res. 40, 735–741.
Yoshii, C., Ueda, Y., Okamoto, M., Araki, M., 2007. Neural retinal regeneration in the anuran amphibian Xenopus laevis post-metamorphosis: Transdifferentiation of retinal pigmented epithelium regenerates the neural retina. Dev. Biol. 303, 45–56.
Yoshimatsu, T., D'Orazi, F.D., Gamlin, C.R., Suzuki, S.C., Suli, A., Kimelman, D., Raible, D.W., Wong, R.O., 2016. Presynaptic partner selection during retinal circuit reassembly varies with timing of neuronal regeneration in vivo. Nat. Commun. 7, 10590.
Yu, R.C., Jahn, R., Brunger, A.T., 1999. NSF N-terminal domain crystal structure: Models of NSF function. Mol. Cell 4, 97–107.
Yun, S., Saijoh, Y., Hirokawa, K.E., Kopinke, D., Murtaugh, L.C., Monuki, E.S., Levine, E.M., 2009. Lhx2 links the intrinsic and extrinsic factors that control optic cup formation. Development 136, 3895–3906.
Zhang, L., Leung, Y.F., 2010. Microdissection of zebrafish embryonic eye tissues. J. Vis. Exp. e2028.
Zhao, X.-F., Wan, J., Powell, C., Ramachandran, R., Myers, M.G., Goldman, D., 2014. Leptin and IL-6 family cytokines synergize to stimulate müller glia reprogramming

and retina regeneration. Cell Rep. 9, 272–84.
Zhu, S., Korzh, V., Gong, Z., Low, B.C., 2008. RhoA prevents apoptosis during zebrafish embryogenesis through activation of Mek/Erk pathway. Oncogene 27, 1580–9.
Zhu, S., Liu, L., Korzh, V., Gong, Z., Low, B.C., 2006. RhoA acts downstream of Wnt5 and Wnt11 to regulate convergence and extension movements by involving effectors Rho kinase and Diaphanous: use of zebrafish as an in vivo model for GTPase signaling. Cell. Signal. 18, 359–72.
Zhu, Y., Carido, M., Meinhardt, A., Kurth, T., Karl, M.O., Ader, M., Tanaka, E.M., 2013. Three-dimensional neuroepithelial culture from human embryonic stem cells and its use for quantitative conversion to retinal pigment epithelium. PLoS One 8, e54552.
Zou, C., Levine, E.M., 2012. Vsx2 Controls Eye Organogenesis and Retinal Progenitor Identity Via Homeodomain and Non-Homeodomain Residues Required for High Affinity DNA Binding. PLoS Genet. 8.
Zuber, M.E., Gestri, G., Viczian, A.S., Barsacchi, G., Harris, W. a, 2003. Specification of the vertebrate eye by a network of eye field transcription factors. Development 130, 5155–5167.